2014

Source tracking and quality assurance of high dose rate (HDR) brachytherapy

Bradley Beeksma
University of Wollongong

Source Tracking and Quality Assurance of High Dose Rate (HDR) Brachytherapy

A thesis submitted in fulfilment of the
requirements for the award of the degree

Master of Science - Research

from

THE UNIVERSITY OF WOLLONGONG

by

Bradley Beeksma
Bachelor of Medical and Radiation Physics
The University of Wollongong, 2014

CENTRE FOR MEDICAL RADIATION PHYSICS
2014

Statement of Originality

This is to certify that the work described in this thesis is entirely my own, except where due reference is made in the text.

No work in this thesis has been submitted for a degree to any other university or institution.

Signed

Bradley Beeksma
First of April, 2014

Abstract

High dose Rate (HDR) brachytherapy utilises a HDR remote afterloader unit to deliver a high activity Ir-192 radioactive source directly into the tumour treatment volume. Since such high source activities are employed for this treatment type, special Quality Assurance (QA) measures need to be employed to ensure accurate radiation dose delivery as calculated by the treatment plan. Real time verification of the remote afterloader and pre-treatment patient specific treatment plan verification should be fundamental to a high dose rate (HDR) brachytherapy quality assurance program. Such QA programs should have real time capabilities of accurately measuring static source dwell positions, precisely measure the time at each dwell location, display real time analysis of error in source positing/timing in comparison to the treatment plan, capable of evaluating transit velocity, track source movement and ideally, real time dosage evaluation and mapping of dose distributions for direct comparison to the treatment plan.

This thesis proposes the development of a new HDR QA smart system so named Brachy*Pix*. The instrumentation and procedures associated with the development of this phantom is designed to address the requirements of an idealistic QA program for HDR brachytherapy. This instrument includes an innovative phantom specifically designed to provide a patient specific, pre-treatment confirmation that a treatment is being delivered according to patient plan. The thesis will focus upon characterisation of epitaxial diodes response to the Ir-192 HDR source for brachytherapy and will continue on to assess the feasibility of the Magic Plate (MP), an innovative CMRP two dimensional silicon detector array, for HDR source tracking and performance

evaluation when combined with the Brachy*Pix* phantom.

Tests for the angular dependence of the single epitaxial diode showed a 15±1% decrease in response when comparing face down to face up orientation of the detector. Depth dose experimental results showed excellent agreement with simulated dose calculation data from the treatment planning system, with subtle variation attributed to positional misalignment. As expected, source velocity was found to be dependent upon intra-dwell position spacing. For the standard clinical treatment step size of 2.5 mm, mean source transit velocity was found to be 15.2±0.6 cm/s. Source transit velocity was shown to be approximately consistent for dwell spacings >20 mm with an average velocity of 31.2±1.8 cm/s. The MP was found to be highly capable of accurately tracking the iridium source by proficiently displaying a visual representation of a transversal reconstruction of source location for both a static and dynamic state. In addition to the visual representation capabilities, the system was proven to be able to numerically locate the local source position in three dimensions with a precision of 0.20 mm. These results give the sanction for continued development of a patient specific pre-treatment quality assurance program.

Acknowledgments

First and foremost I would like to thank Anthony Espinoza and Dr Marco Petasecca. I cannot emphasise how grateful I am to you both for your continuous guidance and support throughout the entire length of this project. I simply could not have completed this work without your assistance and ongoing direction.

Anthony has been a great tutor, guide and collaborator throughout the entire process. His commitment to the project not only kept me on track and focused throughout the entirety of this research but additionally taught me the techniques and provided me with the information essential to the eventual completion of this thesis.

As for Dr Marco Petasecca, six months into my masters and still without a research project he, potentially unknowingly, took me on as his student. Without him I would have never of started let alone been able to complete this work, and for that I am thankful. His knowledge and experience on detectors and data acquisition systems is incomprehensible and he always had solutions to problems I could not figure out. In saying that I sense he learnt a bit from me in terms of PIA phantom design.

In the early phases of my masters, when I was severely lacking in direction, Dr Stephanie Corde-Tehei voluntarily took on the role as my clinical supervisor. Her support, particularly near the beginning of the project was invaluable and her clinical knowledge in the field of radiation oncology is outstanding.

Additionally I would also like to thank the director of medical physics Mr Simon Downes and the entire radiation oncology staff at the Prince of Wales Hospital Syd-

ney, for not only allowing me access the facilities to undertake my research but also on educating me on the fundamental workings of HDR brachytherapy and the entire radiation oncology department.

As for other members of the CMRP, firstly I would like to thank Dr Dean Cutajar for his contributions to the project and in particular for teaching me a very valuable lesson in backing up data. He hit the 'sweet spot' when he successfully managed to retrieve my entire thesis after a major computer failure. Additionally I would like to thank the director of the CMRP Professor Anatoly Rozenfeld. His work behind the scenes has without question greatly influenced not only this project but the course of my life. I also owe thanks to other CMRP staff members Dr Michael Lerch, Professor Peter Metcalfe and Mitra Safavi for their contributions to the project. I would like to thank my friends and colleagues for their support throughout the entirety of this project, in particular 'The Mudlarks' and all members of 'The Batcave'

Lastly I would like to thank my family for their continuous support throughout my medical physics studies and into my career. I couldn't have done it without you.

Contents

List of Figures

List of Tables

Chapter 1

Introduction

With a continually increasing diagnostic rate of cancer amongst Australians [1] radiation therapy techniques are incessantly advancing with the objective of very accurately conforming maximum dose to a well defined target volume, whilst minimising exposure to healthy tissue. The delivery method of High Dose Rate (HDR) Brachytherapy aims to achieve this by localising high activity radiation directly within the target volume. As this treatment method has become an increasingly more viable option, treatment plans have become continually more sophisticated and the number of patients receiving treatment has steadily increased. Consequently, the necessity for development of improved pre treatment quality control systems has become imperative to ensure the accurate and safe delivery of these complex radiation fields.

Due to the high dose rate associated with HDR brachytherapy (5-6 Gy/minute at 5 mm from the source [2, 3]) it is essential that the brachytherapy source be delivered with high precision in regards to dwell positioning and timing. Incorrect implementation of either of these parameters can potentially lead to insufficient tumour control and high dose being delivered to the incorrect treatment volume. Consequently, accurate positional verification of the HDR source is a fundamental part of quality assurance procedures and is well documented in the literature [4–18].

From a clinical perspective, specific quality assurance protocols and procedures will vary between different treatment centres. However, each QA program should re-

flect similarities across all centres. Such clinically patient specific quality assurance procedures should reflect requirements of checking dose prescription (dose and location), comparison of source stopping positions and dwell timings between reports (plan compared to delivery) and an independent verification of treatment plan programs dose calculation (at Prince of Wales Hospital) the prescribed plan from Oncentra (HDR brachytherpay treatment planning software) imported into RadCalc (an independent dose calculation software) for dose comparison and verification).

Although such QA procedures are clinically implemented, currently there is no reported documentation of absolute dose measurement (pre treatment patient specific dosimetry). Coincidently, if there is a problem in the 3D dose calculation or a problem with the file transfer to the console (i.e. what you see on the screen of the HDR computer is not what was expected to be delivered) or disparity in specified catheter to transfer tube attachment, there is no way to pick up these errors and dose delivered to the patient will not correspond to the intended plan.

Although multiple source tracking and positional verification methods are available, currently there are no documented reports in the literature which assess patient specific pre treatment dosimetry techniques for measuring actual dose to be delivered as prescribed by the treatment plan. Such quality assurance methods fail to provide accurate dosimetry and verification of the treatment plan in terms of dwell positioning and timing for individual patient procedures. Such potential for radiation accidents can be prevented by pre treatment dose delivery verification.

In an attempt to rectify this problem, the Centre for Medical Radiation Physics (CMRP) has developed a pre treatment quality assurance system so named Brachy*Pix*. The Brachy*Pix* system incorporates the CMRP developed Magic Plate (MP) silicon diode detector array, to accurately track source positioning and dwell timing for any plan in HDR brachytherapy. As a means of dose verification, the pre treatment dose map acquired by the MP is compared to computed dose map as per the treatment planning system. Variation between the images suggests a misadministration of dose and the problem can thus be noted and rectified. The Brachy*Pix* system is also ad-

vantageous in incorporating the effect of transit dose, neglected by the treatment planning software (TPS).

1.1 Project Outline

This thesis aims to describe the initiation, feasibility, calibration, development and characterisation of the Magic Plate for the Brachy*Pix* HDR pre-treatment dose verification system. Firstly, Chapter 2 of this thesis looks at an overview of radiation therapy, providing a general consensus to the necessity of the field. It explores the ideologies and processes behind radiation therapy; in particular HDR brachytherapy.

Chapter 3 provides a detailed elucidation to the necessity of improved quality assurance within HDR brachytherapy. Firstly, a mathematical explanation of the fundamentals behind the TG-43 protocol are introduced. Since this protocol forms the basis of calculations used in most treatment planning systems, limitations and assumptions made by this protocol are addressed. The chapter continues on to entail a review of the literature which of current approaches to HDR brachytherapy QA, source tracking mechanisms and determination of brachytherapy delivery velocities. The chapter concludes with a fundamental review of silicon diodes and properties associated with using silicon diodes as a radiation dosimeter as per this thesis.

Chapter 4 describes technical details of the detectors and data acquisition systems involved in this thesis. This chapter introduces and provides an insight to the intended design and fabrication of the Brachy*Pix* smart phantom. This chapter goes on to detail the design of silicon epitaxial diodes and components of the Magic Plate detector array. It looks at the Magic Plate's corresponding TERA board electrical read out system and details the high speed X-Tream data acquisition system.

Chapter 5 is dedicated to the experimental procedures undertaken to assess the feasibility of the Magic Plate as a dedicated QA system for HDR brachytherapy. It describes the methods for characterisation of the MP in terms of angular dependence

and depth dose response and examines the applications of the detector system, specifically in its ability to spatially track the iridium source. Results from transit velocity using the X-Tream data acquisition system are also presented. Limitations of the individual detector and respective systems are also addressed. Chapter 6 concludes the findings from this thesis.

Chapter 2

Radiation Therapy

The study of radiation and its use in radiation oncology is a continually evolving field with a broad range of concepts and principles associated within its history and development. Medical uses of X-rays date back to 1895 [19] when Röntgen first discovered that X-rays could be used to identify bone structures; structures; the use of radiation in bracytherapy treatments were practiced soon after in 1898 where sources were placed in contact or close to the target tissue [20]. Since then, extensive research into the properties of radiation has lead to the evolvement of the field of radiation therapy.

2.1 Development of Cancer Modalities

Cancer is defined as the uncontrolled malignant growth (cell division beyond normal limits) of a group of cells caused by a series of changes in the genome. This disease is one of the leading cause of deaths in Australia. In 2010, there was 26 518 reported cases of death as a direct result of the disease. This places cancer second only to cardiovascular disease (32 912 deaths) for mortality rates amongst Australian people [21]. Globally, more than one in three people will develop cancer during their lifetime and about one in four will die from the disease [22].

According to the Australian Institute of Health and Welfare (AIHW) cancer mortal-

ities amongst Australians is declining, however, cancer incidence rates are steadily increasing. The report, *Cancer in Australia: An Overview 2008* [1] showed that in 2007, over 100 000 new cancer cases were diagnosed nationally. This record number of new cases is attributed to Australia's aging population, improved diagnostic technology in the ability to diagnose smaller tumour volumes and increased public awareness of cancer prevalence. A combination of these factors has thus led to more patients presenting for a diagnosis. The report predicted that this number is projected to steadily increase at a rate of 3000 additional new diagnoses per year. The most common cancers for Australian men and women were:

1. Prostate Cancer
2. Colorectal Cancer
3. Breast Cancer
4. Melanoma of the skin
5. Lung Cancer

2.1.1 Treatment Options

After the severity of a diagnosed cancer has been assessed, a treatment option can then be initialised. There is no single effective treatment for any single type of cancer as the best treatment option is often highly patient specific. There currently exists three conventional cancer treatment options; each of which have their own associated benefits and detriments.

- Surgery
- Chemotherapy
- Radiation Therapy

The relative efficiency of each method for a specific clinical site is a matter of debate and often a combination of two or all three of these treatments are used to provide a higher degree of certainty in providing an effective treatment. This is known as a multimodality therapy. For tumors which show no evidence of metastasis and have defined surgical boundaries, radical surgery is often used in conjunction with radiation therapy for optimal treatment. Such is often the case for patients undertaking radical prostatectomy, breast lumpectomy or mastectomy, where radiation is delivered post surgery to treat potential microscopic disease around the clinical site. The use of chemotherapy and another modality is quite common and can be administrated neoadjuvantly (prior to main treatment), adjuvantly (after the main treatment) or in combination with other treatments. Mixed modalities complement each other to enhance toxicity effects to the tumour site.

2.2 Radiation Therapy

Many radiation therapy modalities exist which enable x-ray or gamma radiation to be delivered to the treatment site in various ways. X-ray radiation is commonly delivered externally using linear accelerators via 3D Conformal Therapy (3DCRT), Intensity Modulated Radiation Therapy (IMRT), Image Guided Radiation Therapy (IGRT), Volumetric Modulated Arc Therapy (VMAT), Tomotherapy, and many others. Gamma radiation is typically delivered internally, via means of brachytherapy, Low Dose Rate (LDR) brachytherapy, High Dose Rate (HDR) brachytherapy and Pulsed Dose Rate (PDR) brachytherapy.

The goal of any radiation therapy is to maximise the dose delivered to a well defined treatment volume while sparing dose to healthy surrounding tissue, with the aim of eradicating the disease, prolonging the life and/or improvement of the quality of life of the patient. The process of calculating the appropriate delivery of any radiation therapy for malignant disease is complex and involves many steps. The most critical step in any radiation treatment is the determination of the location, extent and spread

of the disease relative to normal tissue structures. Contouring of disease with an adequate margin is known as target volume localization or defining the planning target volume [23–25]. By spatially conforming high radiation dose to the planning target volume, high probability of tumor control can be achieved due to the induction of damage to the abnormal cell.

To induce cell death, the radiation must irreversibly damage a cell's DNA. Radiation which produces complex double strand breaks (DSB) in the DNA radically damages the DNA beyond repair. Simple DSBs are potentially lethal lesions that occur within the DNA but can be correctly repaired and the cell continues to live. If multiple simple DSB occur within close proximity ($\approx$4 nm) the DNA becomes unrepairable. This is known as Binary misrepair [26].

The actual cell death is caused by a process known as Mitotic Catastrophe. Mitotic Catastrophe is the most important process of cell death in radiation therapy. Mitotic catastrophe is produced by chromosome abnormalities induced by DNA damage caused by DSBs. If the DNA is mis-repaired, when the cells undertakes mitosis, the daughter cells are also seen as damaged which then die by the natural cell death process of apoptosis. Since the cell death relies on cell proliferation, cell death is not often seen until a long time after irradiation. In terms of radiation therapy, this explains why tumour shrinkage is not often immediate following treatment and tumour size should not indicate the successfulness of the treatment. [26]

2.3 Brachytherapy

Brachytherapy is a form of radiation therapy which aims to achieve highly localised dose distributions by placing small, short range radioisotopes with steep dose gradients inside or adjacent to the region requiring treatment. By placing these small radiation seeds wholly within the treatment volume, the radiation affects only localised tissue in close proximity to the source. This minimises exposure to healthy tissue surrounding the treatment area, decreasing the probability of adverse side ef-

fects [2]. From a clinical perspective, brachytherapy is a simple procedure with fewer fractions and lower treatment time, allowing for rapid recovery of patients. This is in stark contrast to curative external beam radiation therapy (EBRT) whose conventionally fractionated EBRT schemes require multiple fractions and up to 6 weeks to complete. Studies in the literature has demonstrated excellent patient outcomes using brachytherapy [27–29] and is often used in conjunction with other modalities such as hormonal therapy, chemotherapy, external beam radiation therapy and surgery to further improve patient outcome [30–33].

Brachytherapy radiation sources are introduced via catheters, needles or applicators placed within the required treatment region. The distinction between LDR and HDR brachytherapy is based on the activity of the isotope and its associated deliverable dose rate. As per ICRU report 38 [34] LDR is characterised by isotopes with dose rate >0.4 Gy/hr and <2 Gy/hr, this is in contrast to HDR which is characterised by isotopes with dose rates >12 Gy/hr [34]. LDR is commonly associated with long term radiation implants where HDR is often associated with short term removable implants.

2.3.1 LDR Brachytherapy

LDR utilises low activity (7.4-37 GBq) radioactive material for interstital implantation into the target volume. With a half-life of 59.49 days [35] and a relatively low peak energy of 28.3 keV, I-125 seeds are the most commonly used isotope for LDR procedures in Australia. For prostate treatments the number of seeds implanted into the target area is primarily dependent upon the treatment site and size of the target volume. For such treatments number of implanted seeds can exceed 150 [2]. LDR brachytherapy procedures are used for direct treatment of tumour sites, low risk patients and for treatment of residual disease following invasive tumor extraction.

2.3.2 HDR Brachytherapy

HDR treatments utilises temporary implantation of a high activity, (typically Ir-192) radio isotope to irradiate the target volume by a process known as remote afterloading. Suitable for relatively small and well localised tumors, HDR brachytherapy is often used in conjunction with external beam radiation therapies as a radiation boost. Extensively steep dose gradients and high dose rates (5-6 Gy/minute at 5 mm from the source [2, 3]) delivers high dosages to a localised volume in a short time. This enables patients to undertake minimal fractionations and short treatment times whilst still achieving high tumor control probability.

The treatment is delivered through the use of catheters inserted directly into or adjacent to the treatment volume. These catheters are introduced in three ways; placed into pre-existing body cavities (eg/ vaginal and cervix treatments) known as intracavitary therapy or surgically inserted in the treatment area (eg/ prostate or breast treatment) known as interstitial therapy or placed into wax moulds, moulded to the patients contour for superficial treatments. Imaging of the patient is then required to gain a visual representation of the insertion of the cathers relative to anatomical structures and assess if the inserts are suitable for treatment. Essentially, the images also provide a data set in which the plan is to be developed on. A variety of imaging modalities are available and depending on the treatment type typically include Computed Tomography (CT), Magnetic Resonance Imaging (MRI) or Ultrasound (US) [36–38]. Images are then transferred to the hospitals brachytherapy treatment planning system (TPS) where calculation of optimal dose to the treatment volume is conducted based on parameters specified by the oncologist. For each catheter, the TPS outputs a file specifying where the source needs to be administrated (dwell positioning) and the corresponding timing interval at each dwell location (dwell timing). By varying the dwell positions and individual dwell times, a complex dose distribution that conforms to the clinical needs of the individual patient can be delivered in the target volume [39].

HDR brachytherapy treatments have several advantages over other radiation treatment modalities. By nature of the treatment type, HDR brachytherapy places the radiation source directly in or near the tumor location. Due to rapid dose fall off, this treatment permits delivery of high doses in minimal fractions, leading to a greater biological effective dose and increased dose localisation. This has the effect of greater sparing of surrounding tissue and negligible entry/exit dose, unable to be delivered even by the most advanced external beam radiation therapy treatment. Additionally, the relatively shortness in the number of fractions prohibits significant tumour cell proliferation. This is in contrast to external beam treatments which often last up to six weeks. HDR brachytherapy is however limited to specific treatment sites and often requires invasive surgery.

Patients receiving HDR brachytherapy are not radioactive after receiving treatment. This is in stark contrast to LDR seed implant patients whose radioactivity continues to emit after release from hospital. For LDR treatments hospital personal and other persons the patient comes into contact with during the treatment procedure are exposed to additional radiation exposure. Modern planning systems and HDR afterloaders provide a more precise positioning and thus better dose distribution than LDR implants [40].

2.3.2.1 HDR Afterloader: Nucletron mHDR-v2 MicroSelectron

For all irradiations performed in this work, a Nucletron microSelectron mHDR-v2 afterloader was used (see figure 2.1) which resides at the Prince of Wales Hospital, Randwick, NSW Australia. The Nucletron microSelectron HDR brachytherapy afterloader treats firstly at the most imminent dwell position before continuing to other specified dwell positions further distances within the catheter (forward stepping). During treatments, the drum is remotely controlled from outside the room. This feeds the source out of the safe, through the selected transfer tube and into a catheter located inside the patient.

HDR remote afterloading therapies typically use a small radioactive Ir-192 pellet

contained within a stainless steel capsule attached to a flexible stainless steel cable. When not in use, the source resides in a tungsten safe housed within the afterloader. The opposite end of the cable is wound around an encoded cable drum. A stepper motor, which is directly coupled to the cable drum, drives the source cable both towards the applicator and retracts it into the safe. Depending on the direction of drum rotation, the source is extended to the required dwell location or entirely retracted back to the safe.

Figure 2.1 MicroSelectron transportable HDR afterloading unit [41]

Dimensions for the Nucletron mHDR-v2 MicroSelectron iridium source shown in figure 2.2 are taken from studies conduced by Daskalov *et al.* and Lliso *et al.* [42,43]. The source consists of a 3.60 mm long, 0.65 mm diameter, high density (22.43 g/cm^3) [42] radioactive Ir-192 core, evenly distributed throughout an enclosed 0.90 mm diameter AISI 316L steel capsule (density of 8.06 g/cm^3 [44]). A 200 mm, 0.70 mm diameter section of highly flexible steel cable is laser welded to the tip of the encapsulation, a 0.15 mm thick tapering segment. This is then adhered to a 4.15 mm long hollow section allocated for source placement. Following the hollow section is a 0.20 mm solid conical section with the external radius of the face being 0.45 mm, totalling the outer capsule length to be 4.50 mm. The remaining cable has length of approximately 1305 mm with an increased cross sectional diameter of 0.90 mm and

density 4.81 g/cm^3 [42]. The capsule and cables small dimensions allow for high flexibility and lower frictional force opposing the motion of the source through the catheter. This inturn permits the source to pass through small diameter catheters and small radii of curvature (1 cm radius) in catheters and applicators.

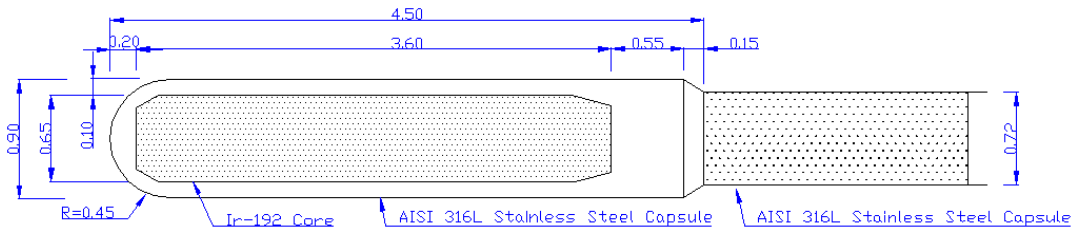

Figure 2.2 Source capsule specifications for the Nucletron mHDR-v2 MicroSelectron iridium source. All measurements are in millimetres

All HDR sources used for measurements in this thesis were all manufactured by Mallinckrodt in Petten, The Netherlands. The activity of the source is approximately 5.1×10^{11} Bq (518 GBq) when first manufactured, although decays to approximately 4.0×10^{11} Bq (10-11 Ci) during the 3 weeks handling and transportation period to Australia. This period of decay is of significance as regulations require a maximum measured dose of less than 0.1 μSv/h at 1 m from the afterloaders shielding safe [41]. The microSelectron-HDR shielding safe can safely only hold a source with a maximum activity of 444 GBq to ensure these regulations are met [41]. The Prince Of Wales Hospital, Sydney exchanges the source at every half life ($\approx$167 GBq) which equates to a source change approximately every three months.

2.3.2.2 Source: Iridium-192

Due to its high specific activity and relative ease of manufacture, Iridium-192 is the most commonly utilized isotope for HDR brachytherapy applications. The isotope is produced in nuclear reactors primarily by neutron activation of stable Iridium-191 metal, which produces minimal unwanted by-products. Iridium-191 has a large cross section for neutron interactions and can be found in pure form (37% concentration of natural iridium.) This permits large concentrations of Iridium-192 to be produced

reasonably easily. Below show the two methods of Iridium-192 production [45].

$$^{191}\mathrm{Ir}(\mathrm{n},\gamma)^{192}\mathrm{Ir}$$
$$^{192}\mathrm{Os}(\mathrm{d},2\mathrm{n})^{192}\mathrm{Ir}$$

According to the LNHB Table of Radionuclides [45] Iridium-192 has a half-life of 73.827 days, and decays by beta minus emission (95.13%) to excited levels of Platinum-192 and by electron capture (4.87%) to excited states of Osmium-192. High energy gamma emissions range from 110.4 keV to 1378.2 keV with the most probable decay at 316.5 keV [45] and mean energy of 370 keV [46].

Chapter 3

Review of HDR Dose Calculation Protocols and Quality Assurance Methods

Due to the high radiation dose rate associated with HDR brachytherapy treatments (5-6 Gy per minute to localized tissues) [2, 3] it is critical that the timing and delivery of the source to the required dwell location is undertaken with the utter most precision. Incorrect positioning of dwell location will result in undesirable dose delivery or the administration of dose to the incorrect treatment volume [47]. Incorrect placement of the source location can result from a variety of parameters; a mismatched catheter length, wrong transfer tube length, variation in the source position, malfunction of the remote afterloading system and inaccuracy of treatment set-up and planning [10].

Patient treatment plans in HDR brachytherapy are developed using treatment planning software such as PLATO or its latest version Oncentra, which calculates 3D dose distributions in the body due to exposure from the brachytherapy source. Most commercial softwares employ algorithms based on the dose distributions described by the AAPM TG-43 protocol [46]. This software bases the intended dose distribution entirely on dwell timing and positioning; thus precise dwell timing and positioning needs to be undertaken to deliver the prescribed dose as per calculated by the TPS. Although rare, the use of in-vivo real time dosimetry during HDR brachytherapy is

employed in some clinical treatments to verify predicted dose from the treatment plan and to allow for urgent intervention if treatment doses are exceeding expected dose levels. These are repeatedly difficult to administer to the correct anatomical locations within the patient and often non-ideal due to the high dose gradients associated with HDR brachytherapy. Some of these studies have shown that some dose incongruities do exist between prescribed and measured dose [4, 48, 49].

Discrepancies between planned dose and administrated dose can a have significant impact on the effectiveness of a treatment. Overdosing of a patient causes unnecessary additional exposure to healthy surrounding tissue. These effects are compounded in treatment sites which are in close proximity to sensitive organs such as the rectum in prostate treatments where over exposure can lead to increased probability of post treatment complications such as rectal toxicity [50]. Under irradiation has the obvious effect of providing an insufficient treatment leading to an increased probability of infield recurrence.

Although most errors in brachytherapy have been the result of human errors rather than failure of the treatment delivery system or error associated with treatment planning, still many accidents have been reported for HDR brachytherapy procedures in the history of the treatment [47, 51, 52]. This reinforces the need for improved HDR QA and highlights the necessity for accurate real time patient specific dosimetric methods and source tracking.

Currently, there are no patient specific independent source position verification procedures nor measurement of delivered dose distribution for individual treatment. It is therefore imperative to develop a patient specific independent quality assurance method that accurately measures and verifies the HDR dwell position and timing within the catheter. This QA verification method will measure absolute dose delivered per patient and ensure the correct operational procedure of the afterloader. These QA measures will reveal and prevent any mistakes before any treatment is administrated allowing the safe execution of a treatment. QA processes should be a fundamental part of HDR undertaken daily prior to treatment delivery.

3.1 The TG-43 Protocol

The Radiation Therapy Committee of the American Association of Physicists in Medicine (AAPM) formed the task group 43 (TG-43) to recommend a dosimetry protocol for dose calculations and a data set for the values of dosimetry parameters for interstitial brachytherapy [46, 53]. This protocol defines recommendations for source strength specifications, calibration standards and dose calculation equations which form the basis of many treatment planning systems. In 2004 AAPM released an updated version of the recommendations [46] to make corrections to the formalisation and to accommodate for newly available sources. Prior to the TG-43 protocol, dose rates were calculated based upon photon fluence around the source in free air geometry. Since Ir-192 seeds are not isotropic point sources, accurate dose distributions in a patient could not be calculated from photon fluence in free space. This problem was rectified in the TG-43 protocol by making use of Monte Carlo simulation data and data obtained from measured dose distributions in water equivalent phantoms.

The TG-43 protocol allows for two-dimensional dose calculations around cylindrically symmetric sources such as those used in HDR brachytherapy. The specification employs a polar coordinate system with the origin at the centre of the source. As shown in figure 3.1, r specifies the radial distance (in cm) from the centre of the radioactive source to the point of interest and θ specifies the polar angle the point of interest makes with respect to the longitudinal axis of the source.

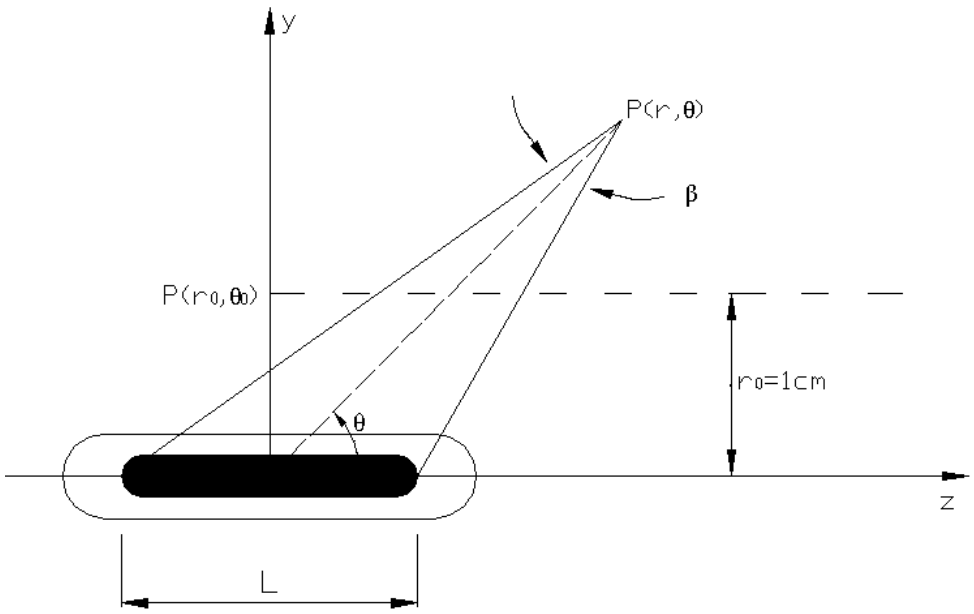

Figure 3.1 Illustration of geometry assumed in the TG-43 dose calculation formalism.

Using this coordinate system the two dimensional dose rate $\dot{\mathrm{D}}(r,\theta)$ at the point of interest $\mathrm{P}(\mathrm{r},\theta)$ can be found using the following equation

$$\dot{D}(r,\theta) = S_K.\Lambda.\frac{G_L(r,\theta)}{G_L(r_0,\theta_0)}.g_L(r).F(r,\theta) \tag{3.1}$$

The inclusion of the subscript L denotes that the line source approximation is used for seed approximation in the data gathered for the geometry function. That is, the source is assumed to have a cylindrical length L, with a zero radius. The remaining parameters given in equation 3.1 are defined as follows.

3.1.1 Air Kerma Strength, S_K

Air kerma strength of a brachytherapy source is the measurement of the sources strength. It is defined as the air kerma rate, $\dot{K}_\delta(\mathrm{d})$ for photons of energy greater than δ (in a vacuum) at a distance of d from the source centre, multiplied by the square of the distance. The distance d is measured in the plane along the transverse bisector of

the source.

$$S_K = \dot{K}_\delta(d)d^2 \tag{3.2}$$

The specification of determining air kerma in a vacuum implies corrections should be made for photon attenuation and scatter in air, or any other medium placed between source and detector. The distance, d, should be large in comparison to source size, usually taken as 1 m. Air Kerma Strength units are specified by the symbol U, where 1U=1μGy.m^2.h^{-1}.

3.1.2 Dose Rate Constant, Λ

The dose rate constant is a specified quantity defined as the ratio of the dose rate at reference location (r_0, θ_0) and Air Kerma Strength. The constant is dependent on the individual radionuclide and includes effects of source encapsulation and scattering within itself and water surrounding the source [46].

$$\Lambda = \frac{\dot{D}(r_0, \theta_0)}{S_K} \tag{3.3}$$

For Ir-192 dose rate constants can be found via Monte Carlo simulations in a study conducted by Williamson [54] or by measured values in a solid water medium by The Interstitial Collaborative Working Group (ICWG) [55].

3.1.3 Geometry Factor, G(r,θ)

Since tabulated data gives information at specific geometrical points, the Geometry Factor allows for increased accuracy in dose rate calculations for cases of extrapolation between discrete data points. The Geometry Factor corrects for reduction of radiation intensity with distance and the size of the source. For a point source approximation, the geometry factor is given by the inverse square law [46].

$$G_p(r, \theta) = \frac{1}{r^2} \tag{3.4}$$

For line source approximations the geometry factor is much more complicated. As depicted in figure 3.1, multiple considerations must be taken into account including; (L) the active length of the source, (β) the angle in radians subtended by the ends of

the active line source with respect to the point of interest P(r,θ) and (θ) the angle the point of interest P(r,θ) makes with the longitudinal axis of the source.

$$G_L(r,\theta) = \begin{cases} \dfrac{\beta}{Lrsin\theta} & \text{if } \theta \neq 0^\circ \\ (r^2 - L^2/4)^{-1} & \text{if } \theta = 0^\circ \end{cases}$$

3.1.4 Radial Dose Function, g(r)

The radial dose function is a dimensionless parameter which accounts for the decrease in dose rate along the transverse axis of the seed with increasing radial distance. This factor accommodates for the effects of attenuation and scatter within the surrounding medium. This function reduces to 1 at the reference point r_0=1 cm and does not account for inverse square law as defined by the geometry factor. For both line and point sources, radial dose function data can be derived using the equation.

$$g(r) = \frac{D(r,\theta_0)}{D(r_0,\theta_0)} \frac{G(r_0,\theta_0)}{G(r,\theta_0)} \tag{3.5}$$

3.1.5 Anisotropy Function, F(r, θ)

An actual brachytherapy source exhibits considerable anisotropy. This means, the dose distribution around the central axis of the source with respect to the transverse plane is directionally dependent. Since the source is not a point source, activity is distributed throughout its length. The source distribution, self absorption by the active element of the source in conjunction with photon attenuation by the encapsulating shell and delivery cable, gives rise to the anisotropy of the source. The 2D anisotropy function takes into account this variation defined by the equation

$$F(r,\theta) = \frac{D(r,\theta)}{D(r,\theta_0)} \frac{G(r,\theta_0)}{G(r,\theta)} \tag{3.6}$$

The anisotropy function reduces to unity along the transverse plane of a source. Off this axis, F(r,θ) typically decreases with: decreasing radial distance, as θ approaches 0° or 180° , increasing encapsulation thickness and with decreasing photon energy.

The 2D formalisation gives the highest degree of accuracy at distances close to the source (<1 cm). However, most HDR treatment planning systems implement the use of a 1D isotropic point-source approximation to simplify the dosimetry calculations (given in equation 3.8). The introduction of 1D anisotropy factor, $\phi(\mathrm{r})$, reduces equation 3.1 to be dependent only on radial distance (r), eliminating the need to know the orientation of the source inside the patient and therefore to evaluate its angle θ.

The anisotropy factor at radius r, can be acquired by the ratio of integrating the dose rate over the entire two dimensional 4π solid angle to the dose rate at radius r on the transverse axis. Shown by the equation

$$\phi_{an}(r) = \frac{\int_0^\pi D(r,\theta) sin(\theta) d\theta}{2D(r,\theta_0)} \tag{3.7}$$

With the inclusion of the 1D anisotropy factor, for a pinpoint source equation 3.1 reduces to the 1D dose rate calculation

$$\dot{D}(r) = S_K.\Lambda.\left(\frac{r_0}{r}\right)^2.g_r(r).\phi_{an}(r) \tag{3.8}$$

or for a line source

$$\dot{D}(r) = S_K.\Lambda.\frac{G_L(r,\theta_0)}{G_L(r_0,\theta_0)}.g_L(r).\phi_{an}(r) \tag{3.9}$$

3.2 Factors not accounted for in the TG-43 Based Brachy therapy Treatment Planning Systems

Anatomical material differences, lack of heterogeneity correction, defined patient boundaries, attenuation by applicator materials and assumption of full scatter conditions introduce amalgamations in some treatment sites during HDR brachytherapy treatments [56]. These inconsistencies may adversely affect patient dose distributions, however, are not taken into account by the broadly used TG-43 protocol. This is a limitation of the system which can lead to oversimplification of dosimetry calculations in some clinical treatment sites.

Even though brachytherapy dose calculations are heavily dependent on scatter conditions and the photon interaction process is dominated by the photoelectric effect cross sections (more so for LDR), brachytherapy planning systems have only recently had heterogeneity corrections made available. These are known as Model based dose calculation algorithms (MBDCAs). MBDCAs offer the possibility of modeling radiation transport in non water substrates (tissue, applicators, air etc) resulting in a much more accurate display of the physical dose delivered to the patient [57].

Such algorithms can have vast differences in dose calculations to those TG43 based algorithms. TG-186 [57] state a difference of a factor of 10 in some cases. Specific to HDR Ir-192 treatments, multiple studies have shown discrepancies in dose using a TG-43 based formalism or a dose to medium calculation based method. Anagnostopoulos *et al.* [58] found that for a HDR Ir-192 esophageal treatment, there was no difference between TG-43 based dose to water ($\mathrm{D_{w,w}}$) and Monte Carlo based dose to medium ($\mathrm{D_{m,m}}$) within the target region, however TG-43 ($\mathrm{D_{w,w}}$) over estimated dose of up to 13% to the spinal cord and 15% underestimation to the sternum bone. Poon *et al.* [59] showed for a HDR Ir-192 endorectal treatment, differences between ($\mathrm{D_{w,w}}$) and ($\mathrm{D_{m,m}}$) were less than 2% for soft tissues, 18-23% in cortical bone, 3-3.5% in spongiosa and 5-7% in femoral bone.

Model based dose calculation algorithms raise certain issues. MBDCA calculated doses are sensitive to the dose specification medium resulting in energy dependent differences between, dose calculated to water in a homogenous water geometry (TG-43), dose calculated to the local medium in the heterogeneous medium and dose calculated to a voxel of water within a heterogeneous medium [57]. MBDCA's can be categorized as semi-empirical or model based. Some semi-empirical methods apply 1D ray-tracing with scaling for correcting total doses due to the presence of high Z materials. Such methods (none are completely 3D) separate primary and scatter dose components and use a 1D ray-tracing for the primary dose and estimate the scatter dose component. Another approach is based on Monte Carlo pre-calculated applicator specific dose in water distributions which aim at accounting for high Z material

shields of the applicator [57]. These semi-empirical approaches allow brachytherapy treatments to be calculated in the same time frame as TG-43 based methods with the benefit of increased accuracy to represent the physical implant [57]. Model based algorithms either openly simulate the transport of radiation in the medium or utilize scatter integration techniques to account for scatter dose. Three main methods of model based algorithms are Collapsed Cone Superposition/Convolution Method, Deterministic Solutions to the Linear Boltman Transport Equation and Monte Carlo based methods.

TG-186 points out that as model based dose calculations algorithms are new to Brachytherapy, caution should be used for early adapters of the model. Key vigilance areas pointed out by TG-186 [57] include, MBDCA doses are sensitive to voxel by voxel interaction cross sections. ICRU/ICRP and conventional CT do not provide useful guidance for assigning interaction cross section values to each voxel, since each patient has a unique source/applicator combination. Having reference data for each possible combination is impractical. Historical prescriptions and isodose lines are based on TG-43 to water, we have no evidence of tissue responses based on dose to the medium. So visualizing dose to medium therefore may alter our prescription without evidence.

The recent Acuros BV algorithm employed by Varian Medical Systems is such a MBDCA which corrects for such inhomogeneities in brachytherapy dose calculations. A 2011 study conducted by T. Nyathi *et al.* [56] was devised to compare the new Acuros BV algorithm to the standardised TG-43 system. This preliminary study compared calculated point doses by Acuros BV against ionization chamber measurements in heterogeneous material and TG-43 dose calculations. 6% and 10% agreement with the ionization chamber was found for the Acuros BV and TG-43 respectively. Previously treated patient plans were recalculated using the Acuros BV system. In one case for a single mammosite brachytherapy plan skin doses as high as a 27% difference between the two algorithms was found. This is attributed to Acuros BV modelling the lack of scatter in lower density materials where TG-43 as-

sumes homogenous water. As a result clinical sites with significant inhomogeneities such as breast, lung and oesophagus are presumably to benefit from inhomogeneity corrections [56]. This study proves that errors exist in TG-43 based brachytherapy treatment planning systems and that simulated dose distributions do not always correspond to delivered dosages.

HDR brachytherapy is a dynamic treatment as the position of the radiation source is varied in time. This leads to the introduction of transit dose; currently neglected in dose calculations by most treatment planning systems. Transit dose occurs during transit between time intra-dwell positions, entry of the source into the patient and as the source is withdrawn from the patient. This dose is dependent upon source activity, number of fractions and source velocity.

Many factors contribute to the difficulties associated with dose calculations and determining the effects that transit dose have on a treatment. Such considerations needed to be accounted for are; acceleration and deceleration of the source, time in transit, time at dwell positions relative to time in transit, number of dwell positions and the resolution of the internal clock of the afterloader [60, 61].

K. Bastin *et al.* [62] attempted to calculate the transit dose delivered during the delivery and retraction of a source. This was done by placing TLDs in a Lucite phantom at distances between 5 mm and 40 mm away from the orthogonal axis of the catheter. The source was delivered to its dwell position for 0.1 s and then retracted. It was found that total transit doses were typically $<$100 cGy but may exceed 200 cGy when using a large number of fractions with a high activity source. The results of this study stated that treatment planning systems cannot assume transit dose to be negligible and should be included within all high dose rate treatment planning systems.

3.3 Current Clinical QA Practices

QA programs ensure that all devices required for treatment planning and delivery continue to function within defined tolerance levels. These tolerance levels shall be set to realistically reflect the capabilities of the equipment and achieve clinically acceptable levels of treatment accuracy. This program often consists of a subset of commissioning tests, which are to be performed at fixed intervals [36]

Recently the Australian College of Physical Scientists and Engineers in Medicine (ACPSEM) Radiation Oncology Specialty Group (ROSG) released a brachytherapy QA recommendation paper [36]. These tests and their frequencies are based of recommendation of various national and international bodies [37,38,63–67]. This document serves as a guideline for the frequency of calibration and quality assurance (QA) of equipment and radioactive sealed sources used for brachytherapy in Australasia, however, the document does not provide information on a procedure in which to carry out such tests. Each of the QA tests are subdivided into categories based on their frequency to be performed. A combination of likelihood of malfunction, clinical impact of malfunction and resources required all combine to assess the frequency at which the tests should be performed. The ACPSEM paper subdivides these tests into daily, at source replacement (quarterly) and annual frequencies for such QA procedures to be performed. A summary of QA procedures, frequencies and their tolerances will be provided below with greater emphasis being provided on the procedures with greater importance.

3.3.1 Pretreatment (Daily)

3.3.1.1 Functionality tests

The functionality of interlocks and safety measures are critical in preventing a radiation accident and minimizing exposures in emergency situations. Therefore, daily testing of such interlocks is imperative to patient safety.

- Door interlocks
- Treatment interrupt button
- Emergency off button
- Room radiation monitor
- Console displays (treatment status indicator, date, time, source strength)
- Data transfer from TPS
- CCTV + Audio system
- Emergency equipment present
- Applicator and transfer tube interlocks

Other recommended pre-treatment tests require validation of the HDR afterloaders accuracy. Such tests must be performed daily as incorrect delivery of such parameters would lead to grievous consequences for the patient. These tests include:

3.3.1.2 Source Positional Accuracy

This is test is to ensure that HDR afterloader is delivering the source to the desired position. As HDR dose distributions are dependent upon source positioning, it is essential for correct treatment that the source goes to the correct location for the programmed dwell position and additionally that this position corresponds to that used in the treatment plan. For a stepping source, the afterloader requires the distance to a specific dwell position (usually the first) from some reference point, the dwell positions are then relative to this absolute position. Therefore precise measurement of this reference position is critical. There are multiple methods in which to verify source positional accuracy. AAPM TG 40 [63] recommends verification of source location using radiographic film supplemented by external markings which reference the desired source delivery position, developing the film shows the agreement

between delivered and expected source position. ESTRO booklet 8 [37] also recommends the radiograph method but also describes a method of delivering the source to a specially designed catheter with ruler makings directly related to distance. Attaching the ruler and focusing a camera on the scale allows the position of the tip of the source to be verified. Both methods are capable of testing the first reference position and subsequent the source step size. Recommended tolerance levels are 1 mm [36, 63].

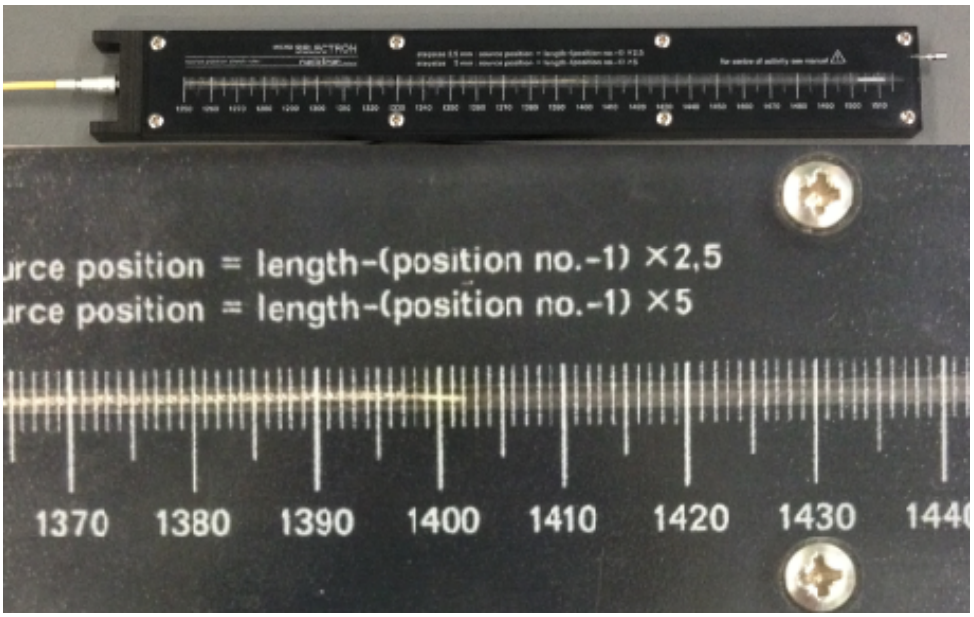

Figure 3.2 Specialised catheter with positional indicators used for daily QA

3.3.1.3 Dwell Time Accuracy

As recommended by ESTRO booklet 8 [37] a simple plan should be established to send the source to a specific position for a designated time. Comparing the programmed treatment time with a stopwatch reading will perform the timer consistency check. Tolerance 1% [36]

3.3.2 At Source Replacement (Quarterly)

Quarterly tests are typically more extensive and time consuming than daily tests.

3.3.2.1 Functionality tests

- Mechanical integrity of applicators, transfer tubes and connectors
- Emergency off in room
- Power failure recovery
- Obstructed catheter
- Check contents of emergency equipment and ensure availability during source exchange

Similarly to the daily tests, other recommended monthly tests require validation of the HDR afterloaders accuracy. These include

3.3.2.2 Source Positional Accuracy

As described in the daily test verification of source location using radiographic film supplemented by external markings which reference the desired source delivery position is recommended. Unlike the daily test, this should be undertaken using film so a permanent record exists of source positioning. Often a jig is used in conjunction with a standard plan for this type of verification (see figure 3.3 below). Consideration of the expansion of metals must always be taken into account. When the source is replaced, the stainless steel cable is often cold. As time passes the metal heats up and expands, this leads to a change in the positioning of the source. For this reason, source positional accuracy should always be checked the next day after the source has been untouched in the safe for a prolonged period of time.

Figure 3.3 QA jig to establish the positional accuracy of a brachytherapy source with film

3.3.2.3 Applicator Length

The length of the transfer tubes are a critical element in the overall source positioning accuracy. Often there are a large number of transfer tubes to accommodate for the use of different catheters. Using a dedicated length gauche or a ruler system that allows measuring the overall length of the catheter and tube combination provides a QA tools for this purpose.

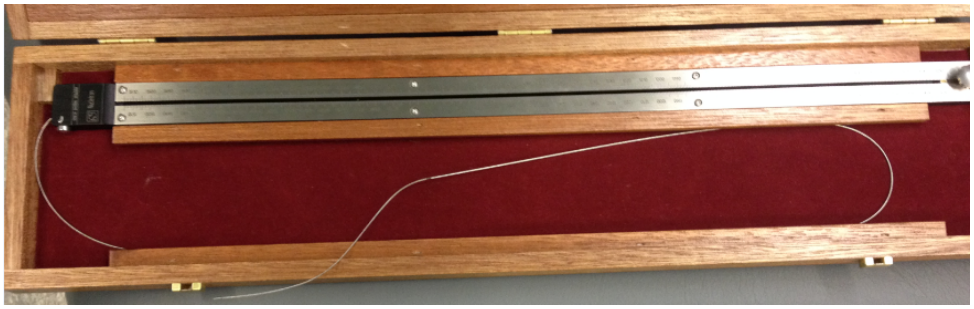

Figure 3.4 Applicator length verification tool

3.3.2.4 Timer Linearity

As described in ESTRO booklet 8 [37] it is recommended to verify the timer linearity. Position an ion chamber close to catheter and deliver the source to the same position within the catheter multiple times with varying dwell times. A linear plot should result by plotting the ionization reading vs dwell time. A tolerance of 1% is recommended [36].

3.3.2.5 Source Strength Calibration

The TPS calculates dwell times based on the source strength or the air kerma rate. Multiple sources [36–38, 64] recommended that the source strength according to the certificate be verified with a suitably calibrated dosimetry equipment traceable to a primary standard. A calibrated well-type ionization chamber is the preferred method for calibration of brachytherapy sources; however a farmer chamber within an air-jig suitable calibrated can also be used. Air kerma can then be calculated based on the protocol given by TEC DOC 1274 [67]. The vendor supplied source strength should not be used as the sole method for source strength specification. The secondary measurement method shall be capable of detecting errors within a 5% uncertainty [36].

Figure 3.5 Well chamber for use in source calibration

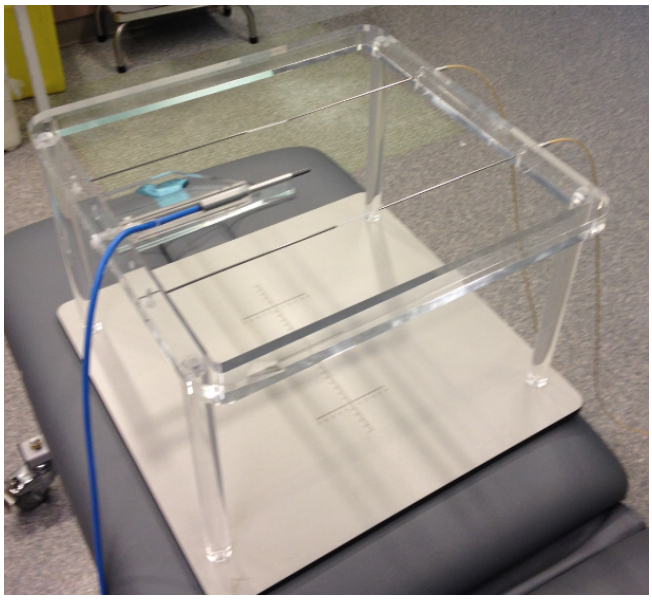

Figure 3.6 In-air jig for use in source calibration

3.3.2.6 Stability Of The Local Standard

ESTRO booklet 8 [37] recommends establishing the drift in response of a well type chamber by comparing the response from a long lived reference source such as Cs-137. By using a uniquely defined insert to ensure reproducibility of positioning of the source, one can verify the chambers signal. ESTRO booklet 8 [37] also suggests An alternative method for checking the chamber's stability is to irradiate it in an external Co-60 beam under reproducible conditions. Only correction for source decay and, if applicable, temperature and air pressure is needed to obtain confidence in the stability of the instrument's reading. Any sudden deviation of more than 0.5% in the check reading might indicate a problem [37, 67].

3.3.2.7 Leakage/Contamination radiation

ESTRO booklet 8 [37] recommends checking contamination of sources or leakage of radioactive material using a wipe test. An absorbent cotton pad is dampened with a suitable solvent such as water or alcohol as this can enhance the collecting efficiency of radioactive material present. The swab should be applied to applicators and transfer tubes as the sources are generally not directly accessible for wipe testing. The radiation from the swab is then analysed with a crystal counter or scintillator based nuclear pulse counter in order to detect any gamma emitting nuclides. As the radiation level to be detected is generally low, a good counting geometry and a long counting time is required to collect a suitable signal, which is high enough to differentiate from the background. The recommended leakage radiation tolerance is 10 μSv/hr [36].

3.3.3 Annual

Annual tests are the most extensive QA tests with the tightest tolerances

3.3.3.1 Functionality Tests

- Hand held radiation monitor

- Hand crank function
- Emergency procedure review
- Applicator damage
- Applicator and catheter attachment

3.3.3.2 Transit Dose Reproducibility

The effect of the transit time increases the dose delivered to the patient beyond that due to the dwell time alone. In general, the further the point of interest is from the dwell position the greater the percentage contribution to the dose is due to transit effects. Using a fixed geometry the consistency of transit time can be measured. The effects of transit can be found from the following equation

$$TransitDose(t) = 1 - \frac{M_{t0}}{M_t(t)} \tag{3.10}$$

Where $\mathrm{M_t(t)}$ is the electrometer reading at time t and $\mathrm{M_{t0}}$ is the electrometer reading with zero dwell time and dose only contributing during source transport. This is determined by programming specific dwell times ranging from 5-120 seconds and extrapolating to t=0. Tolerance 1% [36].

3.3.3.3 In-Air Jig Calibration

Air kerma determination as per the IAEA TECDOC-1274 [67].

3.4 Determination Of Transit Velocity

Several attempts to determine the transit velocity of a high dose rate HDR brachytherapy unit have been reported in the literature with varying results. In the majority of these studies, merely the average speed of the source is measured for transit dose calculations, which is inaccurate as speed of the source is dependent upon step size.

Accurately determining the speed of the source is necessary to calculate the transit dose in brachytherapy treatments and therefore determine the implications this dose has on treatments.

Wong *et al.* [68] used a video camera with shutter speed of 1 ms and a digital stop watch of resolution 0.01 s to calculate source speed. It was reported that the transit speed was found to vary with the step size and path length. For travelled distances of 0.25, 0.5, 1.0, 23.0 and 99.5 cm, average transit speeds were found to be 5.4$\pm$2.3, 7.2$\pm$1.6, 23.3$\pm$7.3, 38.5$\pm$0.7 and 52.9$\pm$1.5 cm/s respectively.

Using an ionisation chamber and a precision electrometer, Sahoo [69] measured charge as a source moved through the catheter. Transit times of 0.03 s and 0.45 s for 0.5 cm and 10 cm were reported for separation between two dwell positions, respectively. The average time for 1 cm travel of the source between two dwell positions was found to be 0.022 s, resulting in an average speed of 45.5 cm/s.

Using a video monitor and stopwatch, Bastin *et al.* [62] measured that for a 32.5 mm dwell spacing, source velocity was 32.5 cm/sec and had a maximum velocity of 45.2 cm/s for large dwell separation distances. Although stating that lower velocities exist for shorter path lengths no attempt at measuring small distances were made. Linear extrapolation was used to estimate source velocity at small dwell separation distances.

Using a simple system consisting of a plastic scintillator block and a charge-coupled device (CCD) camera H. Kojima *et al.* [61] recorded the luminance of the source to accurately measure source positioning and timing in real time. From the produced images, pixel size and luminance blur restricted source position resolution. Source location was determined to be within $\pm 1\,\mathrm{mm}$. The CCD camera's frame rate was fixed at a rate of 30 frames per second, giving a timing resolution of 33.3 ms. The authors concluded that this method enabled a simple, quick, yet effective way of determining parameters such as source position, transit time, dwell time and movement at each dwell position.

Unlike previous indirect measurements of transit velocity, Minamisawa *et al.* [70] measured directly the immediate speed profile of an iridium source in a HDR brachytherapy unit. Measurements were taken for the source travelling from the unit's safe to the end of the catheter and between inter-dwell positions. Directly measuring the source has the effect of drastically reducing error in velocity calculations as some indirect measurements have reported up to 100% standard deviation [69] for small inter-dwell distances. Using an optical fibre based detector system the maximum velocity of the source were found to be 52.0 ± 1.0 cm/s, slightly different to the speed specified by Nucletron of 50 cm/s. The maximum average velocity is reported to be 46.7 ± 0.9 cm/s significantly less than found by Wong *et al.* [68]. The authors demonstrate that the radiation source follows a uniform acceleration and deceleration both of a=113 cm/s^2. This leads to the conclusion that average velocity of the source between different inter-dwell distances is linearly proportional to the travelled distance.

3.5 Current HDR Brachytherapy Quality Assurance Methods Within The literature

3.5.1 Radiochromic Film

Radiochromic film allows the collection of data in a one plane from a radiation exposure. Radiochromic film has been used to verify dwell positioning and dose by comparing relative isodose lines from the plan to point doses extrapolated from the film. Discrepancies between the measured data and TPS data can be usually attributed to positional inaccuracies of the film, mismatch in film calibration conditions and the effect of source anisotropy [4]. Film must be first irradiated and then processed post treatment to check dose distributions and determine dwell positions. The primary problem associated with this is the lack of real time readout and lack of dwell timing information. This is especially unwelcoming in the case of emergency situations and over irradiations, as no information will be provided to staff to interrupt treatment until irreversible damage to the patients healthy tissue has been induced.

D. Rickey *et al.* [5] used a combination of radiochromic film and four photodiode detectors to verify dwell location and dwell timing respectively. Visually inspecting the film, dwell location could be determined using a ruler within 0.5 mm. Scanning the film reduced uncertainty of dwell location to within 0.2 mm however required greater time for analysis. The temporal accuracy of the timing for the QA tool was found to be about 1 ms.

In a study conducted by Aldelaijan *et al.* [6] the dose uncertainty in using radiochromic film as a dosimeter for Ir-192 HDR brachytherapy treatments was investigated. In a dose range of 1-50 Gy, dosimetry could be accurately determined with a dose uncertainty of 4.12%.

3.5.2 Fluoroscopy Imaging

The system described by Lightstone [7] was developed to provide a quick positional and timing verification of an Ir-192 source as a part of the daily quality assurance for the HDR brachytherapy. The apparatus houses a fluorescent screen either side of an applicator. Indicator lines are marked on the fluorescent screen in positions which correspond to the various dwell positions programmed by the daily QA protocol. When the source enters the catheter a glow can be observed using closed-circuit video cameras within the treatment room. This glow indicates the real time positioning of the source. Verification of source positioning can be immediately read out with an accuracy of ± 1 mm and dwell time accuracy within 1 second (for a 60-second dwell time) can be carried out using a stopwatch.

This method is advantageous in: its speed of dwell position verification, ability to visually check source retreatment for safety checks and eliminating confusion of distance between physical end of the catheter and centre of the source. It however provides no hardcopy of verification without video printout, gives no dosimetric information, poor timing resolution and positioning measurements are highly dependent upon the interpretation of the user.

L. Liu [8] incorporated the use of a mobile C-arm fluoroscopic machine to verify dwell positions of a HDR Brachytherapy treatment. Unfavourably, the described method images the positions of the pre treatment check cable safety wire, rather than the actual Ir-192 radiation source. Prior to treatment, this cable delivers a dummy seed to the intended dwell positions as a safety measure. This study describes imaging these positions and visually comparing them to the corresponding positions as per the treatment planning system. This visual inspection is undertaken with a ruler to determine any deviation of source position from the plan. This method provides an indirect QA program which is capable of detecting gross errors in dwell positions, however is unsuitable for millimetre precision of determining absolute dwell position.

3.5.3 Diamond Detector - The Development Of A New Mathematical Algorithm

Nakano *el al* [9, 10] developed a mathematical algorithm to determine a real time verification of a HDR source within the presence of tissue heterogeneity. By placing an array of dosimeters on the patients skin, an independent verification of the source position in three dimensions could be established.

This verification was demonstrated using a diamond detector placed in several locations on the surface of a tissue equivalent phantom. A mathematical algorithm was constructed to estimate the location of the source given measured data from the skin detectors. A limitation of the algorithm is that it may give false source positions if more than half the number of detectors is compromised by the tissue heterogeneity. Thus the locations of detectors must be chosen to avoid tissue heterogeneities as far as possible. The accuracy of the source localization was found to increase with the number of detectors used to compute the estimation of the source position. The resolution to which the 12 detectors can identify the location of the source was within 3 mm. Errors in determination of source positioning, due to tissue heterogeneity, could be reduced by using additional detector increasing the statistical confidence levels. This algorithm could be potentially be used with other dosimetric detectors.

3.5.4 Pinhole Imaging

Duan *et al.* [11] investigated the use of an externally applied, duel pinhole and fluoroscopy imaging system for independent *in vivo* monitoring and verification of a HDR brachytherapy treatment. The system used was comprised of a high resolution pinhole collimator (0.5 mm diameter pinhole), an x-ray fluoroscope and a standard radiographic screen-film combination. The fluoroscopy provides a real-time image of the Ir-192 source for monitoring of the source location and its movement, while the radiographic film provides a permanent record of the source positions. The introduction of the dual-pinhole collimator enables the reconstruction of the source dwell positions in three dimensions. Using a phantom, well recognizable images of a 281 GBq Ir-192 source for dwell times in the clinical range of 2 s to 400 s were achieved. Using this pinhole system and a simple reconstruction algorithm, source dwell positions separated by lateral displacements as small as 1 mm could be clearly resolved. Although the authors claim high resolution source positioning and fluoroscopy can track the source in real time, the authors provided no method or results of dwell timing verification or positional accuracy for dwell times less than 2 seconds.

M Batic *et al.* [12] used high resistivity silicon pad detectors combined with dual pinhole lead pinholes collimators to track the position of the source from distances up to 40 cm in a field of view of approximately $20\times20\times20\,\mathrm{cm}^3$. The system is comprised of 256, $1.4\times1.4\times1\mathrm{mm}^2$ silicon detector pads arranged in 32×8 grid and was developed to follow the movement of the source during therapy. This allows for on-line detection of deviations from planned treatment but can not reconstruct the absolute coordinates of the source. The authors claim that the location of the source can be reconstructed in three dimensions in real time, with a precision of about 5 mm for sources as weak at 37 GBq. Similarly to the previously mentioned Pinhole imaging method, no verification of dwell timing is provided by the authors

3.5.5 Thermoluminescent Detectors (TLD)

TLDs have also been used in dosimetry for HDR brachytherapy. As with most detectors used as an *in-vivo* dosimeter, TLDs encounter difficulties due to the steep dose gradients associated with brachytherapy. The sensitive volume of most TLDs is relatively large, approx 1 mm thick. So in steep dose gradients, as found in HDR brachytherapy treatments, dose volume averaging occurs across the detector. Other problems associated with TLDs include: over response at low energy, incapable of real time dose measurement, require calibration and are time plus labour intensive in regards to annealing read out of the detector. Despite these limitations TLDs are often the clinical dosimeter of choice to verify a dose plan.

Seo *et al.* [13] verified the accuracy of a brachytherapy treatment of a superficial melanoma using in-vivo thermoluminescence dosimetry. They found the received dose in the planning target volume was close to the prescribed dose with a maximum variation of 7.5% and an 8.8% variation in dose given to the middle of the neck. These large discrepancies were attributed to positional error of the TLDs. The energy response of TLDs also needs to be considered.

Meigooni *et al.* [14] investigated this by measuring dose in polystyrene at several distances from a 370 GBq Ir-192 source using ionisation chambers and LiF TLD chips. They found at 10 cm the sensitivity of the LiF TLDs chips varied 8.5% compared to at distances of 1cm. This factor was attributed to the photon spectrum shift with increasing distance in the phantom due to the attenuation of soft photons of which LiF has an increased response to. As a results depth dose correction factors need to be applied to TLDs to minimise error in dose measurements.

3.5.6 Flat Panel Detectors

H. Song *et al.* [15] successfully implemented using a single flat panel detector to accurately track a HDR brachytherapy source and its dwell positions in real time, in three dimensional space. The prototype utilised ball bearings in a tray of known

configuration to cast a shadow on the flat panel detector from the exit radiation of the Ir-192 source. By manual inspection of the projections of the ball bearings onto the flat panel detector, 3D coordinates for the dwell positions were reconstructed within a standard deviation of 1.5 mm. The authors conclude that with automated ball bearing shadow recognition software; this technique possesses the potential of 3D tracking of dwell location and dwell times of a HDR brachytherapy source in real time.

3.5.7 Ion Chamber Array

The MatriXX Evolution two-dimensional ionization chamber array, has been becoming increasingly popular for intensity-modulated radiation therapy (IMRT) plan verification and recently began to show implementation into brachytherapy treatments. The ionization chamber array consists of 1020 single air-vented plane-parallel cylindric ionization chambers (0.55 cm high, 0.4 cm diameter, 0.76 cm detector pitch and 0.07 cm^3 sensitive volume) arranged in a 32x32 matrix (there are no chambers in the corners of the array). The maximum field of view achievable is 24x24 cm^2 with a minimum read out time of 20 ms [16]. The major issue faced with ionization chambers in HDR brachytherapy is dose volume averaging effect. Due to their finite size, this effect may have significant effects on accuracy of dosimetry in the steep dose gradients present in HDR brachytherapy.

Yewondwossen *et al.* [17] utilised the MatriXX Evolution two-dimensional ionization chamber array for dosimetric verification of a HDR brachytherapy treatment by comparing expected TPS calculated dose distributions and measured dose from the 2D array. Three catheters were placed within a Nucletron Freiburg Flap Applicator Set and used to deliver a standard gynae treatment. This entire apparatus was positioned on top of the MatriXX Evolution array to cover the detector area. Slabs of solid water were used to provide full scatter conditions. The mean difference in dose was measure to be 1.67% with a maximum deviance of 11.35%. 98.7% of all pixels were in agreement between planed and measure dose. The authors conclude that the matrix detector can be used for quick and convenient verification of a brachytherapy

plan.

Manikandan *et al.* [18] utilised the MatriXX 2D array as an independent HDR brachytherapy treatment verification as to ensure the treatment is delivered as prescribed. Using this detector array, this study delivered plans of 5mm step size and 2 s dwell time to verify dwell position and step size. Maximum error in dwell positioning was found to be 1.8 mm with average uncertainty in dwell positioning being 0.45 ± 1.99mm at 95% confidence. It was found that step sizes $\leq 1\,\mathrm{cm}$ could not be verified using the MatriXX system. For step sizes 2, 3, 4 and 5 cm 70% of errors were found to be below 1 mm.

3.5.8 The Optimal HDR verification system

The numerous aforementioned studies from the literature all assess HDR brachytherapy QA. Each study reports using various detector types and detector systems; yet each constituent exhibits their own various benefits and downfalls. An optimal pre-treatment verification system should be able to provide instantaneous, real time read-out of source positioning and dwell timing. These parameters should be able to be conducted with a high degree of accuracy with sub millimetre and sub millisecond response in order to accurately provide spatial information whilst the source is in transit. Additionally the system should be able to provide a measured dosimetric analysis of the plan and a comparison of this measured dose to the inputted treatment plan; inclusive of an assessment of transit dose and transit velocity. An ideal dosimeter would be tissue equivalent, have a small sensitive volume providing high spatial resolution in three dimensions, independent energy response, high sensitivity and be independent of dose rate. There is currently no dosimeter in clinical use that provides these desired characteristics.

3.6 Silicon Diodes

As a consequence of silicon's high density ($2.33\,\mathrm{g/cm^3}$) incident radiation exhibits large energy losses within the medium. A Silicon detector will produce around 18000 times more charge than an ion chamber of the same volume [71]. This permits detectors to be manufactured with extremely small sensitive volumes which still provide large enough signals to be measured whilst keeping the statistical noise and measurement times at acceptable levels [72]. This provides them with the ability to achieve high spatial resolution without sacrifice of sensitivity to the incident radiation [73, 74]. This high spatial resolution is needed to resolve dosimetry problems within the steep dose gradient associated with HDR treatments. Despite silicons high density, electrons and holes move almost freely in the semiconductor at room temperature. Importantly, this enables rapid charge collection and thus gives them the capacity to electronically provide fast real time read out information on dose rate and integral dose.

Semiconductor detectors also exhibit high mechanical stability, energy independence (for energies $>150\,\mathrm{keV}$, see figure 3.7) capability to be used in passive mode and a mean ionization energy ($3.6\,\mathrm{eV}$) approximately an order of magnitude lower than what is required for gas ionisation chambers [71, 74, 75]. Additionally, they have a real-time detectable signal and strong technology processing history which makes the fabrication of large volume of device easy and cheap. The aforementioned properties make silicon detectors suitable for use in HDR brachytherapy QA systems and direct patient dosimetry.

3.6.1 Silicon Energy Dependence

A common known property of silicon diodes is the energy dependence of the detector response. This property arises as low energy photons in high atomic number materials have high probability of interaction via the photoelectric process. Due to the increasing cross section of the photoelectric effect in silicon relative to water,

silicon exhibits an over response to low energy photons and thus an over estimation of the absorbed dose. Detector responses will be largely over estimated in low energy photon fields (<150 keV). Photons of this energy are present in HDR energy spectrums [71, 73, 76] with increasing fluence at increasing depth due to Compton scattering [77].

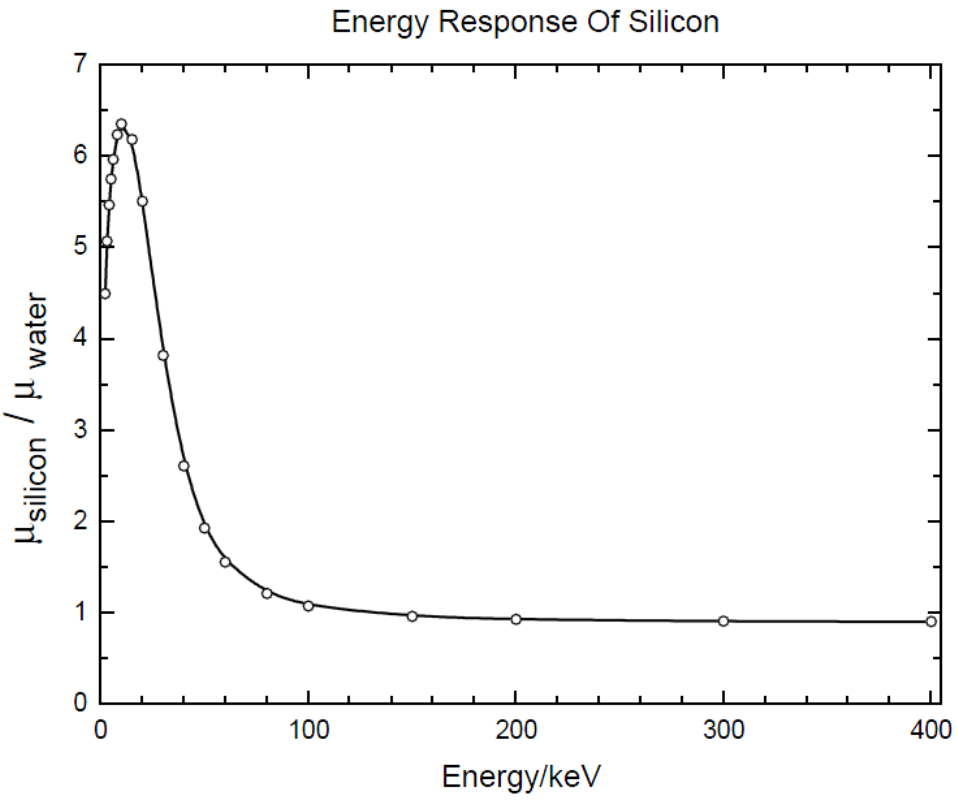

Figure 3.7 Energy response of photon attenuation in silicon relative to water. Produced from data from the NIST XCOM photon cross section database [78]

As figure 3.7 demonstrates, there is no over response in silicon to the higher energy photons. The Ir-192 low energy emissions have a much lower probability of decay and thus contribute to minimal number of counts within the data. So even though these low energy photons respond up to 6.5 times greater, the number of decays (probability of emission) is small so their contribution to the number of counts is minimal. Although still probable, compared to higher energy photon emissions the low percentage of emissions gives minimal rise to the over response effect, making

silicon diodes an eligible dosimeter for HDR dosimetry [79]. For more information on HDR photon energies see section 2.3.2.2.

3.6.2 Silicon Diode Fundamentals

Silicon is typically doped with phosphorus and boron to form p-type and n-type semiconductors respectively. Upon contact, electrons are permitted to diffuse from the n-type to the p-type and holes to flow in the opposite direction. Electrons and holes combine near the junction, where each recombination eliminates and electron and a hole. This results in a region of positive donor ions in the n regions and negative ions in the p region in the immediate vicinity of the junction. These areas of opposite charge create an electric field (ϕ) or build in potential difference, in the order of 10^3 V/cm [75]. This created potential, known as the depletion layer (W) inhibits any further diffusion of carriers across the junction.

3.6.3 Diode Operation as a Radiation Dosimeter

A schematic illustration for a silicon diode in use as a radiation dosimeter is depicted in figure 3.8. With no external voltage applied (nil bias) the detector is said to be operating in passive mode. In this state, if connected to an external circuit, no current is permitted to flow unless carriers are generated by external factors, such as ionizing radiation. Collection of radiation generated carriers is possible without applied external bias due to the electric field which exists across the pn junction.

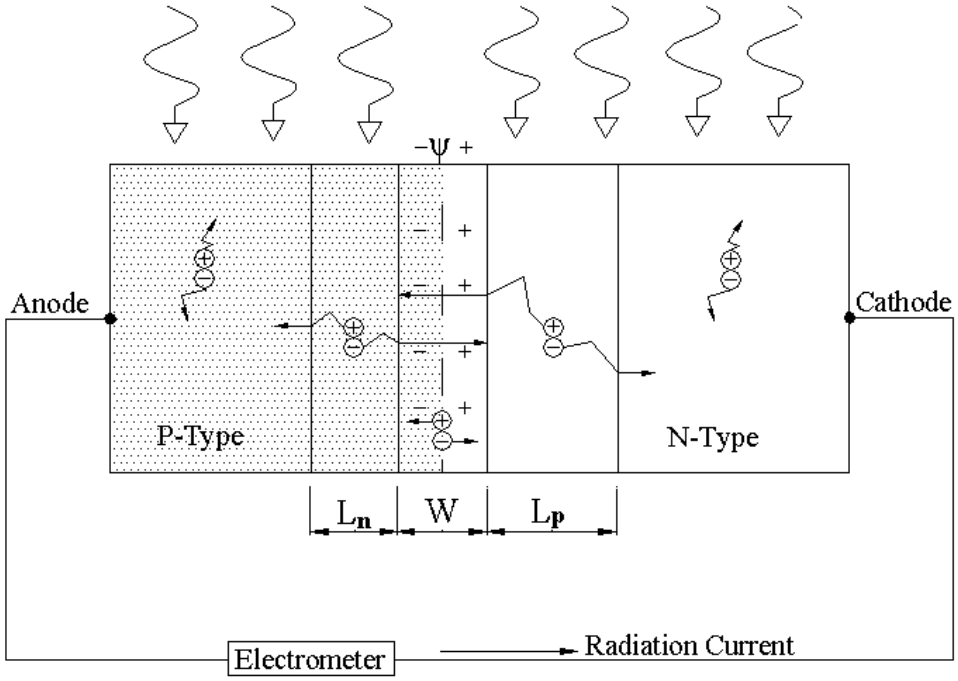

Figure 3.8 Schematic diagram of a silicon pn junction diode in use as a radiation detector.

Radiation incident upon the diode induces electron hole pairs within the p and n type silicon. Excess minority carriers (electrons within the p-type and holes within the n-type) then diffuse towards the pn junction. These carriers are then swept across the junction by the natural built-in potential, collected by the electrometer and registered as current. Carriers created by ionizing radiation outside diffusion lengths L_p on the n-type side and L_n on the p-type side, do not contribute to current. On average these carriers will recombine and achieve equilibrium prior to being swept across the junction by the build-in potential. Carriers created within these diffusion lengths may also diffuse into the region and be swept across the junction, contributing to current.

Applying a reverse bias (negative terminal to the p-type and positive to the n-type) to the semiconductor has the effect of pulling the holes in p-type and electrons in the n-type away from the junction, resulting in the increase of the width of the depletion layer, which is proportional to the square root of the applied potential [71]. Consequently current can not flow across the junction. This is imperative when using

a diode as a dosimeter as there will be no current flow from majority carriers, thus current measured is only due to minority carriers crossing the junction, produced by incident radiation. The measured current is proportional to the dose rate in silicon. Integrating the total counts with respect to time provides the total absorbed dose in the silicon.

The sensitivity of silicon diodes may change over time. This is because ionising radiation creates defects in the silicon lattice. These defects become recombination centres for the minority charge carriers, reducing the minority carriers and thus the sensitivity of the detector. Widely published in the literature suggests that a typical low resistivity diodes sensitivity decrease with increasing radiation damage [80, 81] however, the high resistivity of the epitaxial diode opposes this evidence.

At the Si-SiO2 interface of the epitaxial diode, an increase in radiation increases the number of holes [82]. This results in an increase in the depletion region under the field oxide between the n+ core region and the p+ region, effectively increasing the sensitive volume of the diode [83]. To resolve this issue, epitaxial diodes require a extremely high dose (kGy) to saturate the interface traps and stabilise the detectors sensitivity [83].

3.6.4 Type Of Doping

Minority carriers in p and n-type detectors are electrons and holes respectively. Since each type contains different charge carriers, a variance in the behaviour is seen when comparing the two types of detectors. Post irradiation, this behavioural difference is vastly apparent in regards to detector sensitivity and linearity with respect to dose rate. In an assessment of radiation damage, Osvay and Tarczy [84] first compared sensitivity of p and n type detectors after pre-irradiation by a gamma source. A notable difference between the two types was found where p-type detectors resist radiation sensitivity changes better than n-type. Rikner and Grusell [80] found n-type detectors response became non-linear with respect to dose rate where p-type did not. This is attributed to recombination centres being unable to keep recombination

constant with increasing dose rate. This leads to an increase in diode sensitivity due to larger fractions of the charge being collected [80, 85]. Thus to avoid variances in linearity as a consequence of radiation damage, p-type silicon is used in diodes for radiation dosimeters.

Chapter 4

Materials

As previous chapters demonstrated, there currently exists no QA modality which enables pre-treatment, patient specific dose verification, which also incorporates real-time source tracking and timing of a HDR brachytherapy source. This chapter describes a proposed solution to this problem, the Brachy*Pix* Smart Phantom which incorporates the Magic Plate detector and an application specific phantom. A description of the two electronic data acquisition systems used for this thesis is provided; the TERA and X-Tream read out systems and additional information is then provided on the two detector systems, the Magic Plate detector and the singular epitaxial diode.

4.1 The Brachy*Pix* Smart Phantom

As a solution to the lack of patient specific HDR brachytherapy QA, the CMRP proposes the implementation of a novel technique and instrumentation so named Brachy*Pix*. The patients treatment is delivered to the Brachy*Pix* phantom prior to patient exposure. The final goal of this phantom detector combination aims to highlight any inaccuracies in the treatment prior to patient treatment delivery. This is to be done by real time analysis of dwell pattern, source positioning, dwell timing and verification of total delivered dose based on detector response.

The Brachy*Pix* phantom will contain a radiation transparent detector array (Magic Plate) [86] sandwiched between 18 HDR catheters (9 orientated above and 9 below) within solid water. This configuration is schematically shown in figure 4.1. At time of writing, the furthest progression of the Brachy*Pix* prototype is illustrated in figure 5.13.

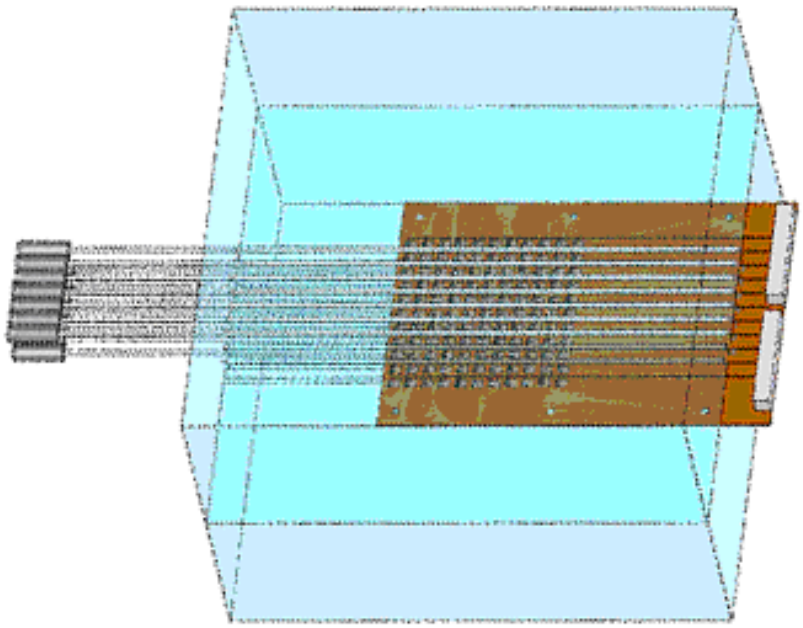

Figure 4.1 Drawing of the proposed Brachy*Pix* Smart Phantom

Using a combination of the Brachy*Pix* phantom in conjunction with the Magic Plate detector array and its corresponding data acquisition systems, this equipment aims to provide:

- Real time, high resolution, accurate pinpoint localization of source location via direct detection.
- High precision timing of source at dwell location and during transit.
- Real time dose distributions and total dose calculation, inclusive of transit dose.
- Real time analysis of error in source positioning and dwell timing in comparison to these planned parameters.

- Provide a software interface which compares planned dose map data and measured.

By characterising and testing the Magic Plate detector array and its corresponding components in its ability to track the HDR brachytherapy iridium-192 source; this thesis has provided the foundations on the initial phases of progression and development for the Brachy*Pix* Smart Phantom.

4.2 Epitaxial Diodes

Silicon epitaxial diodes are used as an alternate to conventional silicon detectors due to a variety of beneficial properties such as increased radiation hardness and smaller sensitive volumes. The difference in epitaxial detector design stems from the construction of the diode itself.

The process involves growing a high quality, thin, semiconducting p-type silicon crystal layer epitaxially (meaning layered upon) on the surface of a heavily p^{+}-doped silicon substrate that has a lattice structure identical to that of grown layer. The thick silicon substrate acts as a supporting structure and crystal seed for the epitaxial growth.

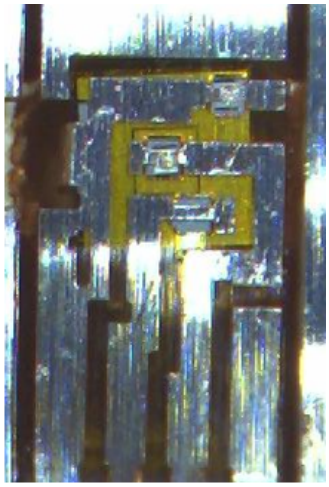

Figure 4.2 Close up of a singular epitaxial diodes sensitive volume and respective aluminium contacts on kapton substrate. Note aluminium contacts are non-symmetrical around the central axis. Assembly of these detectors by this technique is known as the CMRP patented "drop-in-technology"

Experiments undertaken using singular epitaxial diodes described in this thesis are identical to those used on the Magic Plate array. A schematic drawing of the diode is shown in figure 4.3. The diode contains 50 μm thick p-type silicon grown on top of a 375 μm thick 0.001 Ω.cm p^+ substrate. The sensitive volume of the diode is defined by the low resistance (100 Ω.cm) 0.5x0.5x0.05 mm^3 n^+ region. A 0.7 μm thick layer of SiO_2 is grown on the epitaxial layer to allow implantation of the n^+ region in addition to providing a protective layer to the epitaxial layer. To avoid the use of high Z metal contacts above the sensitive area of the detector, thin aluminium contacts are used on the margins of the 0.5x0.5 mm^2 n^+ region in an attempt to minimise energy dependence and improve angular response of the diode; the trade-off being that the diode becomes light sensitive.

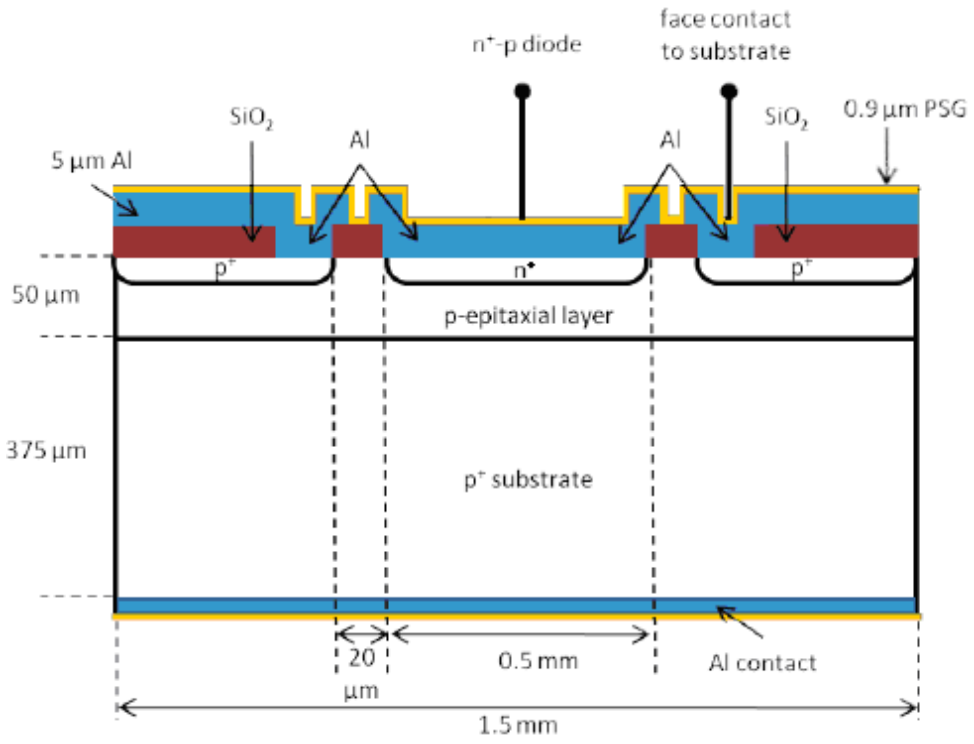

Figure 4.3 2D illustration of epitaxial silicon diode [83]

4.3 Magic Plate

The Magic Plate (MP) is a two dimensional radiation detector consisting of 121 silicon epitaxial diodes of physical size 1.5x1.5x0.425 mm^3, aligned in an 11x11 array, covering an area of 10x10 cm^2 with a pitch of 1 cm. Detectors are mounted to a 0.64 mm think Kapton backing substrate using the CMRP patented drop in technology. The entire diode array has been pre-irradiated to 41.5 kGy to obtain dose response and sensitivity stability. Initially designed for implementation in IMRT verification, the Magic Plate has been further developed for applications in HDR brachytherapy as a 2D array detector for phantom measurements [86]. The MP is equipped with a set of two SCSI-II connectors for readout of the diodes by the pre-amplification board. The readout is based on the TERA chipset. The TERA chips are digitally interfaced to a Field Programmable Gate Array (FPGA) device which controls the commands sent to the TERA, stores the data acquired by the chips and

communicates through an USB2 interface to the software interface RAD-X Dose-View, running on a standard laptop.

Since the detectors of the Magic Plate are light sensitive, the detector system needs to be packaged for protection and to prevent exposure to light. Two pieces of CIRS (Norfolk, VA) Plastic Water Diagnostic Therapy (PWDT) 5 mm solid water were machined and fitted to the Kapton substrate. These solid water cut-outs cover the top and bottom face of the MP array, protecting the diodes for use in phantom studies.

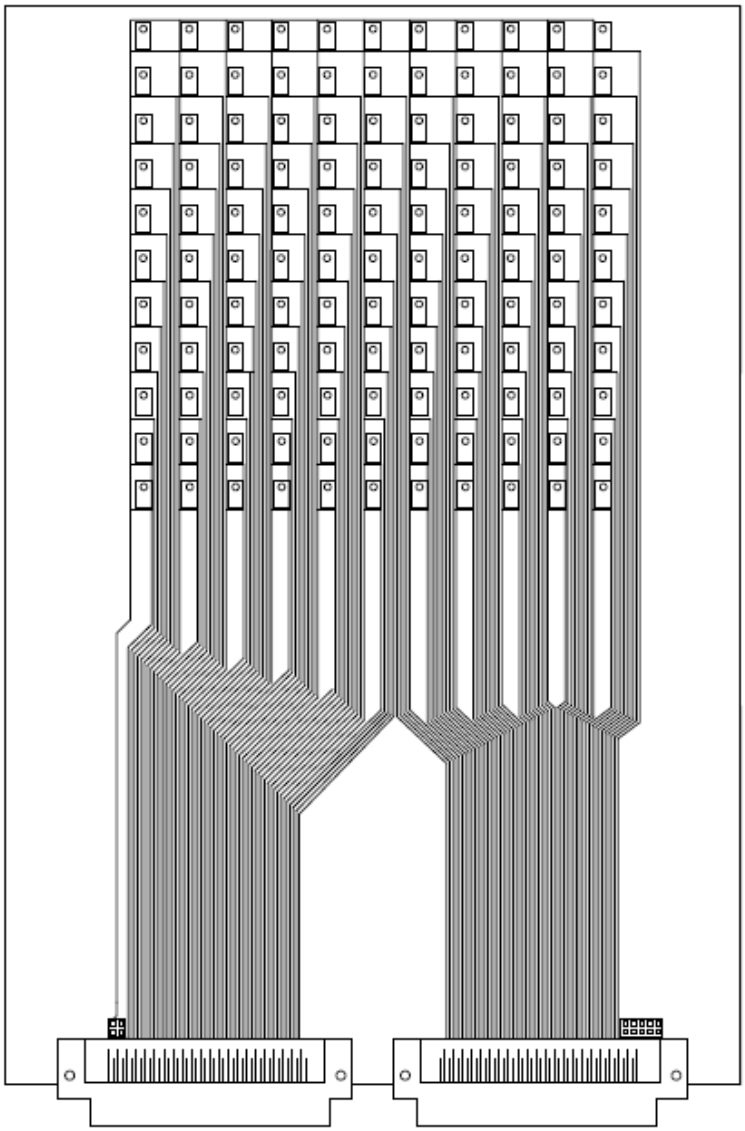

Figure 4.4 Schematic diagram of the Magic Plate 2D array detector.

4.4 TERA Front-End

The TERA chip is a Very Large Scale Integration Application Specific Integration Circuit (VLSI ASIC) designed at the University of Turin microelectronics group and by Istituto Nazionale di Fisica Nucleare (INFN). It was initially designed for use in Hadron therapy to read out ion chamber devices. The CMRP was the first world wide to investigate the use of this chip for solid state detectors. Its system allows for large scale fast integration of charge for up to 64 channels per chip. Two TERA chips are utilised in the MP system to individually read out the current signal of each 121 detectors in the array.

The fundamental basis of the TERA chip is to measure and count the charge created in the detector by the free moving electron hole pairs, generated by radiation incident. The charge is converted into a frequency by a current to frequency converter. If the circuitry counts the number of outputted pulses within a specific timing period using a digital counter, registration of radiation counts can be recorded.

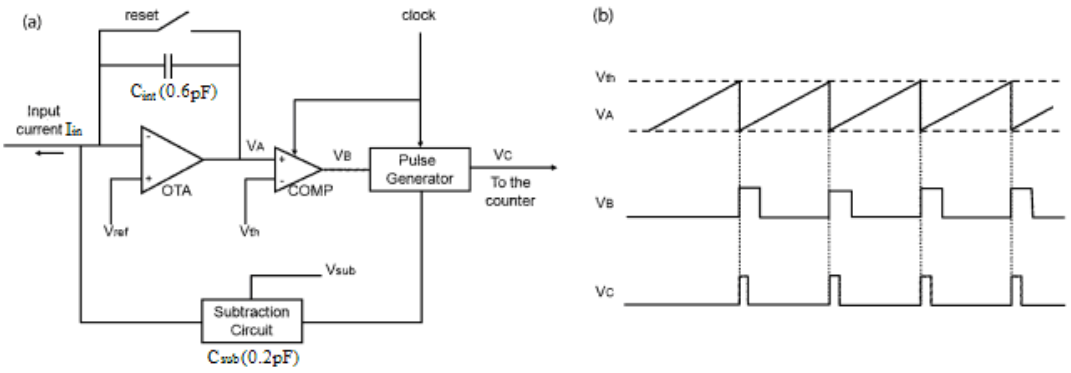

Figure 4.5 Current to frequency converter simplified circuit diagram modified from [87]

The current to frequency converter circuit is a complex process which is implemented using the charge-balancing or recycling integrator technique [88] depicted in figure 4.5 a). The input current from the diode is integrated over the 0.6 pF capacitor C_{int} by the operational transconductance amplifier (OTA). The OTA output voltage ramps

up linearly increasing over time, thus continually increasing the charge stored by the capacitor. The output voltage is fed into the comparator (COMP) which continually compares the output voltage to the set threshold voltage V_{th}. Once the output voltage reaches threshold, the comparator outputs a voltage V_B which sends a calibrated current pulse to the circuit via the pulse generator. This triggers the pulse generator to output two pulses, the first voltage pulse V_C is sent to the digital counter where the event is registered and information is stored as an event. The second pulse from the pulse generator passes through a subtraction circuit which subtracts a fixed amounts of charge (charge quantum Q_C) from the main capacitor C_{int}, thus effectively discharging the capacitor. The decrease in voltage across the capacitor results in a sharp decrease in V_A equivalent to the charge delivered by the subtraction circuit. This cycle is continually repeated unless the input current (I_{in}) is zero [87]. This process results in outputting a voltage representing a sawtooth function as demonstrated in figure 4.5 b).

The slope of the ramp is proportional to the input current; thus a high input current will reach the threshold voltage faster, resulting in a higher frequency of the output pulses. Therefore the input current is related to the output frequency (f) by the following

$$f = \frac{I_{in}}{Q_C} \tag{4.1}$$

The current to frequency converter maximum output frequency is dependent upon the charge quantum, which can be externally varied by altering applied reference voltage and capacitance components of the subtraction circuit. The minimum limit of the charge quantum is set by the resolution of the comparator, which is 0.1 pC [87]. The maximum input current is limited by the pulse generator state machine which has a maximum sample rate of 0.2 μs or 5 MHz [87]. From equation 4.1 this sets the maximum input current ($\mathrm{I_{in}}$) at 5 μA. In the case where input current exceeds this value, the pulse generator continually sends a pulse to the subtraction circuit until the

overload voltage is removed and $V_A < Vth$

The TERA ASIC chip has 64 independent channels, each equipped with a current to frequency converter. Individually coupled to a diode detector, each channel is then connected to an independent digital counter, followed by a 16-bit register to store the counts and respective timing interval data. Designed and developed at the CMRP, this system is read out using a custom C++ user interface named Rad-X DoseView.

4.5 X-tream Data Acquisition System

Originally developed specifically for Microbeam Radiation Therapy dosimetry, the CMRP developed, X-tream system has found many applications in other radiation therapy modalities where high speed, high precision measurements are required. The system combines the use of a single silicon diode coupled to a fast data acquisition electronic interface to accurately acquire a quick, real time readout of dosimetric information. The system demonstrates micrometer spatial resolution at MHz acquisition frequency (microsecond timing resolution) with accurate sensitivity and linearity for over five orders of magnitude of input signal [89].

The X-tream system contains four main constituents; the silicon diode detector, the pre-amplifier, the Central data acquisition System Unit (CSU) and the PC software RadPlot. The X-tream system configuration is shown in figure 4.6.

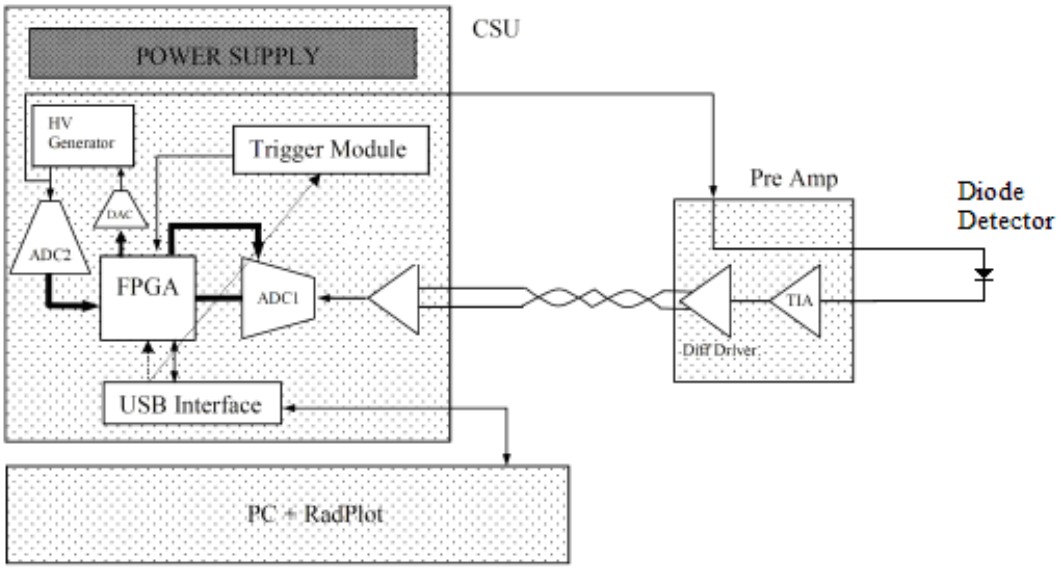

Figure 4.6 X-Tream dosimetry unit showing configuration for a diode detector

Section 3.6.3 explains the operation of diodes as a radiation detector. The preamplifier module (Pre-Amp) amplifies the input radiation induced photocurrent from the diode detector with a gain of 10^5. The sensitivity remains linear over the entire dynamic range of amplification.

The Central data acquisition System Unit (CSU) controls the generated signal from the pre-amp, converts the signal to a digital output, provides and controls the high voltage bias of the detector, regulates all electrical components and provides a communication interface to software via implementation of a standard USB 2.0 link. The driving process behind the CSU is the Field Programmable Gate Array (FPGA). The FPGA samples the inputted data and writes it to a First In, First Out (FIFO) memory buffer. It then sends the sorted information to the PC software RadPlot via USB 2.0 link cable.

RadPlot is a custom graphical interface software developed in C++ by the CMRP. The software sends the firmware to the FPGA by the USB link to acknowledge the device is operational. The software is designed to fully remotely control the system

parameters, in addition to analysing and displaying the data in real time.

Chapter 5

Magic Plate Characterisation

5.1 Angular Dependence

Most silicon diodes display a degree of angular dependence [72,90]. This directional response is caused by geometrical factors synonymous with detector construction. Since detector construction is non-symmetric, a variance in substrate thickness is encountered by radiation incident from dissimilar angles. There are many documented accounts in the literature which attempt to measure the angular dependence of diodes [72, 90–94]. As great as a 25% change in sensitivity, due to variance in the radiation angle of incidence, has been recorded for commercially available diodes.

As for the epitaxial diodes used in the MP array, many factors contribute to the detectors measured non-symmetric behaviour. Factors include experimental misalignment of detectors sensitive volume from the centroid axis, asymmetric diode construction due to thick silicon substrate, non symmetric aluminium mounted contacts (see figure 4.2), intrinsic asymmetry of the silicon substrate and the interface phenomena. This phenomena involves variation of the electron slowing down spectra and multiple scattering effects occurring within the detectors components of varying atomic numbers and between the interface of different materials and detectors surrounding medium. The physical process of stepping the source over the MP 2D array, gives rise to events being recorded with relative source to detector angle varying in both

the polar and azimuth direction. Figure 5.1 illustrates the difference between polar and azimuth angles.

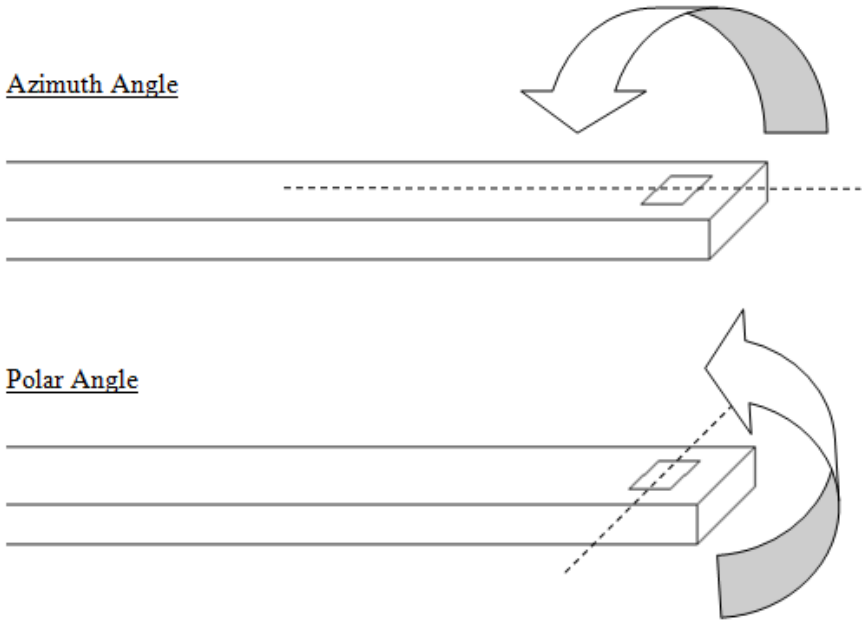

Figure 5.1 Definition of polar and azimuth direction

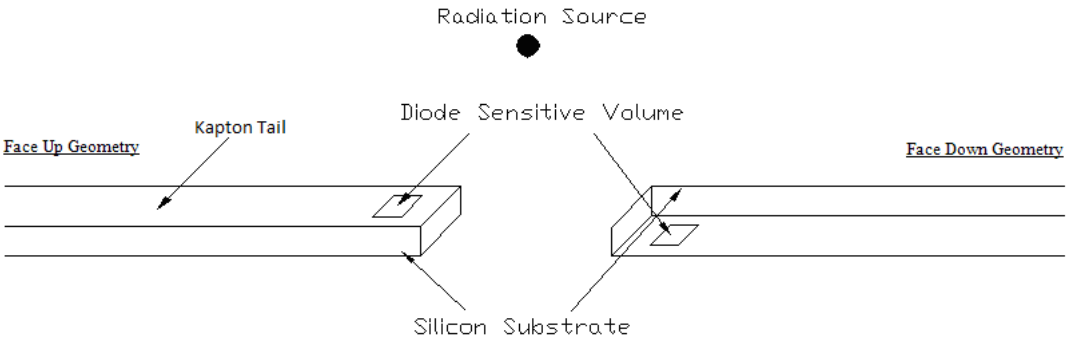

Figure 5.2 Definiton of face up and face down geometry

The design of the Brachy*Pix* pre-treatment quality assurance phantom permits charge to be collected from both face-up and face-down geometries of the detector (see figure 5.2 for clarification). When using this system, not only will detectors located in the immediate vicinity of the source aquire counts, detectors at increasing radial

distance from the source will also receive dose. The angle at which these peripheral detectors measure dose is dependent upon the relative distance from the source position to the detector. This mathematical occurrence is demonstrated in figure 5.3 where the angular incidence of the radiation to the detector increases with increasing radial distance to the source, as indicated by $\theta > \phi$.

Since the detectors are to be used for dosimetry reading and their response is used in the calculation of source positioning, it is critical to measure the angular response of these detectors and determine if correction factors need to be applied based on relative source-detector position.

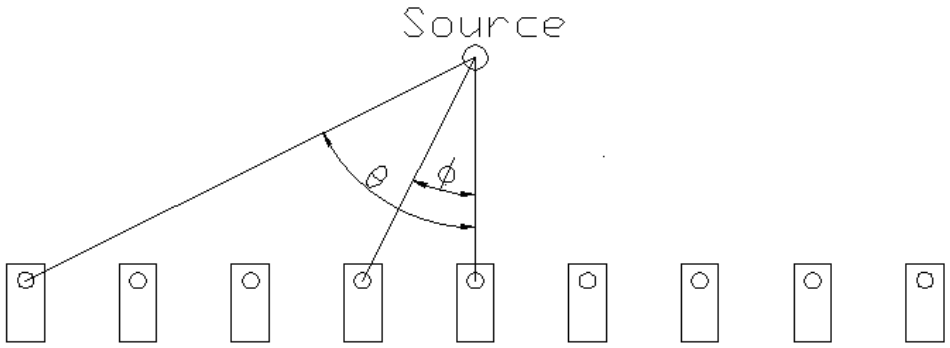

Figure 5.3 Effect of increasing detection angle with increasing radial distance for a fixed source height

5.1.1 Azimuth Direction Angular Dependence

The angular dependence about the transverse axis of the detector was investigated using a single diode identical to those used in the Magic Plate array. The detector was placed centrally inside a rotatable cylindrical phantom in which resided a grove of specific dimensions to the kapton tail geometry. The groove ensured the detector sat flat within the phantom effectively minimising the presence of air gaps between the detector and the cylindrical phantom. The cylindrical phantom itself enabled 360 degrees of rotation within the solid water. See figure 5.4 for clarification.

A HDR prostate brachytherapy catheter was inserted centrally into a 10 mm thick

water phantom and positioned below the cylindrical phantom. The experimental set up was designed so that aligning the two phantoms placed the detectors sensitive volume directly under the catheters last dwell position. In this orientation, the effective distance between the detector and source was 20 mm. A schematic drawing of the experimental set-up is shown in figure 5.4 and figure 5.5 illustrates the physical set-up. The entire apparatus was encapsulated in solid water to form a $30 \times 30 \times 30\,\mathrm{cm}^3$ cube to ensure full scatter conditions during measurement.

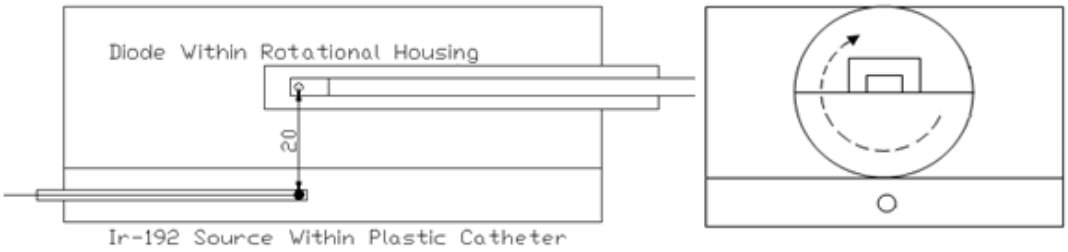

Figure 5.4 Schematic of experimental set up for azimuth angular dependence test. For clarification diode and corresponding kapton tail are shown at 90 degrees relative to the source in first image. Second image shows sensitive volume orientated at 0 degrees relative to the source.

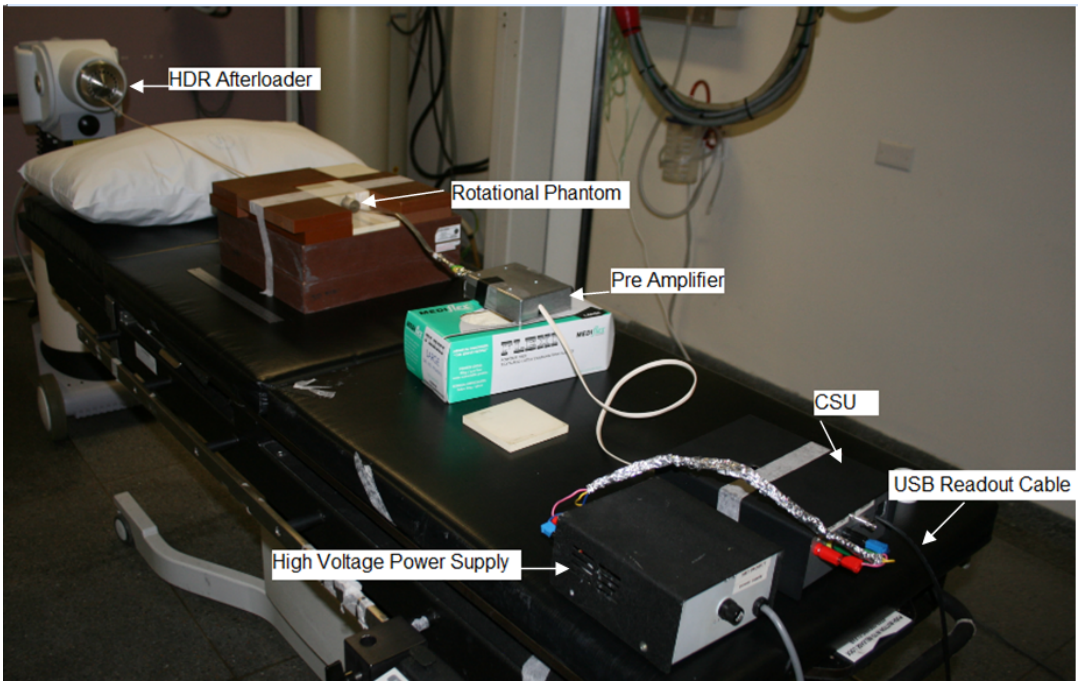

Figure 5.5 Azimuth angular dependence set up showing the detector in the rotational phantom and the data acquisition system.

0° was taken as when the orientation of the detectors sensitive volume was perpendicular, face-up relative to the source. Using a 221.8 GBq Ir-192 source, the Nucletron microSelectron HDR brachytherapy afterloader was programmed to deliver the source to the final dwell position at the end of the catheter for 45 seconds. Counts were recorded at a 1 MHz frequency and averaged over 10 intervals. This corresponds to a 10 μs subset for data acquisition timing period. Therefore, over the 45 seconds timing interval, this equates to 4.5×10^6 samples taken per detector angle. Uncertainty of the detector response was then based on 2 standard deviations of this data (see figure 5.8). The cylindrical phantom was rotated in an anti-clockwise direction in $30^\circ\pm2^\circ$ increments for a full 360° rotation, with measurements taken at every increment.

5.1.2 Polar Direction Angular Dependence

A 225 mm long, 2 mm wide, 50 mm radius semi-circular indentation was cut into a $30 \times 30 \times 1\ \mathrm{cm}^3$ of Perspex. The design of the Perspex phantom enables the catheter to be situated at a constant distance of 50 mm from a central channel and to accommodate a singular diode detector. For a HDR source, the dose gradient at this distance is reduced, thereby reducing errors due to the uncertainties in the placement of the sensitive volume. As depicted in figure 5.7, this configuration enables delivery of the radiation source around the polar axis of the single diode detector. Advertently, this facilitates detector response about about its polar axis.

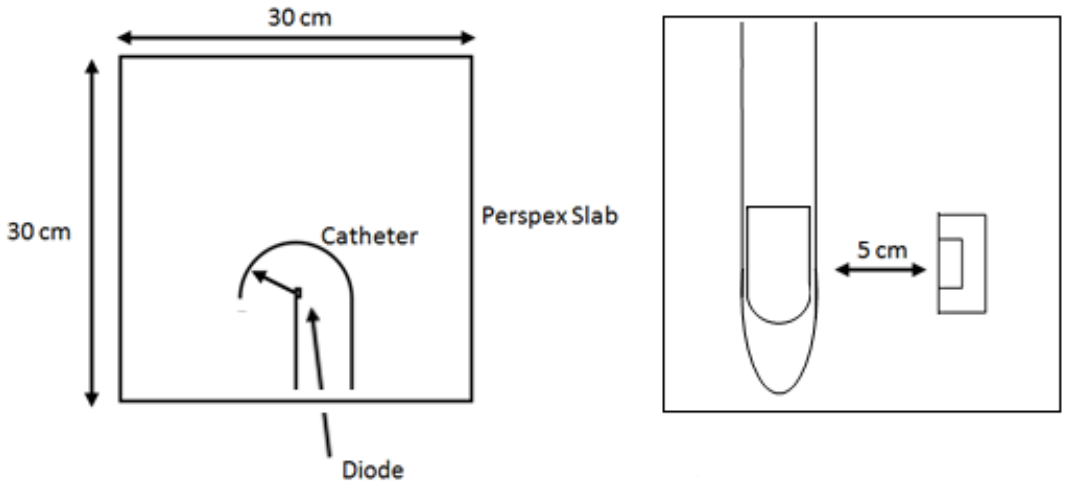

Figure 5.6 Schematic of experimental set up for polar angular dependence test. The image on the right details the source at the final dwell position of the catheter relative to the detector sensitive volume. This orientation is classified as 0 degrees

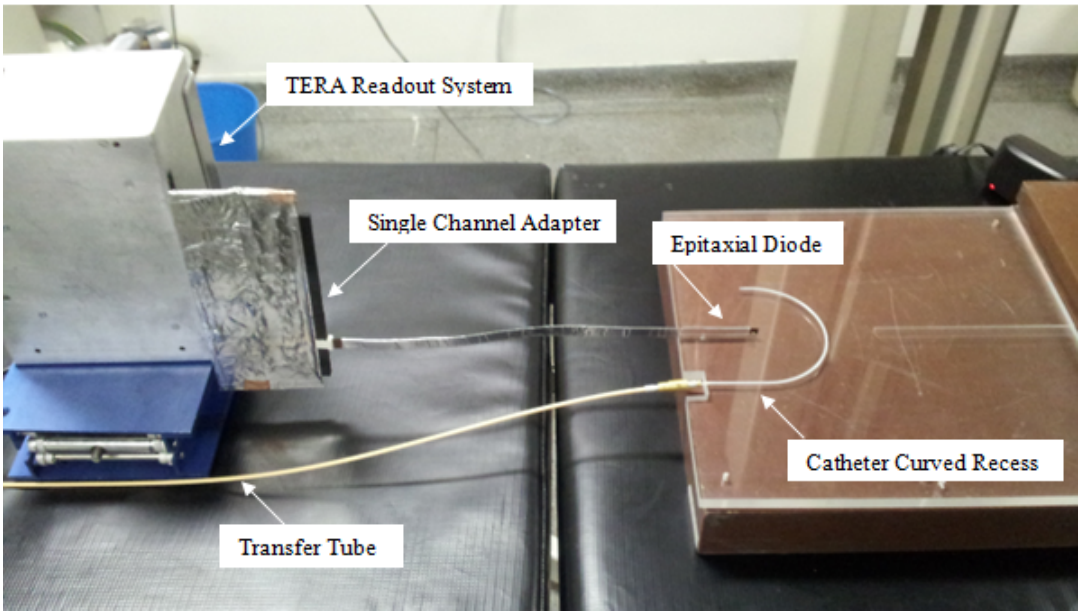

Figure 5.7 Experimental set up of diodes polar directional dependence. The catheter curved recess permits the source to be delivered in a 50 mm arc around a singular epitaxial diode.

The Perspex phantom was so designed that at the final dwell position, the source is aligned orthogonal with the sensitive volume of the detector. When the source is at the final dwell position and detector is orientated with face up geometry, the detector is deemed to be 0 degrees. This is consistent with the azimuth coordinate system. By delivering the source to various locations within the catheter, the relative angle between the source and detector can be controlled, all whilst source to detector distance remains constant. Positional accuracy of the source is routinely documented in the hospitals QA program. As recommended in the literature [36, 37, 63], Prince of Wales Hospital utilizes radiochromic film as an independent modality to assess the HDR afterloaders ability to deliver the source to a predetermined location. The results from the departments routine QA was assessed prior to conducting such measurements to assure that the source position and therefore the polar angle between the source and detector was in accordance to the one planned.

The Nucletron microSelectron HDR brachytherapy afterloader was used to accurately deliver a 214.9 GBq Ir-192 source to specific predetermined incremented lo-

cations within the catheter. Each source delivery location corresponds to 15.0±1.5 degree intervals around the polar axis of the detector, over a range of 180 degrees.

5.1.3 Results: Azimuth Angular Dependence

The angular dependence (A) of the diode is defined as the ratio of the diodes response at an angle (R_θ) over the diodes response when the source was perpendicular to the detector (R_0) in the face up orientation, as described by equation 5.1.

$$A = \frac{R_\theta}{R_0} \tag{5.1}$$

The angular response dependency of the singular diode for a full 360 degree rotation was studied. The directional dependence results are shown in figure 5.8 with the response normalised to 0 degrees. The diode showed noteworthy angular dependence as a considerable decrease in the diodes response was measured as the angle approached 180 degrees. The maximum change in response is seen in between angles 90 and 120 degrees. Stability is again established around the 180 degree mark with fluctuations of only 3.3% over the 120-270 degrees range. Overall, the maximum deviation in percentage of the response was seen at 240 degrees (81.3±2.3% relative to zero degrees). This data set show a variation of 16.6% between the top face (0 degree) and bottom face (180 degree) of the epitaxial detector. Despite this fact, the diode showed stability in the region of interest centred around the face up and face down orientations. This region of interest is $\pm 45^\circ$ around the 0 and 180 degree positions. This will be the maximum angle subtended between the 1 cm equally spaced detectors on the magic plate array and a source situated at a 1 cm depth as per the Brachy*Pix* phantom.

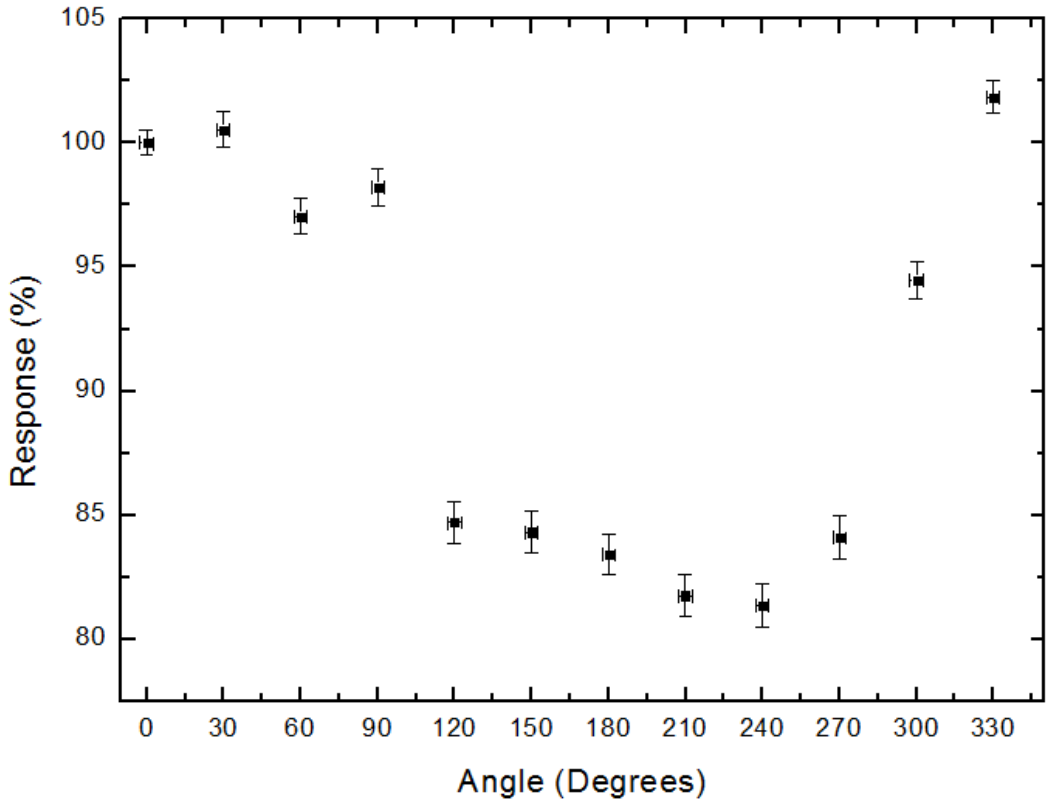

Figure 5.8 Angular response over a 360 degree range for the azimuth direction of the detector. Results are normalised to 100% at 0 degrees, when the detector is in its face up orientation relative to the source.

Due to its design, this type of detector is expected to suffer from angular response dependency. As seen in the literature [72, 90] the behaviour for diodes is characterized by a tendency to under respond as the beam incidence angle increases. These results illustrate accordance with these studies where by the response of the diode is not severely reduced until the angle exceeds 60 degrees. The observed angular dependence arises from a various combination of effects associated with the detector including; varying photon path length through the 375μm p^+ substrate layer, anisotropies inherent in the silicon chip and non-symmetric packaging of Aluminium readout contacts. These factors contribute to variable, direction specific attenuation of photons.

For this result, the apparent non-symmetric angular response of the detector about

180 degrees is primarily attributed a combination of lateral displacement of the detectors sensitive volume in the xy plane and the rotation around the face of the sensitive volume rather than its centre. Placing the detector at a greater distance than 2 cm from the source may reduce the effect of off axis misalignment by reducing the effect of the dose gradient (see figure 5.14). The effects of the lateral displacement of the sensitive volume is illustrated below in figure 5.9.

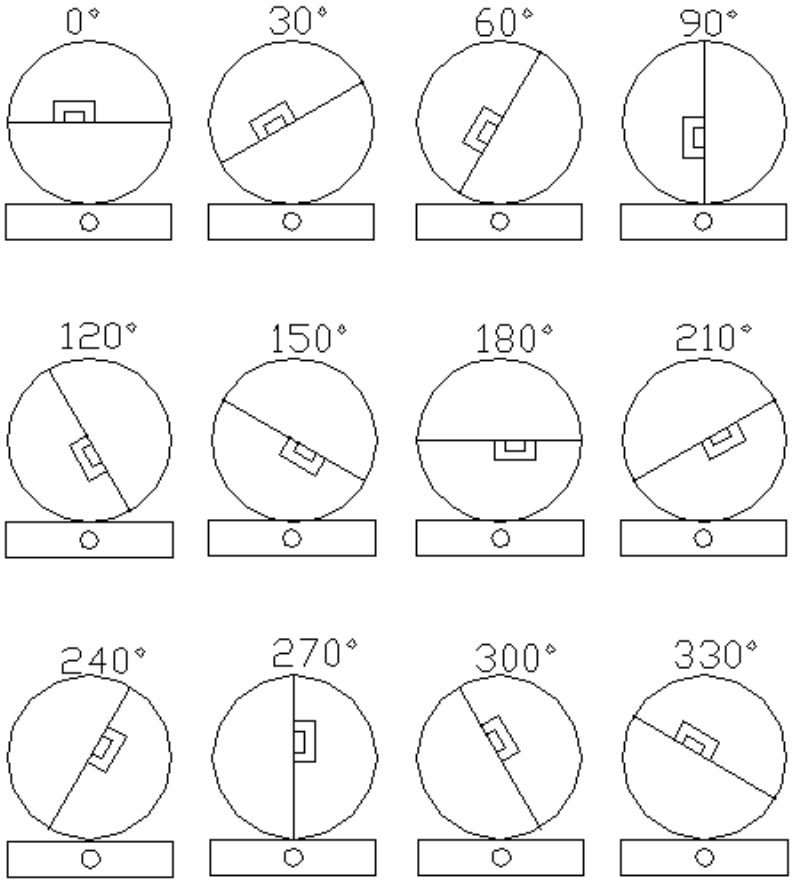

Figure 5.9 Positioning of the diode above the source with varying angle. This demonstrates the effect of the sensitive volume positional error due to detector misalignment in the x-y plane. Note size of sensitive volume and its displacement have been exaggerated for illustration purposes.

For this experimental set up, a slight lateral shift of the sensitive volume from the central axis will have diverse effects on the angular response of the diode due to the variance of depth with the changing angle. For the diode tested, the lateral shift of

the sensitive volume from the central position was estimated at (1.0±0.5 mm). This displacement was apparent due to poorly milled grove within the housing and was unavoidable using this phantom geometry. Since dose gradients in HDR brachytherapy are so high, this small change in position can lead to a large change in detector response. This effect is clearly evident when comparing relatively equivalent angles. As figure 4.3 shows, symmetry exists about the central axis of the epitaxial diode. Therefore, this should translate to symmetric angular dependence for corresponding angles. For example 90 and 270 degrees. However, as results in figure 5.8 indicate, these values do not correspond. Figure 5.9 graphically explains the effect rotating the detector has on detector to source distances where there is a lateral shift of detector placement. As shown in this illustration, the displacement leads to the sensitive volume existing at a minimum distance relative to the source when the detector is rotated to 90 degrees and a maximum distance at 270 degrees.

This variance in depth has maximum ramifications at the 90 and 270 degree positions. At these angles, more significantly than any other, the variance in depth has altered the true angular dependence at these relative detector locations. Despite being at the maximum depth discrepancy; figure 5.8 tells us these values do not correspond to maximum and minimum response of the diode. This is attributed to the thick silicon substrate on the bottom side of the sensitive volume. At 30 degrees, the sensitive volume is placed at the closest distance to the source (due to the lateral displacement effect) with no attenuation from the silicon substrate. This corresponded to the position of maximum measured counts. On the contrary, 240 degrees was determined to have the lowest response since geometrically at this position there is the maximum amount of silicon substrate to attenuate the photons, in conjunction with the greater distance away from the source.

Although extremely difficult to execute, clearly the angular response of the diode used for these experiments could be vastly improved by ensuring the alignment of the detector around the centroid position of the kapton housing. Although difficult to employ, reduction of the silicon substrate thickness and symmetrical contacts would

also decrease the detectors angular dependence. Westermark *et al.* [72] successfully reduced diodes angular dependency by adhering together two identical silicon diodes, with sensitive volumes facing each other. This double diode construction reduced directional dependence whilst improving sensitivity without compromising resolution. However, this was accompanied by undesired effects of an increase on energy dependence and two times the over response to scattered radiation.

5.1.4 Results: Polar Angular Dependence

As with the azimuth response, the polar angular dependence is defined as the response of the diode at an angle relative to the response of the diode when in the face up orientation; as inferred by equation 5.1.

The angular response around the polar axis of the singular diode over a 180 degree range was investigated. The response is normalised to 100% at 0 degrees and the uncertainty calculated based on 2 standard deviations of the data at each dwell location. Due to the configuration of the catheter inside the custom made Perspex phantom, the angle could only be varied from 0 to 180 degrees. Figure 5.10 shows a plot of the polar response of the diode overlayed with the results from the azimuth direction over the 180 degree range. As expected, the diode shows a steadily decreasing response with increasing angle. The maximum variation in response between 0 and 180 degrees is 14.0% reaching the minimum response of 85.97%. This is similar to the 16.6% dependence seen in the proximity of the azimuth direction. Since the Perspex phantom limits delivery angles between 0 and 180 degrees, complete 360 degree comparison cannot be evaluated between the two angular directions with this experimental configuration.

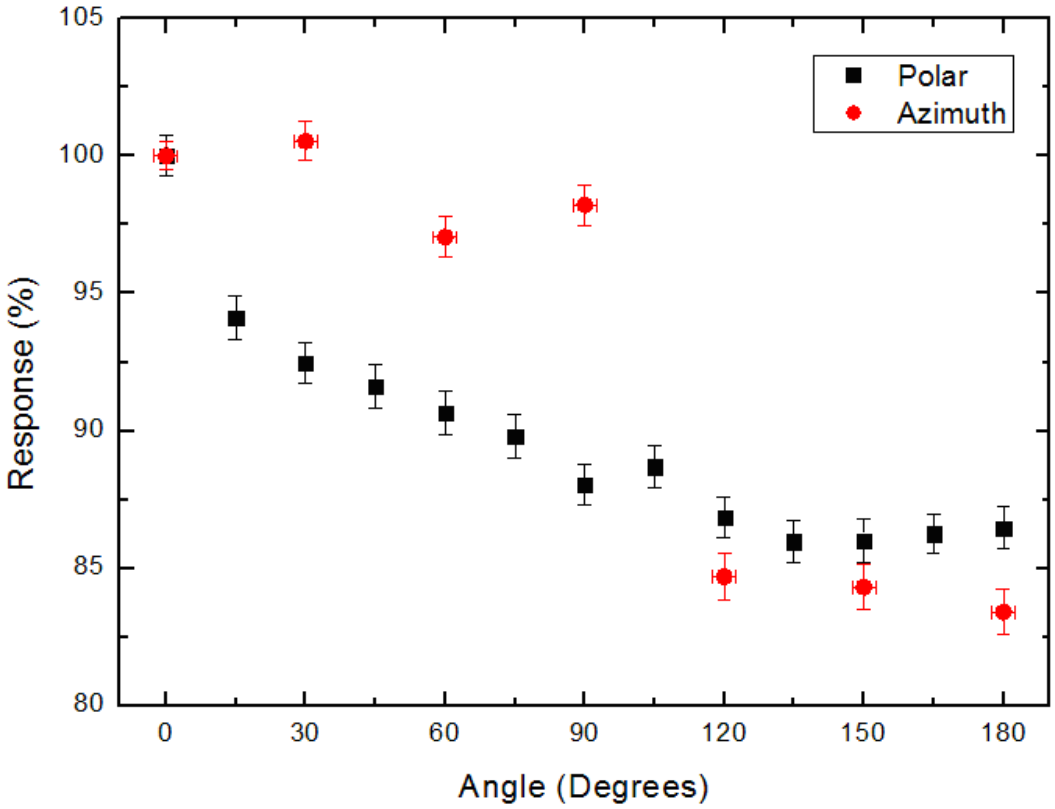

Figure 5.10 Angular response over a 180 degree range for both the polar and azimuth direction of the detector. Results are normalised to 100% at 0 degrees, when the detector is in its face up orientation.

Polar and azimuth plots show correlation with a uniform response within $\pm 7\%$ of variation for angles in the range of $0° \pm 60°$ and $180° \pm 60°$. The maximum deviation between the two data sets occurs at 90 degrees. However, as previously mentioned the data point in the azimuth plot may be presented as an outlier due to uncertainty in positioning associated with the diodes sensitive volume. As mentioned in section 5.1.3, a lateral offset of the sensitive volume of the detector influenced the response in the detector about the azimuth axis. However, this offset is in a plane orthogonal to the polar axis. Consequently, for this experimental orientation, the offset will remain at a constant distance relative to the source. As a result, the response of the detector will not be influenced by any lateral offset for these experimental conditions.

5.2 Depth Dose

The dose distributions surrounding a HDR brachytherapy source often presents complications for dose characterization. The nature of HDR brachytherapy is to implement high dosages directly to the immediate vicinity of the cancerous tissue. Dosages are most significant within a few millimetres of the source and rapidly deteriorate with increasing radial distance. This is characteristic of an Ir-192 source, and is thus why it is most commonly used isotope for these procedures. Since such large dose gradients exist, dosimeters for HDR brachytherapy need to exhibit high sensitivity to such rapid dose gradients. Additionally, this sensitivity must be able to cope with a dynamic range over which the dose can be measured. This is due to the fact there are several orders of magnitude change in dose rate observed with increasing radial distance from the millimetre to centimetre range from the source.

Silicon epitaxial diodes demonstrate such properties and thus are suitable dosimeters for depth dose measurements. However, as explained in sections 2.3.2.2 and 3.6.1 silicon exhibits an amplified response to low energy photons ($<$150 keV). Although this low energy radiation is generally absorbed within short distances of the source, this over response further complicates dose measurements at distances close to the source. At increasing depths, Compton scattering causes an increase in the number of low energy photons relative to the number of high energy photons [77]. In other words the spectrum softens with increasing radial distance from the source.

Percentage depth dose tests measure the reduction in dose as a function of increasing radial distance from the radiation source. Measurement of the diodes response to the Ir-192 energy spectrum at different depths in solid water is critical to assess its validity as a dosimetry device for use in HDR brachytherapy. However, due to the high dose gradients associate with the therapy, accurate dose measurements in regions of close proximity to the source are often difficult to achieve. A slight variation in position in the immediate vicinity of the sourceclose to the source, will lead to a large variation in dose, so the slightest misalignment in detector position can invalidate

results.

The literature shows multiple dose distribution measurements which utilise a vast assortment of dosimeters. Ionization chambers of various types were used by Tolli *et al.* [95], Bahar-Gogani *et al.* [96] and Gromoll *et al.* [97], radiochromic film by Skwarchuk *et al.* [98], Lithium Fluoride Thermoluminescent detectors by Valicenti *et al.* [99], Alanine-Electron Paramagnetic Resonance by Guzman Calcina *et al.* [100], monomer/polymer gels by De Deene *et al.* [101], diamond detectors by Nakano *et al.* [10], MOSFET detectors by Zilio *et al.* [102] and silicon diodes by Williamson *et al.* [103].

In recent publications, measurements using polymer gels have been made within close proximity to HDR sources [101, 104]. In such studies, radial distances are only limited by catheter thickness ($\approx$1 mm) and capsule thicknesses. These cases also report complications when measurements are made in the steep dose gradients close to an HDR source. Monte Carlo calculations thus provide the best means for accurate data on dose distributions at close distances to a HDR source [105, 106].

5.2.1 Single Diode Percentage Depth Dose Experimental Orientation

To evaluate the MP's depth dose response to the HDR radiation, a single epitaxial diode was placed within a small channel housed in a Perspex phantom. This phantom was so designed that when correctly inserted, the detectors sensitive volume sat flush with the surface of the phantom (figure 5.11)

Depth dose analysis was then achieved by placing solid water of varying thickness (ranging from 5-50 mm) between the detector and source. With the exception of the polymer gels, dosimetry at distances less than 5 mm from a HDR source are rarely reported within the literature. Recognising the difficulties accompanied with dosimetry at small distances in a steep dose gradient, the minimum depth measurements were taken at was 5 mm.

A HDR prostate brachytherapy needle was positioned directly above the detector. Precision measurements were undertaken using a dummy seed to align the final dwell position of the catheter directly over the sensitive volume of the detector. The orientation of the diode was positioned face up relative to the radiation source. The entire apparatus was encapsulated in solid water to form a $30 \times 30 \times 30\,\mathrm{cm}^3$ cube to ensure full scatter conditions. Measurements were taken orthogonally to the seed.

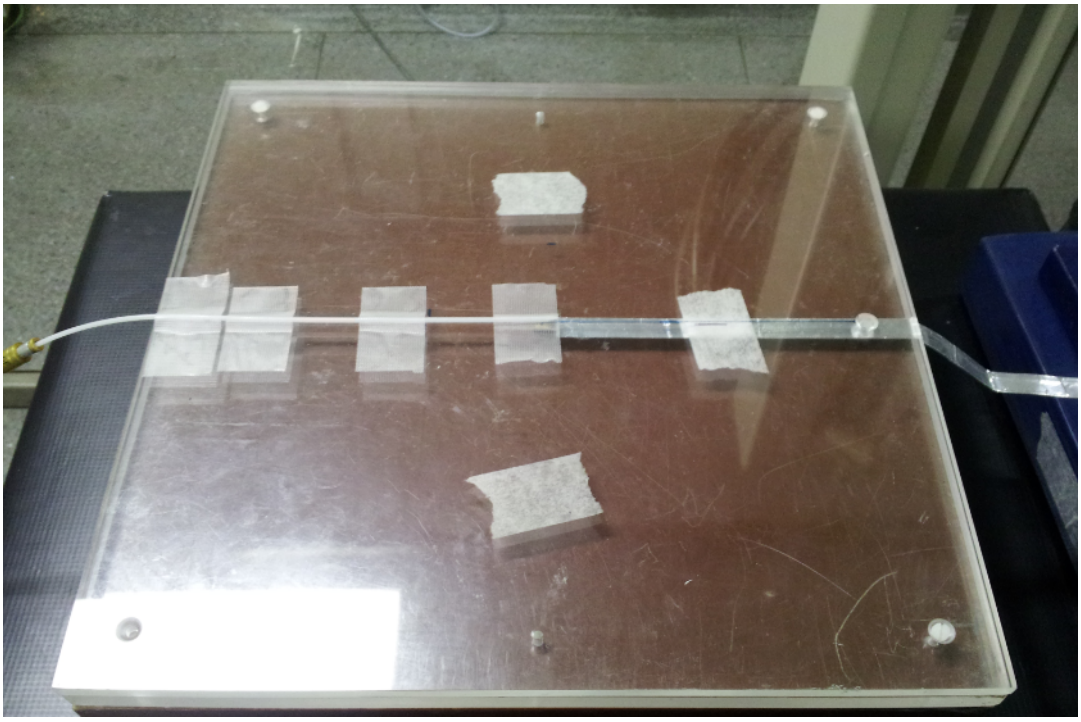

Figure 5.11 Singular epitaxial diode percentage depth dose experimental set up

Using a 208.9 GBq Ir-192 source, the Nucletron microSelectron HDR brachytherapy afterloader was programmed to deliver the source to the final dwell position with a 40 second dwell time. Using the X-tream DAQ system, counts were recorded at a 1 MHz frequency and averaged over 10 intervals, corresponding to $10\,\mu\mathrm{s}$ data acquisition timing period.

5.2.2 PLATO Treatment Planning System Simulated Percentage Depth Dose

The exact same experimental configuration was simulated using the Nucletron PLATO v14.3.7 Brachytherapy Treatment Planning System at Prince Of Wales Hospital, Sydney. In this test, the Ir-192 source was simulated at the final dwell position within a single protate catheter. Reference points were simulated at millimetre increments ($\mathrm{d_n}$) orthogonal to the source, with the first reference point $\mathrm{d_1}$ placed at 5 mm from the source(see figure 5.12.) Assigning 100% dose to $\mathrm{d_1}$, the relative dosages at $\mathrm{d_n}$ were calculated. Extrapolating a line between points provides a basis for experimental comparison to TPS percentage depth dose data.

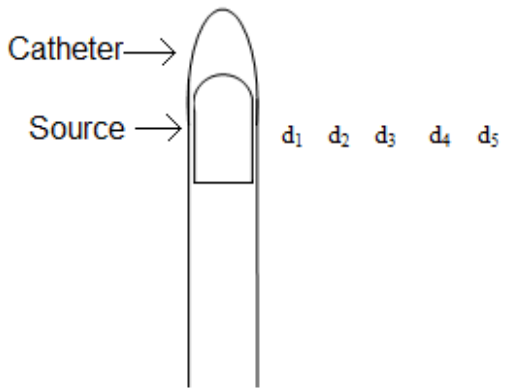

Figure 5.12 Schematic diagram of TPS simulated experimental set up

5.2.3 Magic Plate Depth Dose Experimental Orientation

Although percentage depth dose experiments were already carried out using a singular epitaxial diode, (identical to those used in the magic plate array) undertaking an identical experiment with the Magic Plate will determine if the response of the Magic Plate array is altered due to scattering from the assortment of components associated with the system, particularly the assortment of copper wiring coupled to the electrical read out system of the Magic Plate.

With a similar experimental set up to that of the singular epi-diode, depth dose measurements were performed with the placement of the catheter over the arrays centroid detector. Using the face up orientation, various thicknesses of solid water were placed between the detector and source to provide varying depth (see figure 5.13.) The entire apparatus was encapsulated in solid water forming a $30 \times 30 \times 30\,\mathrm{cm}^3$ cube to ensure full scatter conditions. A Nucletron microSelectron HDR brachytherapy afterloader was used to deliver the 208.9 GBq Ir-192 source to the dwell position aligned over the arrays central detector. Using the TERA readout system, counts were recorded at 100 ms intervals for the duration of the 40 second source exposure time.

A near identical experimental configuration was then performed. By altering only the orientation of the detector system, the face down response of the MP was determined, that is in contrast to the previously used face up orientation. Using this configuration, the entire system is rotated up-side down relative to the source. For this investigation, it was not feasible to create an experimental set-up where the source is positioned at different depths in solid water relative to the detector. For this reason the source remained stationary and the depth of which the detector array was placed relative to the source was varied (reverse geometry). See figure 5.13 for clarification of the MP orientation.

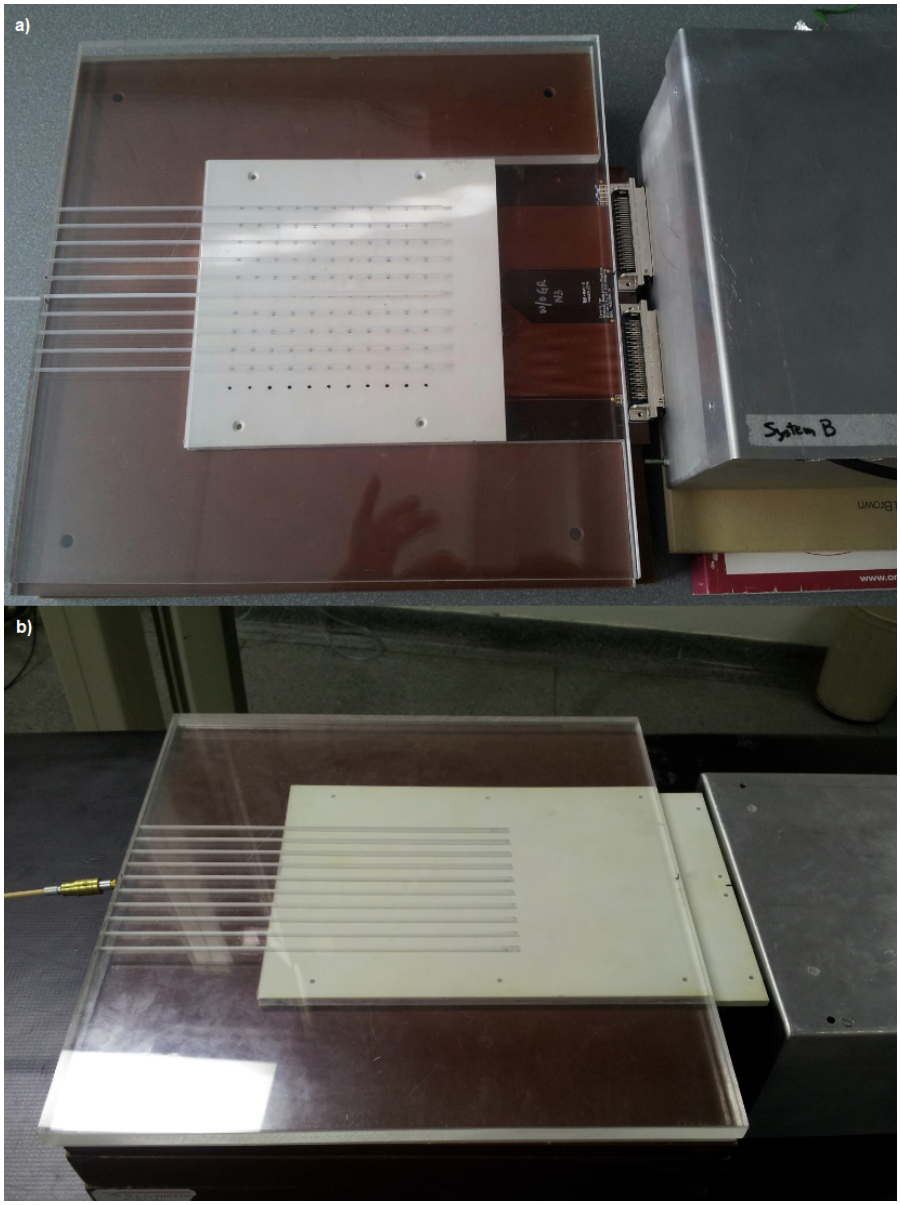

Figure 5.13 Magic plate depth dose experimental set-up a) face up orientation b) face down geometry

5.2.4 Percentage Depth Dose Results

Figure 5.14 shows the depth dose curve obtained with the MP and singular epitaxial diode and compared to Nucletron PLATO TPS data. Correction factors have been applied to the data to account for decay of the isotope and results normalised to the first Magic Plate data point at 6 mm. Results show very good correlation between the

experimental data and the simulated TPS data.

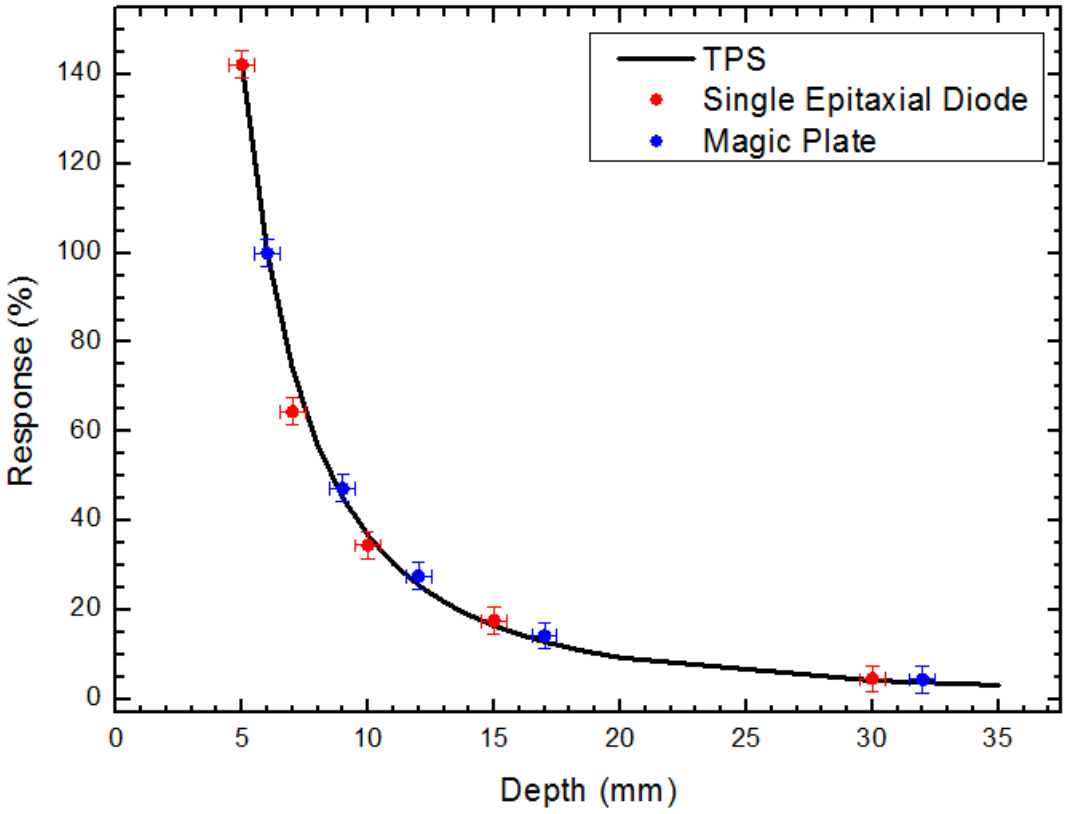

Figure 5.14 Depth dose curve for Ir-192 source. Response measured with singular epitaxial diode and Magic Plate and compared to Nucletron PLATO TPS data.

The MP appears to be slightly over responding compared to the TPS measurements for all depths beyond 6 mm, with the maximum over response of 1.41% at 17 mm depth. This slight variation is attributed to a error in positional accuracy of source delivery and to a lesser extent the over response of silicon to low energy photons (see section 3.6.1.)

The singular epitaxial diode was seen to both over and under respond at varying depths relative to the predicted response of the TPS. Still correlating within uncertainity, a maximim deviation of 9.52% at 7 mm depth. Since the dose gradients associated with Ir-192 sources are so great, a slight variation in position can lead to large deviations in dose. A slight misalignment between the detector and the source

at 7 mm is attributed to the large deviation from the TPS data seen at this close range. The effect of misalignment decreases at increasing depth due to decrease in steepness of the dose gradient. This is apparent in the data as greater depths better correlation between TPS and measured data is observed.

As expected figure 5.15 shows harmonious correlation of percentage depth dose between face up and face down geometries. This result proves the rear face of the MP accurately responses to iridium's radiation spectra in accordance to the detectors front face. As previously demonstrated by the singular epitaxial angular dependence tests (figure 5.10) the rear face of the single diode exhibited 85.97% response compared to the front face of the diode. Using the data from figure 5.15, table 5.1 indicates the ratio of face down response to face up response for the Magic Plate detector array. Results show vastly in accordance, at most depths, to the previously determined 85.97% face down angular dependence of the diode. Since the rear side response using the MP reflects so similarly to that of the single diode, we can conclude the components of the MP array do not influence or add any additional angular dependence. Error margin are calculated based on two standard deviations of the raw data.

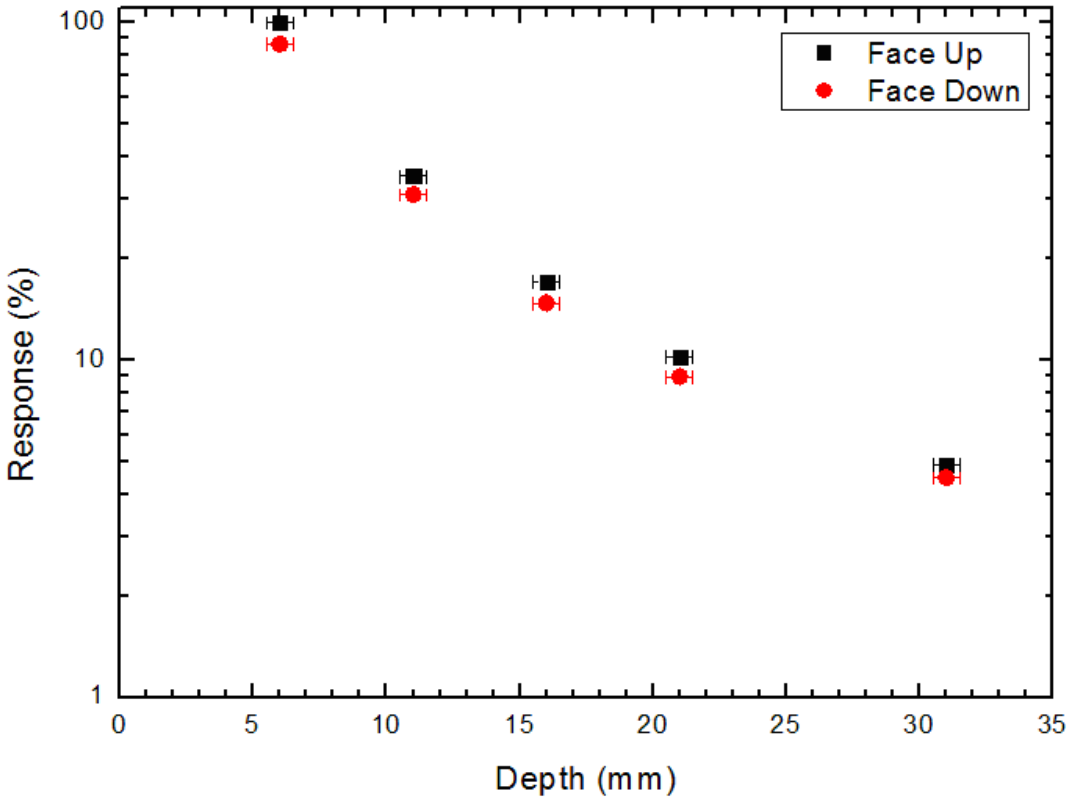

Figure 5.15 Depth dose curve face up and face down orientation of the Magic Plate

	Response (%)		
Depth (mm)	Face Up	Face Down	Face Down/Up ratio (%)
11	35.04	30.91	88.22
16	17.05	14.75	86.51
21	10.19	8.92	87.55
31	4.90	4.48	91.34

Table 5.1 Comparative response of face up and face down geometry of the magic plate

5.2.5 3D Depth Dose Comparison

Assigning 100% dose to the centroid detector at 6 mm, a 3D dose distribution was undertaken where the response of the Magic Plate is compared to an identical simulated experimental set up at each depth using the PLATO Treatment Planning Software.

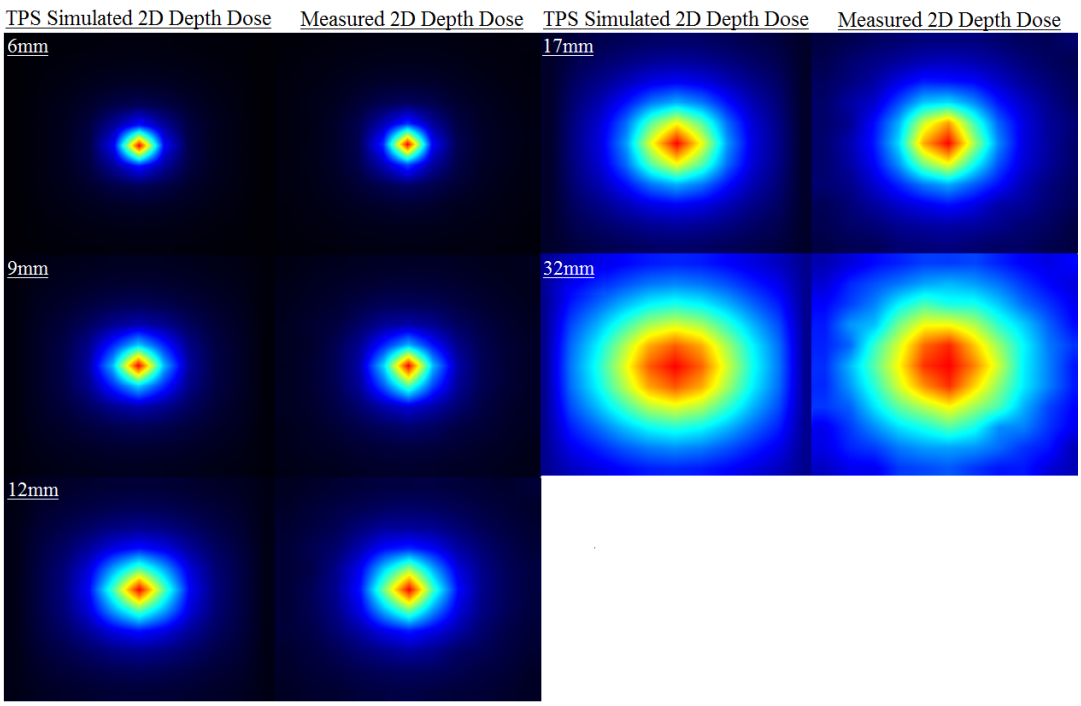

Figure 5.16 TPS simulated and measured 2D depth dose at 6 mm, 9 mm, 12 mm, 17 mm and 32 mm

This result depicts the high dose gradient associated with HDR brachytherapy. The 6 mm dose distribution indicates a highly concentrated dose about the centroid seed position; this is in contrast to the 32 mm image where a much more lateral spread of dose is seen. High correlation is seen between the experimental and simulated data. Notable variations are seen only at greater depths due to limitation of scaling in the colour of the images at lesser depths.

5.3 Source Tracking

As stated in chapter 2, there have been various reports published in the literature which attempt verification of source positioning and dwell timing as means of a quality assurance system for HDR brachytherapy. Ideally, these source tracking systems ought to be high resolution with high sensitivity and exhibit real time instantaneous read out for tracking the source with sub millimetre and sub millisecond accuracy. At

present, there are no clinically implementable devices available for source tracking procedures matching these specifications that also provide additional dosimetric information, inclusive of transit dose. This is typically important since most treatment planning systems do not account for transit dose. Each QA mechanism reports an assortment of limitations associated with their respective detection system; typically restrictions are characteristic of the detector type.

In an attempt to rectify this problem, the CMRP has implemented using the Magic Plates array of 11×11 epitaxial silicon detectors to accurately assess dwell location via direct measurement of the iridium source. Coupling the positional capability of the Magic Plate with the 10 ms read out timing resolution of the TERA system or a singular diode to the X-tream single epitaxial diode acquisition system (1 MHz sampling rate) allows assessment of static dwell positioning and timing, or high resolution transit timing and transit velocity, of the two systems respectively.

5.3.1 Source Tracking Magic Plate Graphical Interface

Developed by the CMRP, the Rad-X Dose View source tracking interface displays a real time 2D graphical display of source positioning (see figure 5.17). The display illustrates to the user an immediate time stamped approximate visual perspective of source location relative to the Magic Plate and a 3D numerical absolute dwell location. Approximate source location is visually illustrated via assigning pixels specific colours based on relative number of counts each detector has received. In addition to source tracking, integral counts are displayed on a separate adjacent graphical display illustrating the generated dose map as per consequence of the radiation source. The tracking and integral maps appear highly pixelated, as diode pitch is 1 cm. Other prototypes currently in development will aim to reduce this pitch to 2 mm. For smoother image appearance, the interface has in inbuilt user option to enable interpolation between detectors. Screen shots of the interface displaying integral dose maps and tracking are displayed in figure 5.23 with and without extrapolation enabled. For data analysis of source positioning, the software enables images to be reloaded and

viewed per specified time interval. This makes it easy to locate and verify source positioning at a specific time interval post irradiation.

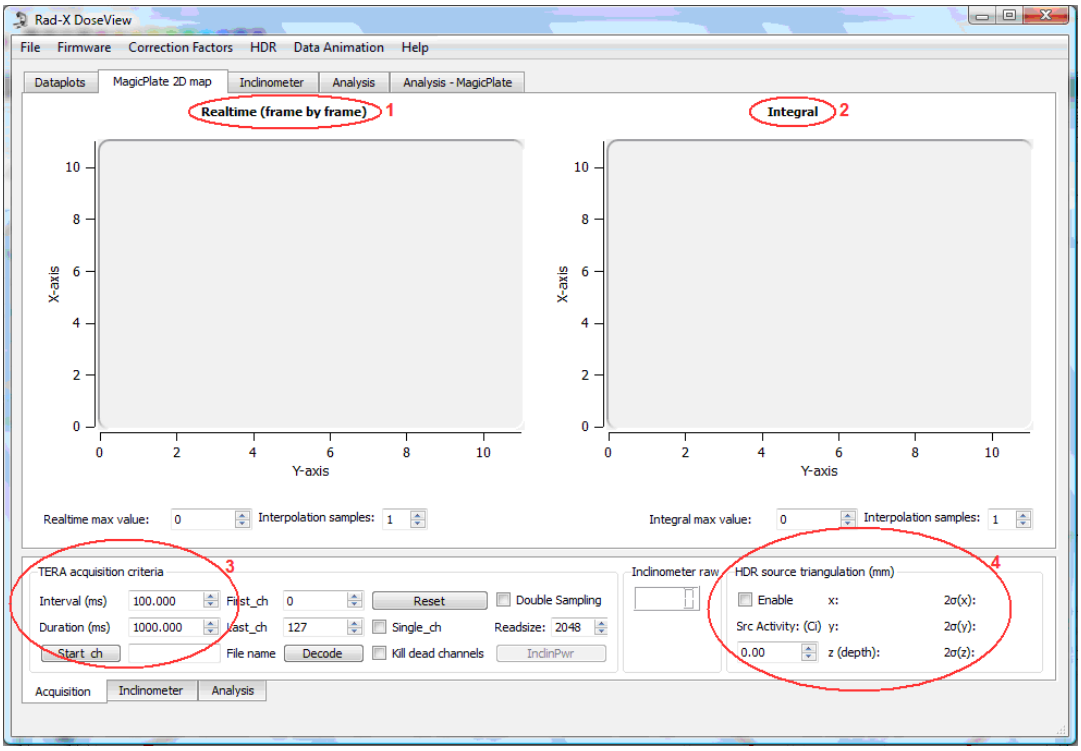

Figure 5.17 Rad-X Dose View source tracking interface. 1) 2D real time display of counts recorded which continually refreshes at the specified interval time. 2) 2D real time display of integral counts over specified duration. 3) Timing acquisition input, interval specifies period of data collection and duration specifies total data acquisition time. 4) Real time numerical source tracking output specifying source position in 3D and associated error in position.

5.3.2 Numerical Source Positioning Algorithm

The nature of a diode permits it to collect charge from a source at any specific distance and from any particular direction; that is to say they accumulate counts without any positional information. However, as seen in section 5.2, the response of the diode is significantly dependent upon radial distance relative to the iridium source. Consequently, based on any given detectors response, information from depth dose experimental data may be used to extrapolate an estimation of the radial distance of the detector to the source. From this information, it is therefore known that the source

is located at this radial distance at any three dimensional point around the detector.

To know the absolute position of the source in 3 dimensions, the radial distance from a minimum of 3 detectors must be known. Given that the detectors on the Magic Plate are fixed at a 1cm pitch, their exact location in the xy plane is constant, and source location can be calculated via the method of triangulation. The point of intersection between the radial distances of the three detectors (r_1, r_2, r_3) divulges source location. This principle is illustrated in figure 5.18.

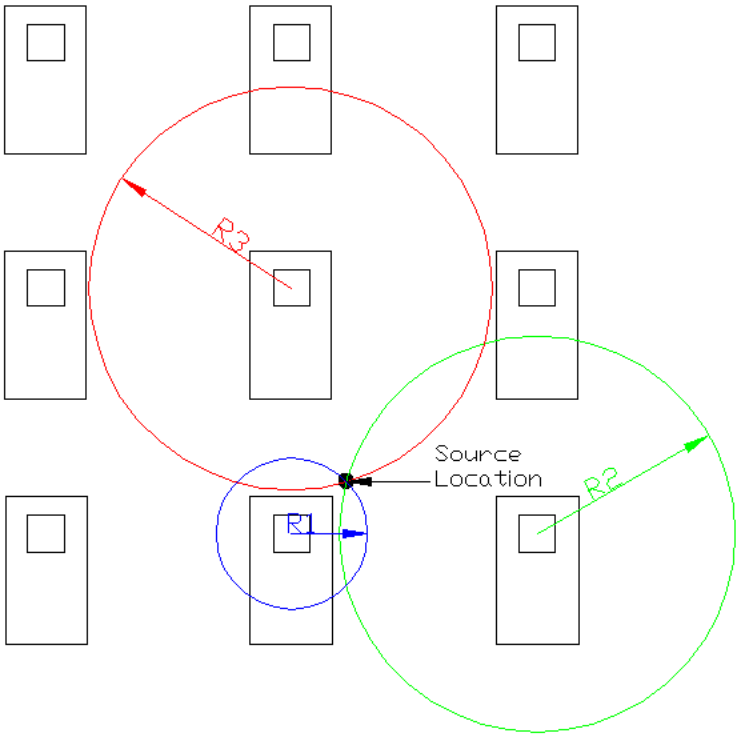

Figure 5.18 2D view of radial intersection triangulation method indicating source location

Prior to radiation exposure, the positional algorithm requires the user to input source activity (units of Curies) at time of measurement. Based on linear interpolation of source strength and the assumption of uniformity of detector response, the software first calculates the expected detector response at a 5 mm depth in water within the specified timing interval prior to any exposure to radiation. As radiation is being delivered, the algorithm then seeks the detector with maximum response within the

array. This detector is therefore known to be closest to the source. The ratio of the measured response of this detector to the previously determined expected response is calculated. Consequently this ratio (the relative response to 5 mm in water) can then be related to the experimental percentage depth dose curve to accurately estimate the radial distance the detector is away from the source. The algorithm seeks the subsequent 2 maximum signals, corresponding to the next two closest detectors, and performs the aforementioned iteration. The radial distance of the three closest detectors ($\mathrm{r}_1, \mathrm{r}_2, \mathrm{r}_3$) is now known.

Given that the pitch between subsequent detectors is constant and the location of each detector is known, the estimated radial distances from these three most proximal detectors are inputted into mathematical algorithms. Based on vector geometry, these algorithms calculate the source location based on the triangulation method depicted in figure 5.18. Coupled to the timing interval, the source location in three dimensions is outputted to a file and displayed in real time on the user interface. Coordinates are displayed in Cartesian coordinates relative to a fixed reference point on the Magic Plate.

Source positions that are input into the treatment delivery system were compared to those determined by the source tracking algorithm. Initial testing showed good agreement between the delivered position and numerically determined position. Esponiza *et al.* [107] demonstrated that difference between the prescribed position and the measured position of the HDR source was 0.5 mm for approximately 75% of measurements. Discrepancy of measured and prescribed source position was attributed to measuring the source whilst in transit.

5.3.3 Reconstruction of Linear Source Movement

Initial tests for assessing the Magic Plates capabilities of source tracking were undertaken by evaluating the response over a singular channel. A single prostate brachytherapy catheter was placed 5 mm above the central column of the 11×11 array of the Magic Plate and held in place with tape and bolus material as depicted in figure 5.19.

Using the Nucletron microSelectron HDR brachytherapy afterloader, the source was stepped with a 10 mm step size (MP detector pitch) over 90 mm with a static time of 5 seconds at each dwell location and then retracted. A dummy source was placed in the catheter as a representation of the radiation source position. The catheter was then aligned visually over the diode array with the intent to align each dwell position directly over the sensitive volume of each detector as the source is stepped. Data was aquired at a 100 ms timing interval.

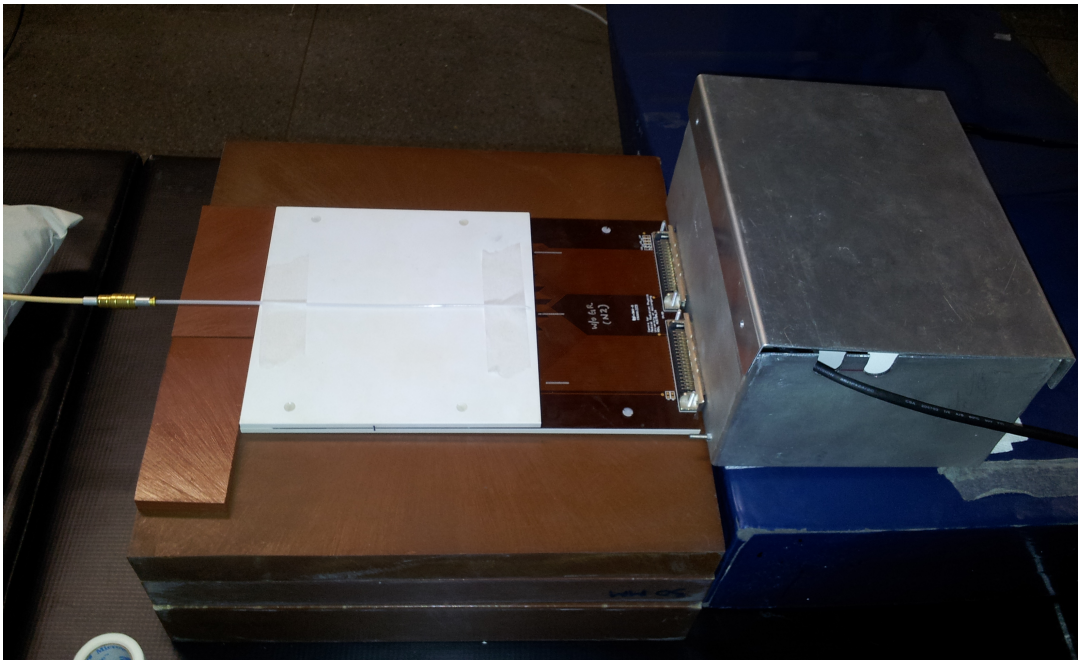

Figure 5.19 1D source tracking experimental set up. Image shows a catheter positioned over the central channel of the Magic Plate

5.3.4 Tracking of a Parabolic Source Trajectory

The curved catheter phantom, used for the polar angle tests (see image 5.7) was re-used to test the visual source tracking aspect of the Rad-X Dose View interface. The afterloader was programmed to drive the HDR source to the final dwell position of the catheter for a dwell time of 5 seconds and then retract. The catheter was placed within the curved recess of the Perspex phantom and positioned above the Magic Plate at a depth of 11mm. Alignment of the Perspex phantom and Magic Plate positioned the

first row of detectors in the array parallel with the straight portion of the catheter; the catheter then curved around a 5 cm radius over the 11 detector rows straightening again over the last row within the array. Figure 5.20 schematically demonstrates the position of the catheter relative to the Magic Plate diode array for this test.

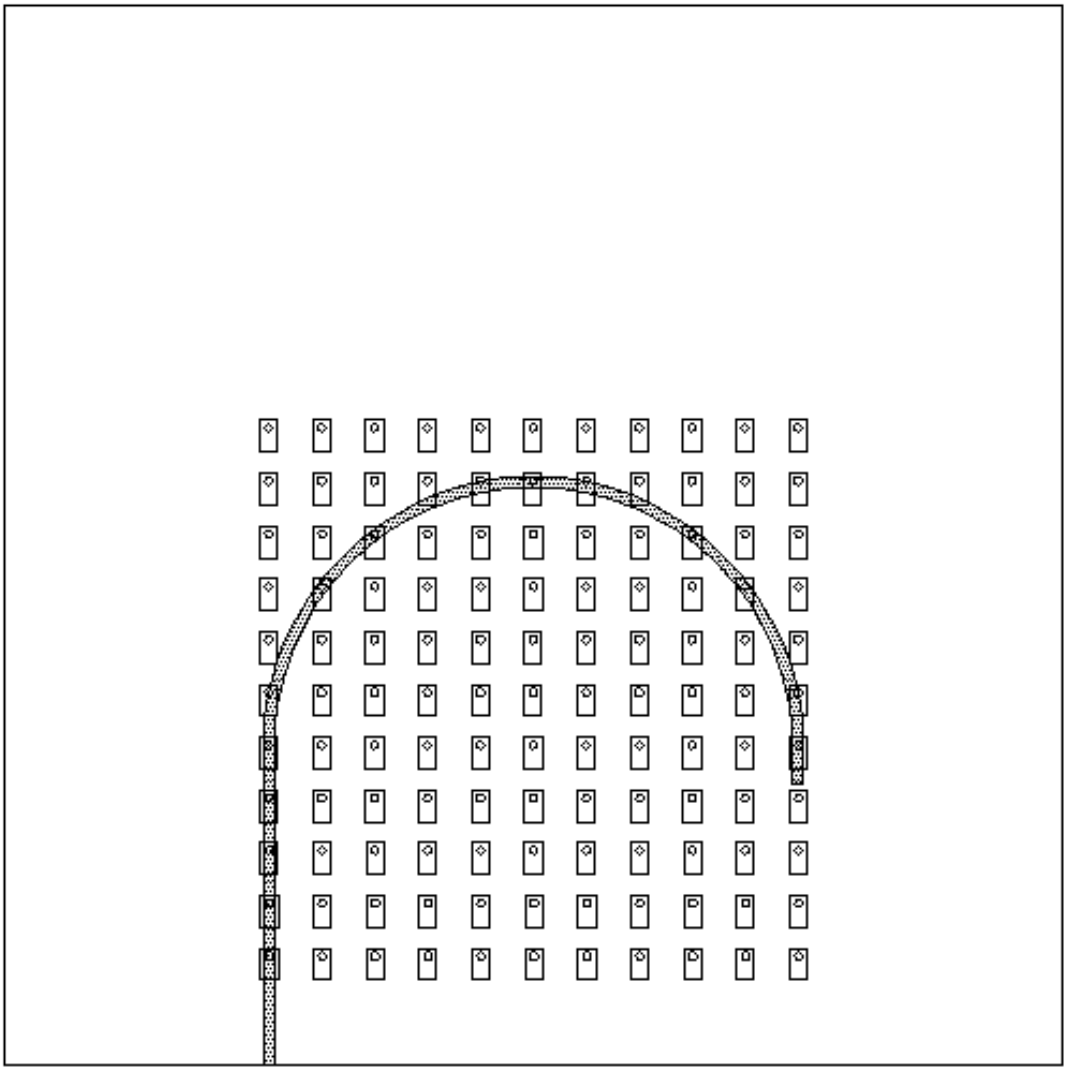

Figure 5.20 Graphical representation of catheter position relative to diode array of the Magic Plate used for source positioning and integral dose experiment.

5.3.5 Results: Reconstruction of a Linear Source Movement

Figure 5.22 shows the response of an individual detector in time. Maximum detector response for channels 63, 60, 59 and 57 correspond to the first, fourth, fifth and seventh dwell positions, when the source is orientated over each detector channel of the Magic Plate respectively. Width of the peaks are 5 seconds, corresponding to the 5 second dwell time of the source. From this figure a misalignment of the catheter over the detectors sensitive volume is evident. If alignment was accurate, symmetry would exist (resembling a pyramid function) around the maximum response in each image. However, for each channel the response is greater as the source is approaching than as it retreats.This results suggests that the source is over shooting the detectors sensitive volume as each detector response is greater on source approach than as it recedes. The large spike at 50 seconds is the response as the source is retracted from the catheter over the detectors sensitive volume. This result illustrates the Magic Plates ability for application in HDR quality assurance programs in terms of source tracking and positional verification.

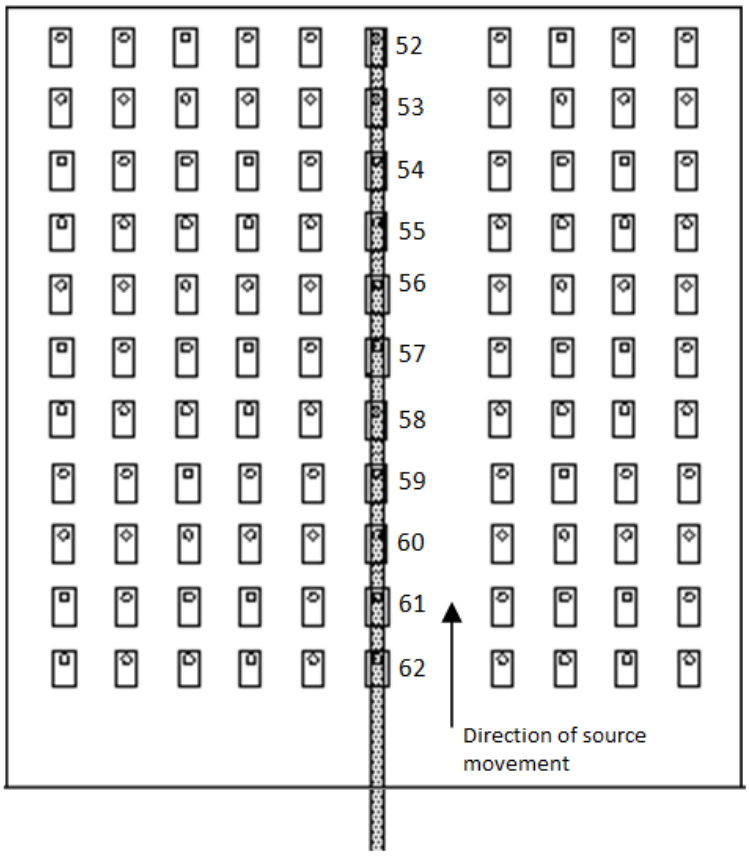

Figure 5.21 Schamatic of the catheter relative to the Magic Plate. The figure illustrates the set-up for 1D source tracking. The figure depicts the naming configuration used by the central channel in the Magic Plate array.

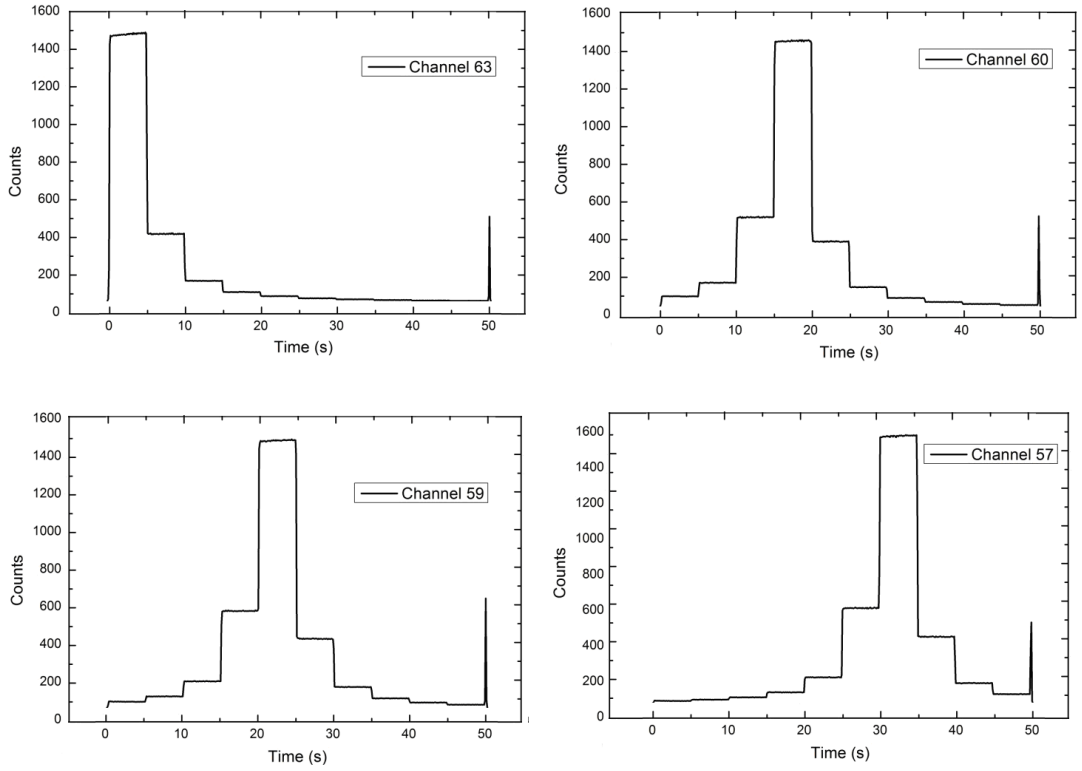

Figure 5.22 Four selected channels showing 1D tracking of the HDR source over the Magic Plate in time.

5.3.6 Results: Tracking of a parabolic source trajectory

The source was tracked in real time as it passed through the curved catheter. Images 1-5 of figure 5.23 indicate screen shots at 100 ms intervals of source transition and below it the corresponding integral dose. Image 6 of figure 5.23 shows a screen shot of the source in a static position at the end of the catheter, after 5 seconds.

Analysing images 1-3 of figure 5.23, the source is evidently in transit as it is positioned at different locations in time. The source is static at the final dwell position over the fifth detector of row eleven in images 4-6. Image 1 shows when the source first enters the catheter; integral counts are minimal (approx 700 at source location). As depicted in integral images 2-4, as the source begins to track around the catheter, counts increase at a faster rate for pixels located proximal to the catheter then for

pixels at greater radial distances. This is expected due to greater dose rates at a decreased radial distance to the source. This trend is shown to continue in images 5-6 when the source reaches its static position; rescaling of the counts diminishes colour in pixels at locations distant to the source. After 5 seconds (image 6) evidence of the catheter is no longer evident as counts have scaled to 40 000 at the source location and the remainder of the image appears almost homogenous.

The real time, frame by frame source positioning images seem highly pixelated as interpolation between detector response has been disabled; this is in stark contrast to the integral dose image where extrapolation has been enabled. Adversely, diode pitch of the detectors on the Magic Plate array restricts the resolution of the images and consequently accuracy of dwell positioning. The resolution of the image is thus restricted to 1cm $\times$ 1cm. With extrapolation disabled clear indication of counts being received by individual detectors can be seen for the entire array. Enabling extrapolation (as done for integral counts in figure 5.23) provides a user friendly quick estimation of dose distribution between detectors. Mapping integral counts in this way can quickly and effectively draw attention to regions of under or over irradiation.

These images give clear indication of source location in real time for a quick visual inspection of source location. The resulting image is clearly comparable to catheter orientation as indicated in figure 5.20, effectively proving the mechanism viable for visual verification of catheter positioning and tracking.

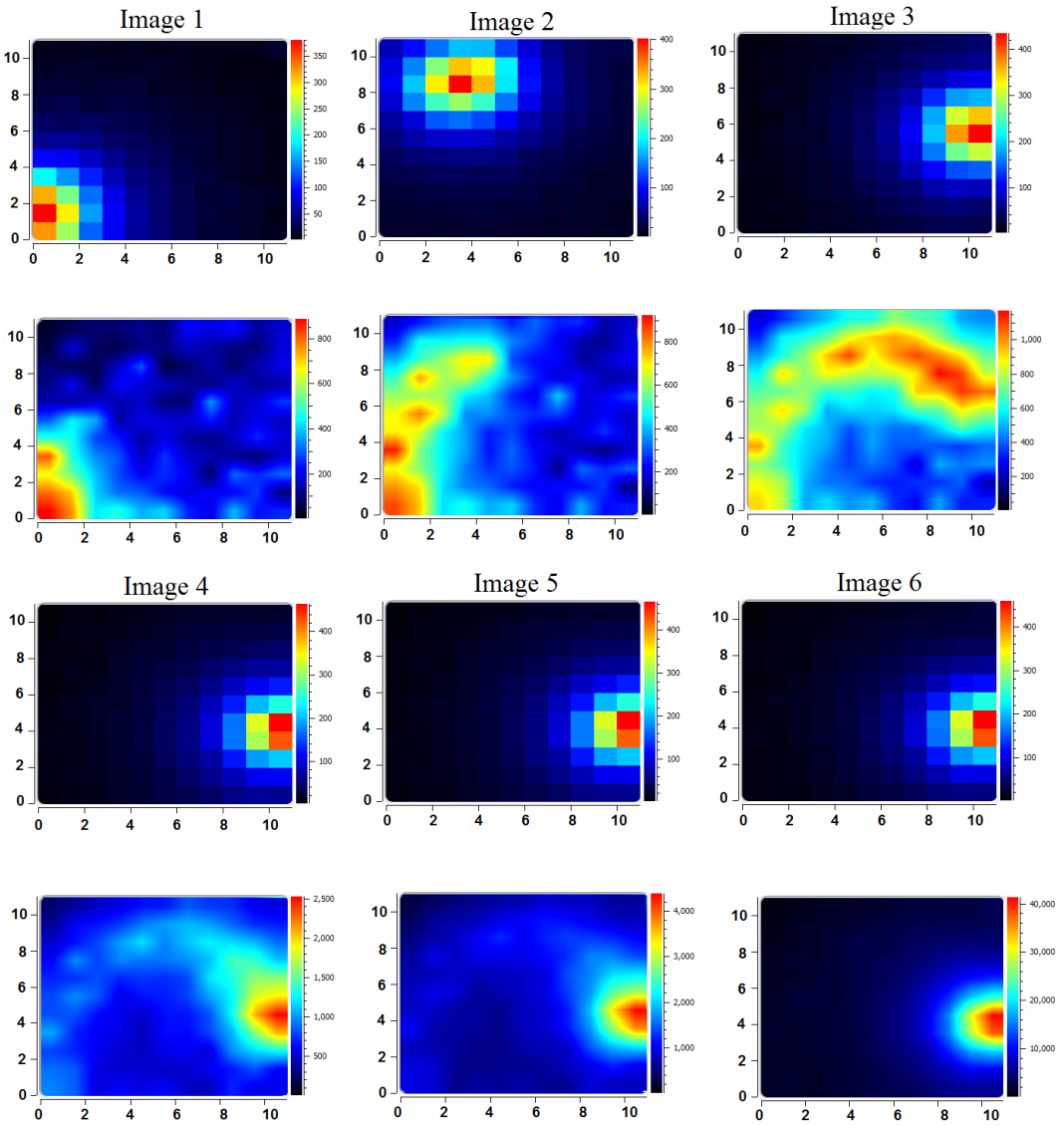

Figure 5.23 Screen shots of Rad-X Dose View source tracking interface at 100 ms intervals. Figure shows source positioning and corresponding dose per timing interval.

Multiple tests were undertaken to test the tracking capabilities of the system. To simulate the Brachy*Pix* smart phantom and verification of an actual patient treatment, 5 catheters spaced 10 mm apart were placed equidistant both above and below the Magic Plate. Random dwell positions and dwell times were entered for each catheter, effectively establishing a random dose distribution. Catheters 1-5 were orientated above the Magic Plate and catheters 6-10 were orientated below as per figure

5.24. The Magic Plate was used for tracking the source at each dwell position and monitoring the overall dose distribution.

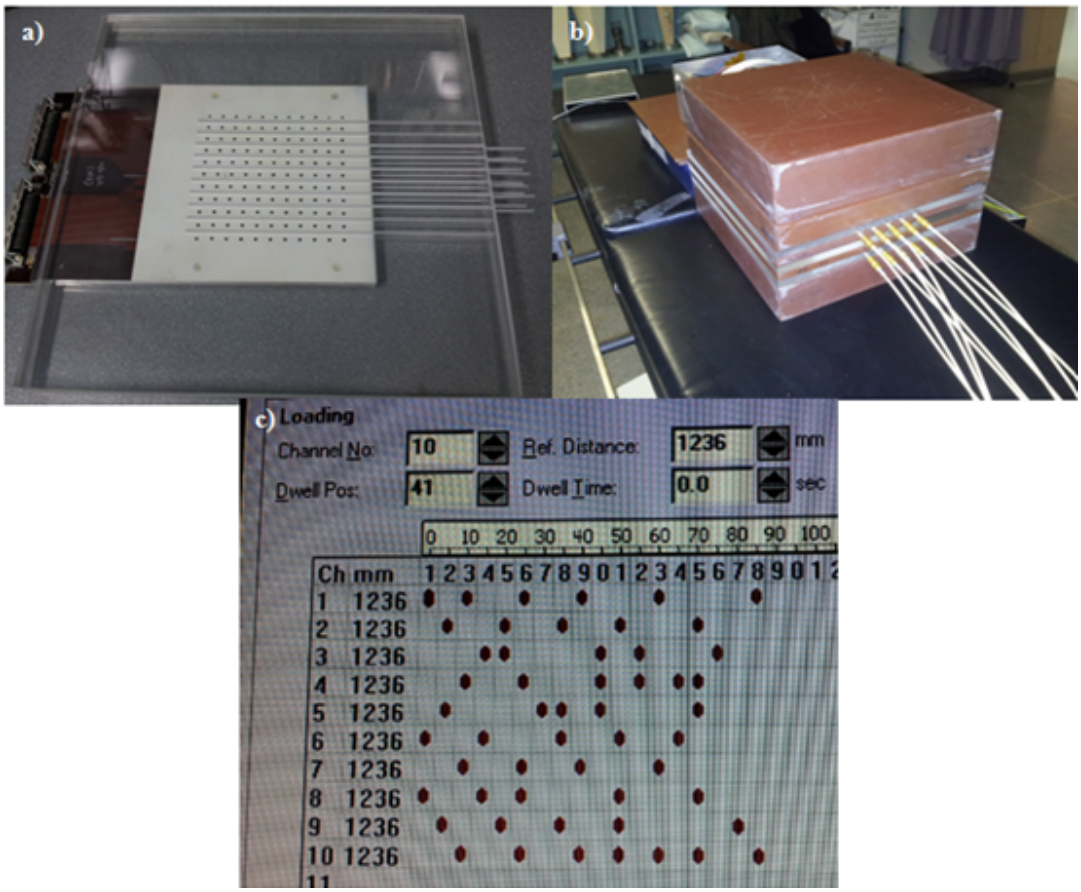

Figure 5.24 a) Catheter orientated above and below the Magic Place, b) Experimental set up with delivery tubes attached to catheters c) Screen shot of delivery system loading program indicating treatment plans randomised dwell positions and timing.

Figure 5.25 illustrates screen shots of the Rad-X Dose View source tracking interface for different dwell locations and the respective dose distribution in time for catheters 1,3,5,7 and 10 respectively. This figure gives clear indication of the respective dose distribution applied by each individual catheter on the plans overall dose distribution.

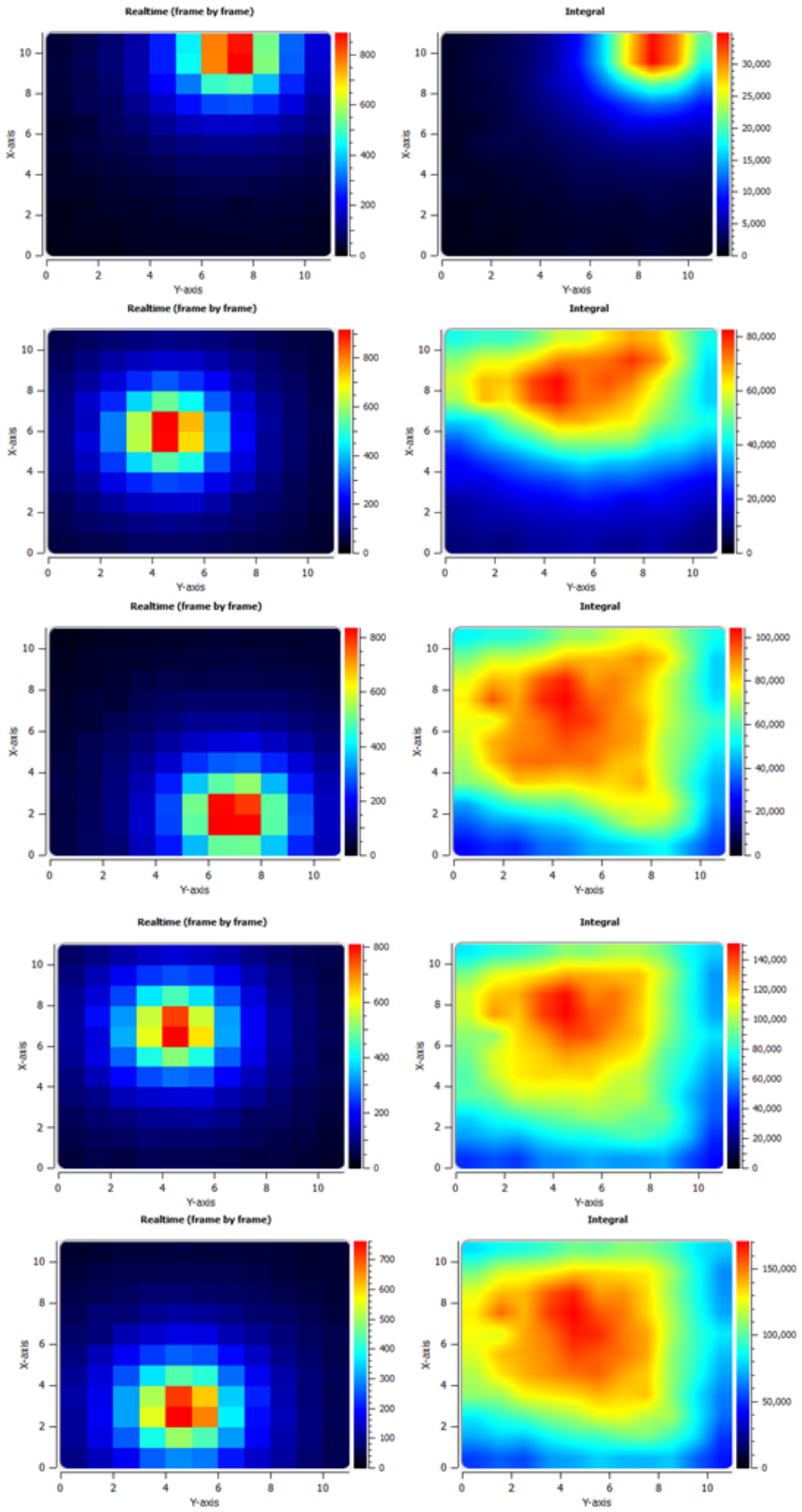

Figure 5.25 Tracking of source positioning and the respective dose distribution of 10 catheters due to randomised dose plan.

5.4 Transit Velocity

Due to a relatively high source velocity, tracking of the HDR source in transit and calculation of transit dose becomes difficult in HDR QA systems since data acquisition readout systems are often simply not fast enough to gather sufficient data. At present time the MPs data acquisition system electronics can not resolve information for timing intervals less than 10 ms. Consequently, insufficient data is acquired while the source is in transit. As a result, high resolution source tracking of the source in transit and determination of source velocity cannot be undertaken using the current MPs electronics. As described in section 4.5, the X-Tream data acquisition system is capable of sampling charge from a singular diode at a frequency of 1 MHz. This corresponds to a timing interval of 1 μs, sufficiently fast enough sampling rate to gather information about the source while in transit. This system was coupled to a singular epitaxial diode in an experimental procedure to analyse the effects of dwell positioning on transit velocity.

5.4.1 Intra Dwell Spacing Effect On Transit Velocity

To evaluate the dependency of distance between dwell positions on the source mean velocity, a single diode was placed 10 mm below the final dwell position of a catheter. Using a 278.3 GBq Ir-192 source, the Nucletron microSelectron HDR brachytherapy afterloader was programmed to deliver the source for 5 seconds at two different dwell locations of varying distance. The relative distance between dwell positions tested was 2.5, 5.0, 7.5, 10. 15, 20, 25, 30, 50, 75, 100 and 150 mm. Measurements were taken 3 times at each dwell separation using the X-tream system at a 1 MHz acquisition frequency. Having a known distance between dwell positions and evaluating the time of the source in transit, the average transit velocity between dwell positions can be estimated. For each distance between dwell positions, uncertainty of source velocity was based on 2 standard deviations of the calculated velocity for the three tests.

Figure 5.26 depicts the response of the diode in time for 20 mm relative distance between dwell positions. The first plateau indicates when the source is at its first dwell position; stationary for 5 seconds, then driven to the second dwell position. The increase in counts is due to the secondary dwell position being at a lesser radial distance to the detector then the first. This does not affect the results as timing between points is independent upon the diodes response. Figure 5.27 is simply is a magnification of figure 5.26 indicating the time in transit for 20 mm dwell separation distance between dwell locations.

The average transit velocity was determined by dividing the distance between dwell positions by the average time it took for the source to move from its static position at the first dwell location and become static at the secondary dwell position. Difficulties in evaluating when the source is in a state of absolute rest due to the deceleration of the source and slight variation between data sets was the main cause of errors; particularly at dwell separation distances of 7.5, 50 and 150 mm. Results are shown in figure 5.28

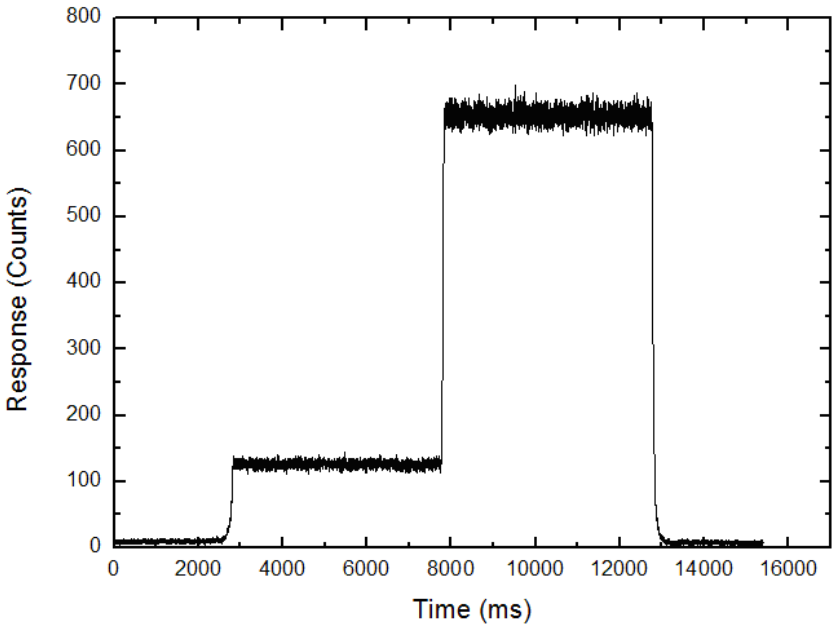

Figure 5.26 Single diode response using the X-tream system of source in transit for 20 mm dwell separation distance between dwell locations.

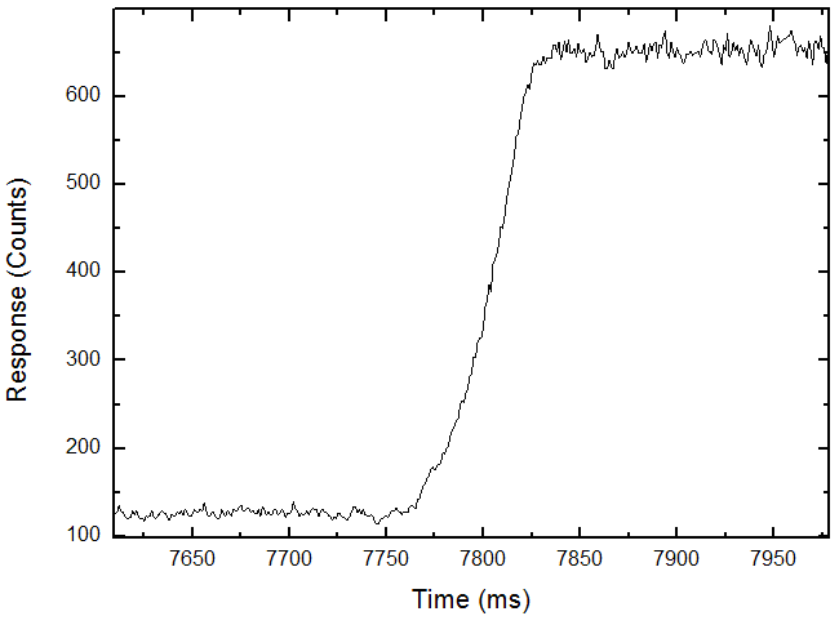

Figure 5.27 Magnification of Figure 5.26 when source is in transit. Figure indicates movement of the source in time.

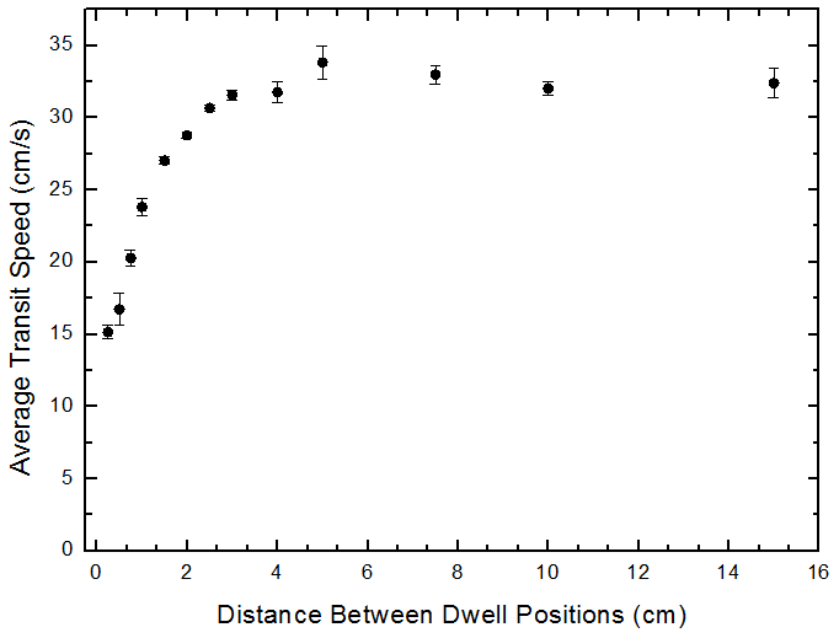

Figure 5.28 Effect of dwell spacing on mean transit velocity

As expected, figure 5.28 shows mean transit velocity increasing as distance be-

tween dwell positions increases; this trend continues at a lesser rate as the source approaches its maximum speed. Velocity begins to taper off at the 28-29 cm/s region (2 cm dwell separation) reaching a maximum speed of 33.8±1.1 cm/s at 5 cm dwell separation distance.

As described in section 3.4 there have been a wide number of attempts to directly measure the source velocity of a HDR afterloader. Values found within the literature have a large variation and often an associated large uncertainty, which demonstrates the difficulty of this type of measurement. With a maximum velocity of 33.8 ± 1.1 cm/s, transit velocity results recorded by the X-Tream system are slightly lower, but comparable to those found in the literature. With an uncertainty margin of 100%, Sahoo *et al.* [69] reported velocities of 45.5 cm/s. Bastin *et al.* [62] reported velocity of 32.5 cm/s for a 32.5 mm step size. Minamisawa *et al.* [70] stated a maximum velocity of 52.0 ± 1.0 cm/s. Wong [68] declared a maximum velocity of 52.9 ± 1.5 cm/s where Nucletron states a specified speed of 50 cm/s [41] and does not consider velocity as a function of step size. As treatment planning systems do not take into account transit dose [46], if transit speed as measured per the X-Tream system are smaller than that stated by Nucletron, than patients will be receiving a dose greater than what is currently expected. Depending on the treatment type, this relative increase in dose may have a clinical impact to the patient.

Minamisawa [70] state that the radiation source follows a uniform acceleration and deceleration both of 113 $\mathrm{cm/s^2}$, however as figure 5.27 demonstrates, acceleration is not uniform. This figure depicts displacement in time, which by definition is velocity. Since the gradient of this slope is not uniformly linear but resembles a more parabolic shape (most evident by comparing the slope of the cure between times 7775-7800 and 7800-7825) than the acceleration can therefore not be constant over this time.

Chapter 6

Conclusion

This thesis characterised silicon epitaxial diodes response to radiation spectra from an iridium-192 source, evaluated their use as a pre treatment quality assurance detector and examined their functionality for real time tracking of the source for HDR brachytherapy. This investigation has characterised the response of silicon epitaxial diodes to the radiation spectra present in HDR brachytherapy in terms of their angular dependence and depth dose response.

As expected, the diode displayed a consistency in its angular dependency about both the polar and azimuth axis. A continuous decreasing response was seen as relative source to detector angles tended towards 180 degrees, with a $15\pm1\%$ decrease in response when comparing 0 and 180 degree orientation of the detector. Although this angular dependency of the epitaxial diode is non ideal and should be taken into account for source tracking measurements, the dependency is minimised as angles of interest are only $\pm45^{\circ}$ of the detector front and rear side.

Strong correlation of depth dose response was seen between experimental measurements and with simulated data from the PLATO treatment planning system with source to detector distances between 5 and 32 mm. Subtle variations were attributed to positional misalignment of the detector at greater depths and to a lesser degree contribution of low energy scatter over responding within the silicon. The sensitivity of the detector deteriorated with increasing radial distance from the source. Having

a high sensitive at greater depths, whilst still achieving accuracy at distance close to the source is difficult due to the high dose gradients associated with an iridium-192 source. Placing the depth of the detector between 10 and 20 mm yielded the best response.

Employed in a 11 x 11 epitaxial diode array, the Magic Plate has shown sufficient ability in tracking and establishing localisation of source positioning in visually in two and numerically in three dimensions. The 2D tracking interface provides a real time visual representation of the source positioning and dose distribution of the treatment. This visual representation will enable the therapist to immediately detect gross errors in the treatment whilst the 3D tracking algorithm will provide numerical acute detail. These results provide proof of concept for source tracking and demonstrates the eligibility of the Magic Plate as an appropriate detector for use in HDR brachytherapy QA. These results sanction the use of the Magic Plate for continued development on a patient specific pre-treatment quality assurance program.

The current timing of the TERA readout systems is not sufficient in effectively measuring the transit time of the source which is why it was measured using the X-Tream high speed readout system. Developed at the CMRP, the X-Tream high speed readout system was used for direct measurements of the source transit velocity. As expected source velocity was found to be dependent upon intradwell position spacing. The greater intra-dwell spacing, the greater the velocity the afterloader was able to deliver the source to its next dwell position. A maximum mean transit velocity of 33.8 ± 1.1 cm/s was established for a 5 cm dwell separation distance. For the standard clinical treatment step size of 2.5 mm, mean source transit velocity was found to be 15.2 ± 0.6 cm/s.

6.1 Future Work

Future developments and prospects leading from the findings of this thesis will primarily be in terms of improved detector design. Decreasing the angular dependence

of the diode will be a major factor in addition to improving the sensitivity of the detector. This aims to improve the diodes response at greater depth and provide improved accuracy of source tracking. To achieve the prospect of higher resolution and improved source tracking is to redesign the Magic Plate by increasing the number of diodes on the array and by decreasing the spacing between subsequent detectors. Additionally to improved detector design, the development of the Brachy*Pix* smart phantom will begin to be implemented. Initial designs of the Brachy*Pix* phantom will house spacing for only prostate needles, however, re-designs will evidently incorporate the ability to track the source through any HDR catheter configuration. Software developments aim to provide an interface with TPS software to provide real time verification of source positioning. Applying a gamma index to results will help quantify the difference between treatment plan and delivered dose.

Bibliography

[1] AIHW (Australian Institute of Health and Welfare) and AACR (Australiasian Association of Cancer Registries), "Cancer in Australia: An Overview, 2008," (2008). Cancer series no. 46. Cat No CAN 42. Canberra: AIHW.

[2] P. Metcalfe, T. Kron, and P. Hoban, *Radiation Detection and Measurement*. John Wiley and Sons, Third ed., (2000). Ch 14.

[3] L. Zuofeng, M. Thomas, P. Jatinder, and L. Chihray, "A quality assurance test tool for high dose rate remote afterloading brachytherapy units," *J Medical Physics*, vol. 25, no. 2, pp. 232–235, (1998).

[4] J. Truong, "Verification of brachytherapy treatment planning system using gafchromic film in gynaecological hdr treatment," *J Australas. Phys. Eng. Sci. Med*, vol. 32, no. 1, pp. 44–50, (2009).

[5] D. Rickey, D. Sasaki, and J. Bews, "A quality assurance tool for high-dose-rate brachytherapy," *Med. Phys.*, vol. 37, no. 6, pp. 2525–32, (2010).

[6] S. Aldelaijan, H. Mohammed, and N Tomic et al, "Radiochromic film dosimetry of HDR 192-Ir source radiation fields," *J Med Phys*, vol. 11, no. 38, pp. 6074–6083, (2011).

[7] A.Lightstone, "Fluorescent screen for high dose rate (HDR) brachytherapy quality assurance," *J Medical Dosimetry*, vol. 30, no. 3, pp. 143–144, (2005).

[8] L. Liu, "A dwell position verification method for high dose rate brachytherapy," *Journal of Applied Medical Physics*, vol. 5, no. 1, pp. 1–5, (2004).

[9] T. Nakano, N. Suchowerska, D. McKenzie, and M. Bilek, "Real time verification of HDR brachytherapy source location: Implementation of detector redundancy," *Phys. Med. Biol.*, vol. 50, pp. 319–327, (2005).

[10] T. Nakano, N. Suchowerska, M. Bilek, D. McKenzie, N. Ng, and T. Kron, "High dose-rate brachytherapy source localization: positional resolution using a diamond detector," *Phys. Med. Biol.*, vol. 48, pp. 2133–2146, (2003).

[11] J. Duan, D. Macey, P. Pareek, and I. Brezovich, "Real time monitoring and verification of in vivo high dose rate brachytherapy using a pinhole camera," *Med. Phys*, vol. 28, no. 2, pp. 167–173, (2000).

[12] M. Batic, J. Burger, V. Cindro, G. Kramberger, I. Mandic, M. Mikuz, A. Studen, and M. Zavrtanik, "Verification of high dose rate Ir-192 position during brachytherapy treatment," (2010). Nuclear Instruments and Methods in Physics Research A 617, 206-208.

[13] H. Seo, M. Haque, R. Hill, and C. Baldock, "In-vivo dosimetric verification of a HDR brachytherapy surface mould," *Australas. Phys. Eng. Sci. Med.*, vol. 31, no. 4, p. 519, (2008).

[14] A. Meigooni, J. Meli, and R. Nath, "Influence of the variation of energy spectra with depth in the dosimetry of Ir-192 using LiF TLD," *Phys Med Biol*, vol. 33, pp. 1159–1170, (1988).

[15] H. Song, J. Bowsher, S. Das, and F. Yin, "Tracking brachytherapy sources using emission imaging with one flat panel detector," *Med. Phys.*, vol. 36, no. 4, pp. 1109–1111, (2009).

[16] J. Herzen, M. Todorovic, F. C. amd V. Platz, D. Albers, A. Bartels, and R. Schmidt, "Dosimetric evaluation of a 2D pixel ionization chamber for implementation in clinical routine," *Phys. Med. Biol.*, vol. 52, pp. 1197–1208, (2007).

[17] M. Yewondwossen and J. Meng, "Commissioning of brachytherapy TPS Using a 2D-Array of ion chambers," (2010). The 6th International Conference on 3D Radiation Dosimetry, Journal of Physics: Conference Series 250.

[18] A. Manikandan, S. Bilab, P. David, R. Holla, T. Vivek, and N. Sujatha, "Relative dosimetrical verification in high dose rate brachytherapy using two-dimensional detector array IMatriXX," *J Med Phys.*, vol. 36, no. 3, pp. 171–175, (2011).

[19] P. Spiegel, "The first clinical x-ray made in America-100 years," *American Journal of Roentgenology*, vol. 164, no. 1, pp. 3–12, (1995).

[20] S. Nag, R. Dobelbower, and G Glasgow et al., "Inter-society standards for the performance of brachytherapy: a joint report from ABS, ACMP and ACRO," *Critical Reviews in Oncology/Haematology*, vol. 48, pp. 1–17, (2003).

[21] Australian Bureau of Statistics, "Causes of death, Australia, 2010," (2010).

[22] Jacob Van Dyk, *The modern technology of radiation oncology: A compendium for medical physicists and radiation oncologists*. Medical Physics Publishing, First ed., (1999).

[23] ICRU Report 50, "Prescribing, recording and reporting photon beam therapy," *Journal of the ICRU*, (1993).

[24] ICRU Report 62, "Prescribing, recording and reporting photon beam therapy," *Journal of the ICRU*, (1999).

[25] ICRU Report 83, "Prescribing recording reporting photon-beam intensity modulated radiation therapy," *Journal of the ICRU*, (2010).

[26] M. Joiner and A. van der Kogel, *Basic Clinical Radiobiology*. CRC Press, fourth ed., (2009).

[27] T. Pickles, M.Keyes, and J. Morris, "Brachytherapy or conformal external radiotherapy for prostate cancer: A single-institution matched-pair analysis,"

International Journal Of Radiation Oncology Physics, vol. 76, no. 1, pp. 43–49, (2010).

[28] D. Brachman, T. Thomas, J. Hilbe, and D. Beyer, "Failure-free survival following brachytherapy alone or external beam irradiation alone for T1-2 prostate tumours in 2222 patients: Results from a single practice," *Int. J. Radiation Oncology Biol. Phys*, vol. 48, no. 1, pp. 111–117, (2000).

[29] T. Mate, J. Gottesman, J. Hatton, M. Gribble, and L. V. Holleneke, "High dose-rate afterloading using 192-iridium prostate brachytherapy: Feasibility report," *Int. J. Radiation Oncology Biol. Phys*, vol. 41, no. 3, pp. 525–533, (1998).

[30] A. Gerbaulet, I. Kunkler, and G.Kerr et al, "Combined radiotherapy and surgery: local control and complications in early carcinoma of the uterine cervix - the Villejuif experience, 1975-1984," *Radiation and Oncology*, vol. 23, pp. 66–73, (1992).

[31] M. Resbeut, C. Alzieu, and L. Gonzague-Casabianca et al, "Combined brachytherapy and surgery for early carcinoma of the uterine cervix: Analysis of extent of surgery on outcome," *Int. J. Radiation Oncology Biol. Phys*, vol. 50, no. 4, pp. 873–881, (2001).

[32] R. Galalae, A. Martinez, T. Mate, and C. Mitchell et al, "Long-term outcome by risk factors using conformal high-dose-rate brachytherapy (HDR-BT) boost with or without neoadjuvant androgen suppression for localized prostate cancer," *International Journal Of Radiation Oncology Physics*, vol. 58, no. 4, pp. 1048–1055, (2004).

[33] A. Martinez, G. Gustafson, and J. Gonzalez et al, "Dose escalation using conformal high-dose-rate brachytherapy improves outcome in unfavourable prostate cancer," *Int. J. Radiation Oncology Biol. Phys*, vol. 53, no. 2, pp. 316–327, (2002).

[34] ICRU Report 38, "Dose and volume specification for reporting intracavitary therapy in gynecology," *Journal of the ICRU*, (1985).

[35] M. Unterweger, D. Hoppes, F. Schima, and J. Coursey, "Radionuclide half-life measurements," October (2010). NIST Physical Measurement Laboratory.

[36] C. Dempsey, R. Smith, T. Nyathi, A. Ceylan, L. Howard, V. Patel, R. Das, and A. Haworth, "Acpsem brachytherapy working group recommendations for quality assurance in brachytherapy," *Phys Eng Sci Med*, (2013).

[37] J. Venselarr and J. Perez-Calatayud, "European guidelines forquality assurance in radiotherapy, estro booklet no 8, a practical guide to quality control of brachytherapy equipment," *ISBN 90-804532-8 ESTRO Belgium*, (2004).

[38] R. Nath, L. Anderson, and J Meli et al., "Code of practice for brachytherapy physics: report of the aapm radiation therapy committee task group no 56," *Med Phys*, vol. 24, no. 10, pp. 1557–1598, (1997).

[39] M. Evans, S. Devic, and E. Podgorsak, "High dose-rate brachytherapy source position quality assurance using radiochromic film," *Medical Dosimetry*, vol. 32, no. 1, pp. 13–15, (2007).

[40] S. Nag, *High dose rate brachytherapy: A textbook*. Futura, New York, (1994).

[41] Nucletron, "Microselectron HDR afterloader and source specifications," (2012). www.nucletron.com/en/ProductsAndSolutions/Pages/microSelectionDigital.aspx.

[42] G. Daskalov, E. Loffler, and J. Williamson, "Monte Carlo-aided dosimetry of a new high dose-rate brachytherapy source," *Med Phys*, vol. 25, no. 11, pp. 2200–2208, (1998).

[43] F. Lliso and J. Perez-Calatayud et al, "Fitted dosimetric parameters of high dose-rate 192Ir sources according to the AAPM TG43 formalism," *Med Phys*, vol. 28, pp. 654–660, (2001).

[44] R. Taylor and D. Rogers, "An egsnrc monte carlo-calculated database of tg-43 parameters," *Med Phys*, vol. 35, no. 9, pp. 4228–4241, (2008).

[45] E. Browne, "Table of radionuclides iridium-192," December (2003). Laboratoire National Henri Becquerel.

[46] M. Rivard, B. Coursey, L. DeWerd, W. Hanson, M. S. Haq, G. Ibbott, M. Mitch, R. Nath, and J. Williamson, "Update of AAPM task group No. 43 report: A revised AAPM protocol for brachytherapy dose calculations," *Med Phys*, vol. 31, no. 3, pp. 633–674, (2004).

[47] International Atomic Energy Agency, "Lessons learned from accidental, exposures in radiotherapy," (2000). Safety Report Series No. 17, IAEA, Vienna.

[48] C. Scarantino, B. Prestidge, and M. Anscher et al, "The observed variance between predicted and measured radiation dose in breast and prostate patients utilizing an in vivo dosimeter," *Int J Radiation Oncology Biol*, vol. 72, pp. 597–604, (2008).

[49] S. Oh, J. Scott, T. Suh, and S. Kim, "Measurements of dose discrepancies due to inhomogeneities and radiographic contrast in balloon catheter brachytherapy," *J Med Phys*, vol. 36, pp. 3945–3954, (2009).

[50] T. Akimoto, H. Muramatsu, and M. Takahashi, "Rectal bleeding after hypofractionated radiation therapy for prostate cancer: correlation between clinical and dosimetric parameters and the incidence of grade 2 or worse rectal bleeding," *Int. Journal Radiation Oncology*, vol. 60, no. 4, pp. 1033–1103, (2004).

[51] J. Valentin, "Prevention of high-dose-rate brachytherapy accidents," *ICRP Publication 97*, vol. 35, no. 2, pp. 1–9, (2005).

[52] United States Nuclear Regulatory Commission, "Loss of an iridium-192 source and therapy misadministration at Indiana Regional Cancer Center, In-

diana, Pennsylvania on November 16, 1992," (1993). Report NUREG-1480, Washington, D.C.

[53] R. Nath, L. Anderson, G. Luxton, K. Weaver, J. Williamson, and A. Meigooni, "Dosimetry of interstitial brachytherapy sources: Recommendations of the AAPM Radiation Therapy Committee Task Group No 43," *Med. Phys*, vol. 22, no. 2, pp. 209–234, (1994).

[54] J. Williamson, "Comparison of measured and calculated dose rates in water near I-125 and Ir-192 seeds," *Med.Phys*, vol. 18, no. 4, pp. 776–86, (1991).

[55] L. Anderson, R. Nath, and K. Weaver, "Interstitial brachytherapy: Physical, biological and clinical considerations," (1990). Interstitial Collaborative Working Group (ICWG), Raven, New York.

[56] T. Nyathi, S. Mannings, and A. Mishra, "Dosimetric validation and evaluation of the brachytherapy dose calculation algorithm Acuros BV: A paradigm shift," (2011). Presented at the South African Association of Physicists in Medicine and Biology annual conference.

[57] L. Beaulieu, A. Tedgren, J. Carrier, S. Davis, F. Mourtada, M. Rivard, and R Thomson el al, "Report of the task group 186 on model based dose calculation methods in brachytherapy beyond the tg-43 formalism: Current status and recommendations for clinical implementation," *Med Phys*, vol. 39, pp. 6208–6233, (2012).

[58] G. Anagnostopoulos, D. Baltas, and E Pantelis et al, "The effect of patient inhomogeneties in oesophageal Ir-192 HDR brachytherapy," *Phys Med Biol*, vol. 49, pp. 2675–2685, (2004).

[59] E. Poon, J. Williamson, T. Vuong, and F. Verhaegen, "Patient specific Monte Carlo dose calcuations for high dose rate endorectal brachytherapy with shielded intracavity applicator," *Int J Radiat Oncol Biol Phys*, vol. 49, pp. 2675–2685, (2004).

[60] M. Bidmead, "A practical guide to quality control of brachytherapy equipment," (2004). Brussels, ESTRO booklet 8.

[61] H. Kojima, T. Hanada, S. Katsuta, A. Yorozu, and K. Maruyama, "New method for obtaining position and time structure of source in HDR remote afterloading brachytherapy unit utilizing light emission from scintillator," *Journal of Applied Clinical Medical Physics*, vol. 10, p. 2983, (2009).

[62] K. Bastin, M. Podgorsak, and B. Thomadsen, "The transit dose component of high dose rate brachytherapy: Direct measurements and clinical implications," *Int. J. Radiation Oncology Biol. Phys.*, vol. 26, pp. 695–702, (1993).

[63] G. Kutcher, L. Coia, and M Gillin et al., "Comprehensive qa for radiation oncology: report of aapm radiation therapy committee task group 40," *Med Phys*, (1994).

[64] Canadian Association of Provincial Cancer Agencies (CAPCA), "Standards for quality control at canadian radiation treatment centres: Brachytherapy remote afterloaders," *CAPCA Cananda*, (2006).

[65] R. Elfrink, I. KolkmanDeurloo, and H van Kleffens et al, "Quality control of brachytherapy equipment in the netherlands and belgium: current practice and minimum requirements," *Radiother Oncol*, (2002).

[66] Swiss Society of Radiobiology and Medical Physics (SSRMP), "Dosimetry and quality assurance in high dose rate brachytherapy with iridium-192, recommendations no 13," *SSRMP, Switzerland*, (2005).

[67] International Atomic Energy Agency (IAEA), "Iaea-tecdoc 1274 calibration of photon and beta ray sources used in brachytherapy," *IAEA, Vienna*, pp. 1011–4289, (2002).

[68] T. Wong, W. Fernando, P. Johnston, and I. Bubb, "Transit dose of an Ir-192 high dose rate brachytherapy stepping source," *Phys. Med. Biol*, vol. 46, pp. 323–331, (2001).

[69] N. Sahoo, "Measurement of transit time of a remote after-loading high dose rate brachytherapy source," *Med. Phys.*, vol. 28, no. 8, pp. 1786–1790, (2001).

[70] R. Minamisawa, R. Rubo, R. Seraide, J. Rocha, and A. Almeida, "Direct measurement of instantaneous source speed for a HDR brachytherapy unit using an optical fiber based detector," *Med. Phys.*, vol. 37, no. 10, pp. 5407–5411, (2010).

[71] F. Attix, *Introduction to radiological physics and radiation dosimetry*. John Wiley and Sons, (1986).

[72] M.Westermark, J.Arndt, B.Nilsson, and A.Brahme, "Comparative dosimetry in narrow high-energy photon beams," *Physics in Medicine and Biology*, vol. 45, no. 3, pp. 685–702, (2000).

[73] G. Rinker and E. Grusell, "General specifications for silicon semiconductors for use in radiation dosimetry," *Phys. Med. Biol*, vol. 32, no. 9, pp. 1109–1117, (1986).

[74] G. Lutz, "Silicon radiation detectors," (1995). Nuclear Instruments and Methods in Physics Research, Section A, 367, pp21-33.

[75] A. Rosenfeld, "Electronic dosimetry in radiation therapy," (2006). Radiation Measurements, Vol 41 (Supplement 1), S134-S153.

[76] K. Eklund and A. Ahnesjo, "Modeling silicon diode energy response factors for use in therapeutic photon beams," *Phys. Med. Biol*, vol. 54, pp. 6135–6150, (2009).

[77] D. Cutajar, *Spectroscopic dosimetry: The development of the urethral minidosimetry system*. PhD thesis, University Of Wollongong., (2011).

[78] National Institute of Standards and Technology, "NIST XCOM database," (2013). http://physics.nist.gov/PhysRefData/Xcom/html/xcom1.html.

[79] K. Tanderup, S. Beddar, C. Anderson, G. Kertzscher, and J. Cygler, "In-vivo dosimetry in brachytherapy," *Medical Physics*, (2013).

[80] G. Rinker and E. Grusell, "Effects of radiation damage on p-type silicon detectors," *Phys. Med. Biol*, vol. 28, no. 11, pp. 1261–1267, (1983).

[81] M. Bruzzi and M Bucciolini et al, "Epitaxial silicon devices for dosimetry applications," *Applied Physics Letters*, (2007).

[82] A. Rosenfeld and V. Pugatch et al, "Strip detectors for short range particles.," *Nuclear instruments and methods in physics reserch section A: Accelerators, Spectrometers, Detectors and associated equipment*, vol. 326, no. 1, pp. 234–238, (1993).

[83] J. Wong, *Implementation of silicon based dosimters, the Dose Magnifying Glass and Magic Plate for the dosimetry of modulated radiation therapy*. PhD thesis, University Of Wollongong, (2011).

[84] M.Osvay and K. Tarczy, "Measurements of gamma-dose rates by n- and p-type semiconductor detectors," *Phys.Stat.Sol*, vol. 27, no. 1, pp. 285–290, (1975).

[85] J. Shi, W. Simon, and T. Zhu, "Modeling the instantaneous dose rate dependence of radiation diode detectors.," *Med Phys*, vol. 30, no. 9, pp. 2509–2519, (2003).

[86] J. Wong, I. Fuduli, M. Carolan, M. Petasecca, M. Lerch, P. Metcalfe, and A. Rosenfeld, "Characterization of a novel two dimensional diode array the Magic Plate as a radiation detector for radiation therapy treatment," *Med. Phys.*, vol. 39, no. 5, pp. 2544–2558, (2012).

[87] G. Mazza, R. Cirio, M. Donetti, A. Luparia, F. Marchetto, and C. Peroni, "A 64-channel wide dynamic range charge measurement ASIC for strip and pixel ionization detectors," *IEEE transactions on nuclear science*, vol. 52, no. 4, pp. 847–853, (2005).

[88] B. Gottschalk, "Charge-balancing current integrator with large dynamic range," *Nuclear Instruments and Methods in Physics Research*, vol. 207, no. 3, pp. 417–421, (1983).

[89] M. Petasecca, A. Cullen, I. Fuduli, A. Espinoza, C. Porumb, *et al.*, "X-Tream: a novel dosimetry system for Synchrotron Microbeam Radiation Therapy," *Journal of Instrumentation*, vol. 7, pp. 1–15, (2012).

[90] P. Higgins, P. Alaei, B. Gerbi, and K. Dusenbery, "In vivo diode dosimetry for routine quality assurance in IMRT," *Medical Physics*, vol. 30, no. 12, pp. 3118–3123, (2003).

[91] P. Jursinic, "Angular dependence of dose sensitivity of surface diodes," *Medical Physics*, vol. 36, no. 6, pp. 2165–2171, (2009).

[92] E. York, R. Alecu, and L. Ding, et al, "AAPM Report No. 87," (2005). American Association of Physicists in Medicine, College Park, MD.

[93] J. Eveling, A. Morgan, and W. Pitchford, "Commissioning a p-type silicon diode for use in clinical electron beams," *Med. Phys.*, vol. 26, pp. 100–107, (1999).

[94] P. Lee, J. Sawicka, and G. Glasgow, "Patient dosimetry quality assurance program with a commercial diode system," *Int. J. Radiat. Oncol., Biol, Phys.*, vol. 29, pp. 1175–1182, (1994).

[95] H. Tolli and K. Johansson, "Absorbed dose determination at short distance from 60-Co and 192-Ir brachytherapy sources," *Phys. Med. Biol.*, vol. 43, pp. 3183–3194, (1998).

[96] J. Gogani, G. Wickman, L. Johansson, and B. Johansson, "Assessment of the relative dose distribution around an 192 Ir line source using a liquid ionization chamber," *Med. Phys.*, vol. 26, pp. 1932–1942, (1999).

[97] C. Gromoll and A. Karg, "Determination of the dose characteristics in the near area of a new type of 192 Ir hdr afterloading source with a pinpoint ionization chamber," *Phys. Med. Biol.*, vol. 47, pp. 875–887, (2002).

[98] M. Skwarchuk, T. Ochran, R. Komaki, J. Cundiff, and E. Travis, "The use of radiochromic film to measure dose distributions resulting from high dose rate192-iridium single catheter treatments," *International Journal of Radiation Oncology Biology Physics*, vol. 34, no. 1, pp. 173–181, (1996).

[99] R. Valicenti, A. Kirov, A. Meigooni, V. Mishra, K. Das, and J. Williamson, "Experimental validation of monte carlo dose calculations about a high-intensity Ir-192 source for pulsed dose-rate brachytherapy," *Med.Phys.*, vol. 22, pp. 821–829, (1995).

[100] Carmen S Guzman Calcina, Adelaide de Almeida, Jose R Oliveira Rocha, Felipe Chen Abrego, and Oswaldo Baffa, "Ir-192 HDR transit dose and radial dose function determination using alanine/EPR dosimetry," *Phys. Med. Biol.*, vol. 50, pp. 1109–1117, (2005).

[101] Y. De-Deene, N. Reynaert, and C. De-Wagter, "On the accuracy of monomer/polymer gel dosimetry in the proximity of a high-dose-rate 192 ir source," *Phys. Med. Biol.*, vol. 46, pp. 2801–2825, (2001).

[102] V. Zilio, O. Joneja, Y. Popowski, A. Rosenfeld, and R. Chawla, "Absolute depth-dose-rate measurements for an 192Ir hdr brachytherapy source in water using MOSFET detectors," *Medical Physics*, vol. 33, no. 6, pp. 1532–1539, (2006).

[103] J. Williamson, H. Perera, Z. Li, and W. Lutz, "Comparison of calculated and measured heterogeneity correction factors for 125I, 137Cs and 192Ir brachytherapy sources near localized heterogeneities," *Med Phys*, vol. 20, pp. 209–222, (1993).

[104] M. McJury, P. Tapper, V. Cosgrove, P. Murphy, S. Grifn, M. Leachk, S. Webb, and M. Oldham, "Experimental 3D dosimetry around a high-dose-rate clinical

192 Ir source using a polyacrylamide gel (PAG) dosimeter," *Phys. Med. Biol.*, vol. 44, pp. 2431–2444, (1999).

[105] J. Williamson and Z. Li, "Monte Carlo aided dosimetry of the microselectron pulsed and high dose-rate 192-Ir sources," *Med. Phys.*, vol. 22, no. 6, pp. 809–819, (1995).

[106] D. Baltas, S. Giannouli, A. Garbi, and F. Diakonos et al, "Application of the Monte Carlo integration (MCI) method for calculation of the anisotropy of 192Ir brachytherapy sources," *Phys. Med. Biol.*, vol. 43, no. 6, pp. 1783–1801, (1998).

[107] A. Espinoza, B. Beeksma, and Marco Petasecca et al., "The feasibility study and characterisation of a two dimensional diode array in magic phantom for high dose rate brachytherapy quality assurance," *Medical Physics*, (2013).

[108] G. Knoll, *Radiation Detection and Measurement*. John Wiley and Sons, third ed., (2000).

[109] G. Obe, C. Johannes, and D. Schulte-Fronlinde, "DNA double-strand breaks induced by sparing ionizing radiation and endonucleases as critical lesions for cell death, chromosomal aberrations, mutations and oncogenic transformation," *Mutagenesis*, vol. 7, no. 1, pp. 3–12, (1992).

[110] D. Parkin, P. Pisani, and J. Ferlay, "Global cancer statistics," *CA: A Cancer Journal for Clinicians*, vol. 49, no. 1, pp. 33–64, (1999).

[111] National Institute of Standards and Technology, "XCOM: Photon Cross Sections," (2012). http://physics.nist.gov/PhysRefData/Xcom/Text/XCOM.html.

[112] J. Wong and M. Carolanet al, "Asilicon strip detector dose magnifying glass for IMRT dosimetry," *Medical Physics*, vol. 37, no. 2, pp. 427–439, (2010).